# SPATIAL DISTRIBUTION AND EVOLUTION OF A SEASONAL SNOWPACK IN COMPLEX TERRAIN: AN EVALUATION OF THE SNODAS MODELING PRODUCT

By

Brian Trail Anderson

A thesis

submitted in partial fulfillment

of the requirements for the degree of

Master of Science in Hydrologic Sciences

Boise State University

May 2011

BOISE STATE UNIVERSITY GRADUATE COLLEGE

## DEFENSE COMMITTEE AND FINAL READING APPROVALS

of the thesis submitted by

Brian Trail Anderson

Thesis Title: Spatial Distribution and Evolution of a Seasonal Snowpack in Complex Terrain: An Evaluation of the SNODAS Modeling Product

Date of Final Oral Examination: 25 February 2011

The following individuals read and discussed the thesis submitted by student Brian Trail Anderson, and they evaluated his presentation and response to questions during the final oral examination. They found that the student passed the final oral examination.

| | |
|---|---|
| James P. McNamara, Ph.D. | Chair, Supervisory Committee |
| Alejandro N. Flores, Ph.D. | Member, Supervisory Committee |
| Hans-Peter Marshall, Ph.D. | Member, Supervisory Committee |

The final reading approval of the thesis was granted by James P. McNamara, Ph.D., Chair of the Supervisory Committee. The thesis was approved for the Graduate College by John R. Pelton, Ph.D., Dean of the Graduate College.

ACKNOWLEDGEMENTS

I would like to thank those who helped make this work possible. Thanks to my wife Amanda for her patience, understanding, and support during this process. Also, thanks to all my family and friends who have encouraged me to pursue my education, I could not have done it without you. My thanks and appreciation goes out to my advisor Dr. James McNamara for providing me with this opportunity. He was always willing and available for assistance and guidance both on the snow and in the office and provided me with flexibility to pursue my interests in science. Thank you to my committee: Dr. Hans-Peter Marshall whose guidance and expertise in snow science and technology greatly improved this work, and Dr. Alejandro Flores for his suggestions and assistance. I could not have collected these datasets without the many hours of field assistance from: Alden Shallcross, Ivan Geroy, Ryan Warden, Patrick Kormos, Dave Eiriksson, Erik Boe, Alison Burnop, Scott Havens, Pam Aishlin, Ben Wickham, and others. My thanks go out to Cindy Busche and Christina Rivas at the Boise WaterShed Environmental Education Center and Karen Viskupic, James Belthof, and David Wilkins for their help with the GK-12 fellowship. Thanks to the staff at the Boise NRCS Snow Survey Office and the Agricultural Research Service for the loan of snow survey equipment and training.

Funding was provided from the National Oceanic and Atmospheric Administration - National Weather Service, The Geological Society of America Student Research Grant, The National Science Foundation GK-12 Program, and the Boise State Geoscience Department.

ABSTRACT

Hydrologists and water managers have been attempting to accurately estimate watershed scale snow water equivalent (SWE) for over a century. Extensive monitoring networks, remote sensing technology, and sophisticated modeling approaches have greatly improved these estimates; however, water inputs from snow in mountainous areas are still subject to considerable uncertainty due to SWE spatial variability. In an attempt to improve the understanding of physical processes and controls influencing SWE spatial variability, a field campaign to measure the spatial and temporal distribution of SWE within the Dry Creek Experimental Watershed (DCEW) was conducted during 2009 and 2010. These measurements are compared to a distributed SWE data assimilation and modeling product from the National Weather Service called the Snow Data Assimilation System (SNODAS) to estimate the sub-pixel variability and accuracy of the model estimates, as well as attempt to understand model deviation from observed conditions. These data are evaluated using the variogram to assess the evolution of SWE variability and spatial correlation lengths throughout the winter. Correlations between snow depth and landscape characteristics are explored to determine the most influential physical processes influencing SWE distribution. Specifically, this work indentifies the relative importance of differential accumulation, redistribution, and differential ablation at three spatial scales. Results from this work indicate that at the watershed scale (27 $km^2$), elevation is the most important control on snow distribution, while at the SNODAS pixel scale (1 $km^2$), and 1 meter spaced transect scale, differential solar radiation is a stronger

control on SWE distribution during ablation. Comparison of transect scale and SNODAS pixel scale observations with SNODAS show the model under-predicts SWE throughout the winter at two out of three sites, and over-predicts during ablation at one site. SNODAS captures the watershed scale elevation trend, but under-predicts the magnitude of SWE at assumed maximum accumulation.

TABLE OF CONTENTS

LIST OF TABLES

LIST OF FIGURES

# CHAPTER 1: INTRODUCTION

Snow is an important part of the hydrologic cycle in many regions, affecting both global energy fluxes and regional water availability. Snow-derived runoff provides domestic and irrigation water for an estimated 1 billion people worldwide (Barnett *et al.*, 2005). Accurate assessments of the distribution of SWE and the timing of melt are critical for predicting runoff magnitude, and understanding surface and climate processes. Recent climate studies show reduced seasonal snowpack and earlier timing of melt in the Western United States (Cayan *et al*., 2000) reinforcing the need to improve SWE modeling capability in semi-arid regions for water management, hydrologic forecasting, and for improving understanding of climate processes.

The National Weather Service's National Operational Hydrologic Remote Sensing Center (NOHRSC) has developed an integrated modeling and data assimilation product called the Snow Data Assimilation System (SNODAS). SNODAS products combine an energy and mass balance snow model, called the NOHRSC Snow Model (NSM) with satellite snow cover estimates and remote ground-based observational data assimilation to simulate SWE with 1 $km^2$ resolution. This product provides spatially distributed SWE and melt water input estimates at daily time steps for the Continental United States and a portion of Canada (Carroll *et al.,* 2006). While the overall ability of the NSM to model the snowpack in one dimension at a single point has proven to be relatively accurate based on validation work by Rutter *et al.* (2008), SNODAS products have not been thoroughly validated in a distributed fashion at mid elevation where

snowpack properties at this scale (1 $km^2$) are inherently heterogeneous and snow model driving data are subject to large uncertainty. Understanding the relevant processes and influencing factors that cause SWE spatial variability within a watershed will help improve distributed modeling efforts and lead to better distributed snow models.

### 1.1 Project Description

The purpose of this study is to gain a better understanding of the sources of snow variability that may lead to poor model performance. It is expected that a model operating at a 4 $km^2$ resolution will not perform optimally in regions where significant spatial variability occurs over tens of meters. A benefit of evaluating models in highly instrumented watersheds is that insight can be gained into reasons why models fail, rather than just the fact that they do. To that end, this work investigates the physical processes and landscape characteristics that control snow distribution at different scales by quantifying the variability of SWE in both space and time. Ultimately, this work aims to improve estimates of watershed scale SWE for hydrologic modeling and water balance investigations within a hydrologic research basin. Often in snow hydrology, investigations are interested in capturing peak SWE within a basin to determine how much water is held in the snowpack just prior to melt. Snow surveys in this study were conducted repeatedly at the same locations throughout the winter in an effort to answer the question: *how does SWE variability develop?* It is hypothesized that SWE spatial variability can be explained by three processes that interact through time. These processes include: 1. differential accumulation, 2. redistribution, and 3. differential ablation.

To test this hypothesis, snow depth and SWE measurements were made at multiple sites over two winters in the Dry Creek Experimental Watershed (DCEW). Snow water equivalent predictions from SNODAS were obtained from the National Snow and Ice Data center and compared with ground truth observations to evaluate the accuracy and sub-pixel variability of the SNODAS model. Field data are analyzed using

variogram analysis to gain an understanding of the correlation lengths at which variability occurs and how snow cover spatial variability changes throughout the winter. SWE measurements are combined with landscape characteristics to indentify correlations between observed SWE and elevation, aspect, slope, solar radiation, vegetation, and wind.

The results of this work indicate that SNODAS model predictions are often not representative of conditions on the ground. This finding, while representative of only three grid cells within a model of thousands of grid cells, is significant because there has been, as of yet, no evaluation of this distributed modeling framework (Barrett, 2003). Regardless of the accuracy of SNODAS at these locations, it is important to understand the causes of snow spatial variability and their influence through time. Greater understanding of these processes will benefit the future development of snow hydrology models and ultimately lead to better distributed snow models.

## 1.2 Background

Efforts to monitor the volume of SWE in the mountains have been ongoing since the early 20th century in the form of snow surveys. Dr. James E. Church, a classics professor from the University of Nevada, is often cited as the pioneer of the snow survey. His initial work from 1905 to 1911 involved monitoring the snowpack in the Sierra Nevada Mountains and lead to the creation of the Mt. Rose "Federal" snow sampler (Helms *et al*,. 2008). Today, the Natural Resources Conservation Service (NRCS) monitors SWE across the western United States with a combination of manual snow measurement sites called snow courses and with remote automatic sites known as SNOTEL stations. Snow courses are measured twice monthly and typically consist of 5 SWE samples along a linear transect. SNOTEL sites send real-time observations of SWE, snow depth, and a variety of meteorological data. The data from these sites are extremely valuable to water managers and hydrologists alike for use in predicting stream flow; however, because SNOTEL stations are only measurements at a single location within a basin, the data from them may not accurately represent the distribution of snow within a basin. Recent studies have shown that basin-wide SWE estimates may be biased due to instrument location (Molotch and Bales, 2005) and SNOTEL sites must be considered as point index estimates. Bales *et al.* (2006) also points out that SNOTEL sites are limited at both extreme high and low elevations where a significant amount of SWE may go unaccounted for, and the effects of climate variability on SWE may be missed.

SWE in mountainous areas often shows a high degree of spatial variability, owing to the influence of complex terrain and wind, combined with the multiple physical processes that accumulate and melt snow. A snowpack is a dynamic medium in a

constant state of flux. Snow crystals begin their existence in the atmosphere, growing in a variety of morphologies as a result of temperature and vapor pressure conditions in clouds. Once a snow crystal has grown large enough to have a downward velocity and survive sublimation, it can become deposited on the ground. The spatial variability of snow that is present directly after deposition is the result of temperature and precipitation lapse rates in the atmosphere, wind intensity, topography and underlying surface roughness, and vegetation (DeWalle and Rango, 2008). Snowfall amounts in mountainous regions trend linearly with elevation due to orographic uplift of air masses. With the exception of high alpine regions where steep rock walls and high winds obscure snow accumulation, more snow and precipitation in general falls at higher elevations than at lower elevations. Snow deposition on the ground is often affected by the magnitude and direction of winds during a snow event. If a snowstorm comes in with significant winds, exposed areas are scoured and snow deposition occurs preferentially near areas where airflow separation occurs, such as leeward sides of ridges, forest canopy openings, and other convex barriers (DeWalle and Rango, 2008). Snow also covers and fills in around small scale surface roughness from shrubs, rocks, logs, and etc. Forest canopies also reduce accumulation of snow on the ground by interception. Snow intercepted by forest canopy melts or unloads from the tree but is subject to considerable sublimation and evaporation. Drip from melting snow intercepted by the tree canopy can cause melt of the underlying snowpack as well.

After being deposited on the ground, snow crystals continue to change. The snowpack settles and the snowflake structure begins to metamorphose as a result of differing temperature and vapor pressure in the pack. Wind events can redistribute newly

fallen snow if the snow surface remains erodible and wind speeds are strong enough. Based on work done in the Canadian prairies by Li and Pomeroy (1997), threshold wind speeds for snow redistribution were determined to be approximately 15 and 22 miles per hour for dry and wet snow, respectively.

Energy fluxes into and away from the snowpack cause it to ablate differentially. Solar, longwave, and turbulent fluxes make up the bulk of energy that melts snow (Armstrong and Brun, 2008). In complex terrain, differential solar input to the snowpack is the result of slope and aspect values as described by Lee (1963) and Frank and Lee (1966). Differential ablation is strongly linked to differences in solar radiation inputs from complex terrain especially in open areas without considerable vegetation. The presence of forest canopies can affect the solar radiation input by reducing the transmitted solar radiation through the canopy. Longwave radiation emissions from the vegetation itself can cause localized ablation near trees and shrubs. Turbulent fluxes of sensible and latent heat are important energy flux terms as well; however, the requirement to measure vertical wind, humidity, and temperature profile values above the snow surface and estimate the snow surface roughness length make calculation of these fluxes complex. Turbulent fluxes are also important for patchy, shallow snow cover due to the transfer of sensible heat from snow free areas to snow covered areas as described by Granger *et al*. (2006). The spatial variability resulting from these processes makes monitoring and modeling SWE at the watershed scale subject to large uncertainty.

Typical gridded modeling discretizations are subject to what is known as "sub-pixel variability" (Blöschl, 1999). In general terms, model grid cells are often too coarse to adequately represent the variability in SWE that is present on the landscape. Pixel-

based snowmelt models treat each pixel as uniform snow cover representing average snow distribution within the pixel. During ablation, when patchy or variable snow cover dominates, error can be introduced into runoff predictions by effectively calculating melt from areas that are snow free or vice versa. This problem has confounded SWE distribution investigations for some time because validation of distributed model predictions is challenging. Obtaining enough samples to adequately estimate the mean SWE over a basin or even a modeling pixel is a time consuming and labor-intensive effort that to date is only possible via exhaustive manual surveys. The cost and effort required for such an endeavor makes this approach unfeasible for operational hydrologic monitoring (Elder *et al*., 1991).

Attempts have been made to remotely sense SWE from space borne and airborne platforms using passive microwave technology, but as of yet none of these approaches are used operationally by water resource management agencies. Difficulties related to snow microstructure, and liquid water within the snowpack has confounded passive microwave approaches to monitoring SWE. Because passive microwave response retrieval algorithms are sensitive to heterogeneities within the snowpack, such as snow microstructure, no single retrieval algorithm will work in all snow types and land cover types (Rango *et al.*, 1989; Schmugge *et al.*, 2002).

Satellite derived imagery has been useful in determining snow covered area (SCA), which has then been used to infer snow water equivalent based on the concept of a depletion curve (Luce *et al*., 1999; Homan *et al*., 2011). A depletion curve relates SCA to SWE assuming that SWE can be inferred from SCA using a distribution function that embodies the watershed characteristics.

It has often been noted that certain landscape characteristics influence patterns of SWE and snowmelt consistently from year to year. Elder *et al*. (1991) was successful in using topographic and radiation parameters, such as elevation, slope, and potential solar radiation, to map zones of similar snow properties. Anderton *et al*. (2004) determined that wind exposure and distribution of SWE prior to melt were the most important factors related to snowpack disappearance in a small catchment in the Spanish Pyrenees. It has been noted in such studies that non-linear relationships exist between SWE and landscape features that influence SWE. In turn, researchers have adopted non-linear classification schemes, such as binary decision trees (e.g., Elder *et al*., 1998), to relate SWE to landscape properties for the modeling of SWE.

Future work aims to resolve the snow spatial variability problem using airborne radar. Current missions form both NASA and the European Space Agency are focused on the use of active Ku band and dual X band radar to retrieve SWE measurements from space with spatial resolutions of less than 100 meters (Rott *et al*., 2010).

### 1.3 Study Site

DCEW is a 27km$^2$, dominantly southwest facing, semi-arid mountain front, draining a north trending ridge and the foothills north of Boise, Idaho (located at 43° 43'N, 116° 07'W; Figure 1.1). Boise State University and the Agricultural Research Service established DCEW in 1998 as a field laboratory to investigate cold region watershed processes. Elevations within DCEW range from 950 m at the lower stream gage to 2130 m at Deer Point. Vegetation is predominantly sagebrush (*artemisea tridentata),* bitterbrush (*prushia tridentata),* and mixed grasses and a variety of riparian vegetation at lower elevations. Higher elevations within DCEW give way to forested areas composed mostly of Douglas Fir (*Pseudotsuga menziesii),* Ponderosa Pine *(Pinus ponderosa),* Green Alder (*Alnus viridis),* and Ceanouthus *(Ceanothus Americansus).*

Soils in DCEW are generally coarse textured sandy loam, the result of weathering of the granitic Idaho Batholith. Soils are shallow and well drained, meaning overland flow is not common (LaMontange, 2009; McNamara *et al*., 2005; Williams *et al*., 2009).

There are three weather stations within the basin collecting standard precipitation and meteorological data at elevations of 1100 m, 1610 m, and 1850 m. There is also a nearby SNOTEL site outside DCEW at the Bogus Basin Ski Resort at 1932 m that collects weather data as well as time series measurements of SWE from a snow pillow. The lower elevations within the basin receive only occasional intermittent snow that usually does not last more than a couple days, while the higher elevations are generally snow covered from December until May. This study focuses on three sites at the middle to upper portions of the basin with elevations greater the 1600 m.

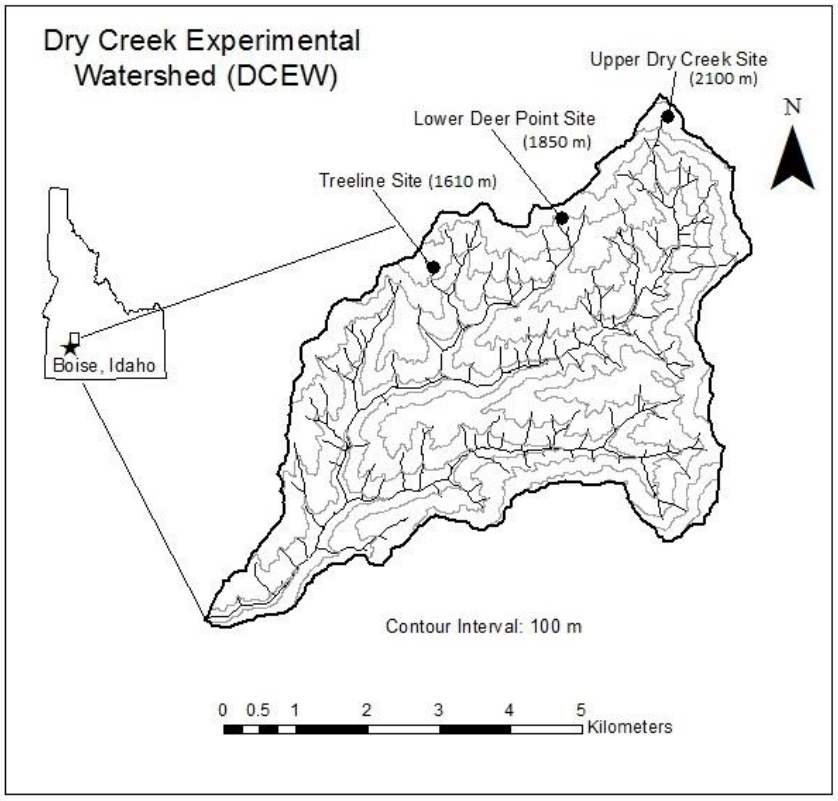


**Figure 1.1** Dry Creek Experimental Watershed showing three study sites

1.3.1 Climate

Climate in Southwest Idaho is driven by pacific maritime conditions with the greatest amounts of moisture supplied during winter and spring months by prevailing westerly winds originating from the Aleutian Low (Williams, 2005). The Boise area and lower portions of DCEW are defined as having a cold semi-arid climate, BSk in Köeppen classification system. The upper portions of DCEW are classified as Dsa, moist continental climate with dry summers.

There is a significant (~300%) increase in precipitation with elevation. Annual average precipitation increases from 310 mm in Boise (900 m), to 570 mm at Treeline (1610 m), to approximately 1000 mm at Bogus Basin SNOTEL (1932 m) (LaMontange,

2009). DCEW typically experiences hot and dry summers and cool and wet winters with approximately 70-80% of annual precipitation falling from December-June. Precipitation versus elevation trends based on total cumulative precipitation from the Lower Weather, Treeline, and Bogus Basin weather stations during the 2009 and 2010 winter months (Oct-May) are shown in Figure 1.2.

Temperatures are also highly elevation dependent. Boise typically experiences temperatures 5-10 °C warmer than Bogus Basin. However, inversions are a common occurrence in the winter and Bogus Basin may experience warmer temperatures than the valley floor. Temperature versus elevation trends based on average daily air temperatures from the Lower Weather, Treeline, and Bogus Basin weather stations during the 2009 and 2010 winter months (Oct-May) are shown in Figure 1.3.

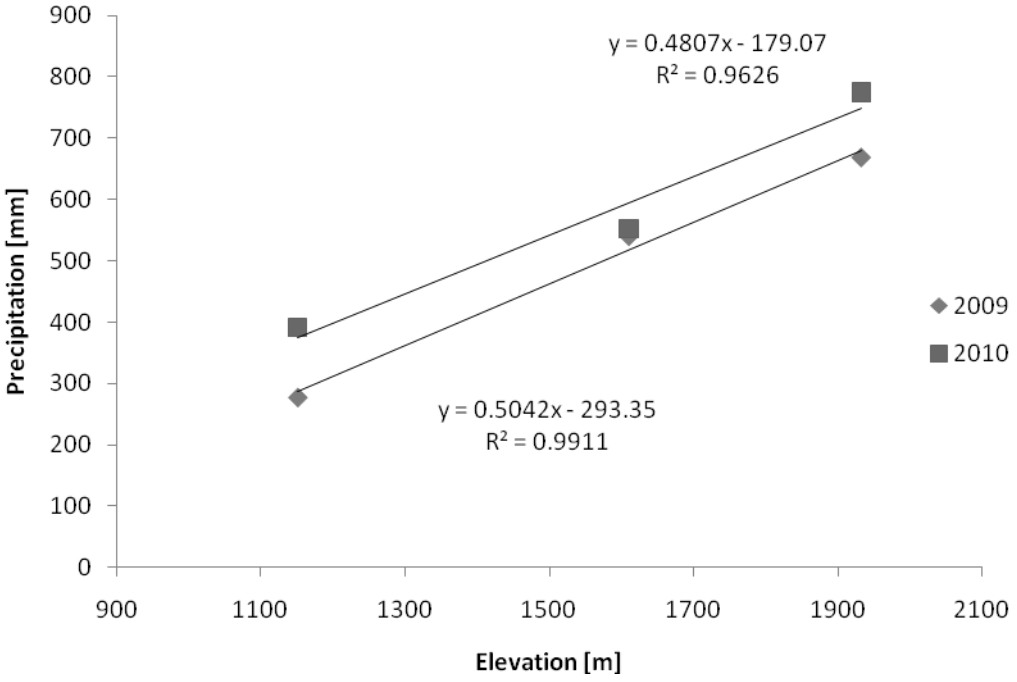


**Figure 1.2** Total Oct-May precipitation versus elevation during 2009 and 2010.

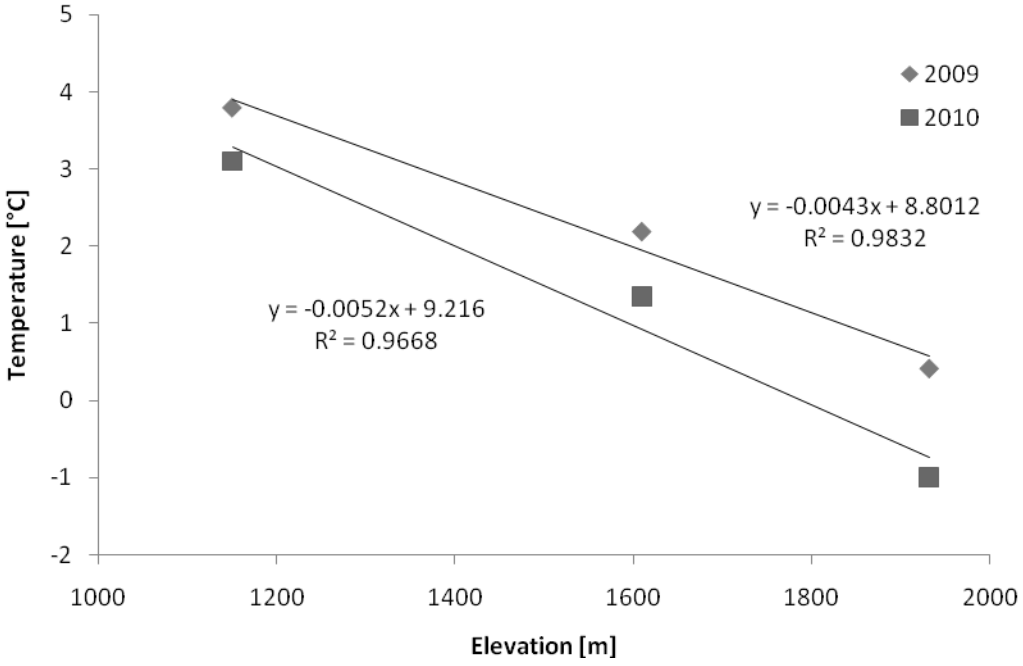


**Figure 1.3** Average Oct-May temperature versus elevation during 2009 and 2010.

1.3.2 Treeline

The Treeline site (1610 m) is a 0.02 $km^2$ instrumented sub-basin with a meteorological station that lies in a sagebrush steppe ecotone transitioning to mixed conifer forest. Snow cover at Treeline is often shallow, patchy, and variable from year to year. Precipitation at Treeline can be variable, with some years receiving more rain than snow, and vice versa. Topography at this site includes steep opposing hillslopes that show the same snow spatial patterns from year to year. Snow tends to melt out quickly on the southwest-facing slope and remains throughout the year on the northeast-facing slope.

### 1.3.3 Lower Deer Point

The Lower Deer Point site (1850 m) is on a ridge knob and includes a meteorological station and soil moisture site that is surrounded by mixed conifer forest, alder, and heavy ceanothus underbrush. This site is typically snow covered throughout the winter. Snow distribution at Lower Deer Point is influenced by vegetation occurring at different densities throughout the site due to logging operations that occurred in the vicinity in past years.

### 1.3.4 Upper Dry Creek

The Upper Dry Creek site (2100 m) is the upper portions of the Bogus Experimental Catchment (Kormos, 2005) that contains scattered conifer trees, and ceanothus and alder shrubs. This uninstrumented site is the highest elevation portion of DCEW and holds the deepest, most persistent snowpack throughout the basin. It is hypothesized that wind is an important influence at this site due to its high elevation and sparse forest canopy.

### 1.3.5 2009-2010 Snow and Meteorology

Precipitation during 2009 was marked by a distinct break in precipitation events during late January and February, while 2010 experienced consistent amounts throughout the season (Figure 1.4). The 2009 and 2010 snow amounts were relatively similar within DCEW. The Bogus Basin Snow Course reported April 1$^{st}$ SWE measurements that were 90 and 88 percent of the 1971-2000 average, respectively (Figure 1.5). The Bogus Basin Road Snow Course, one half mile from and the same elevation as the Treeline site,

reported March 1st SWE measurements of 45 (2009) and 156 (2010) percent of the 1971-2000 average, while April 1st measurements showed 126 (2009) and 56 (2010) percent (Figure 1.6) (March 1st typically being the maximum for this site). This discrepancy illustrates the shallow, variable snowpack that is typical of this lower elevation site. During both years, DCEW experienced significant snowfall events later in the season when significant ablation had occurred.

Wind speed and direction during winter months plays a critical role in accumulation and redistribution of snow. Wind data from Treeline and Lower Deer Point are shown for both the 2009 and 2010 winter months (Oct-May) in Figures 1.7 and 1.8. Wind data from both sites show a dominant wind direction of Northwest during 2010 and more predominantly Southeast during 2009.

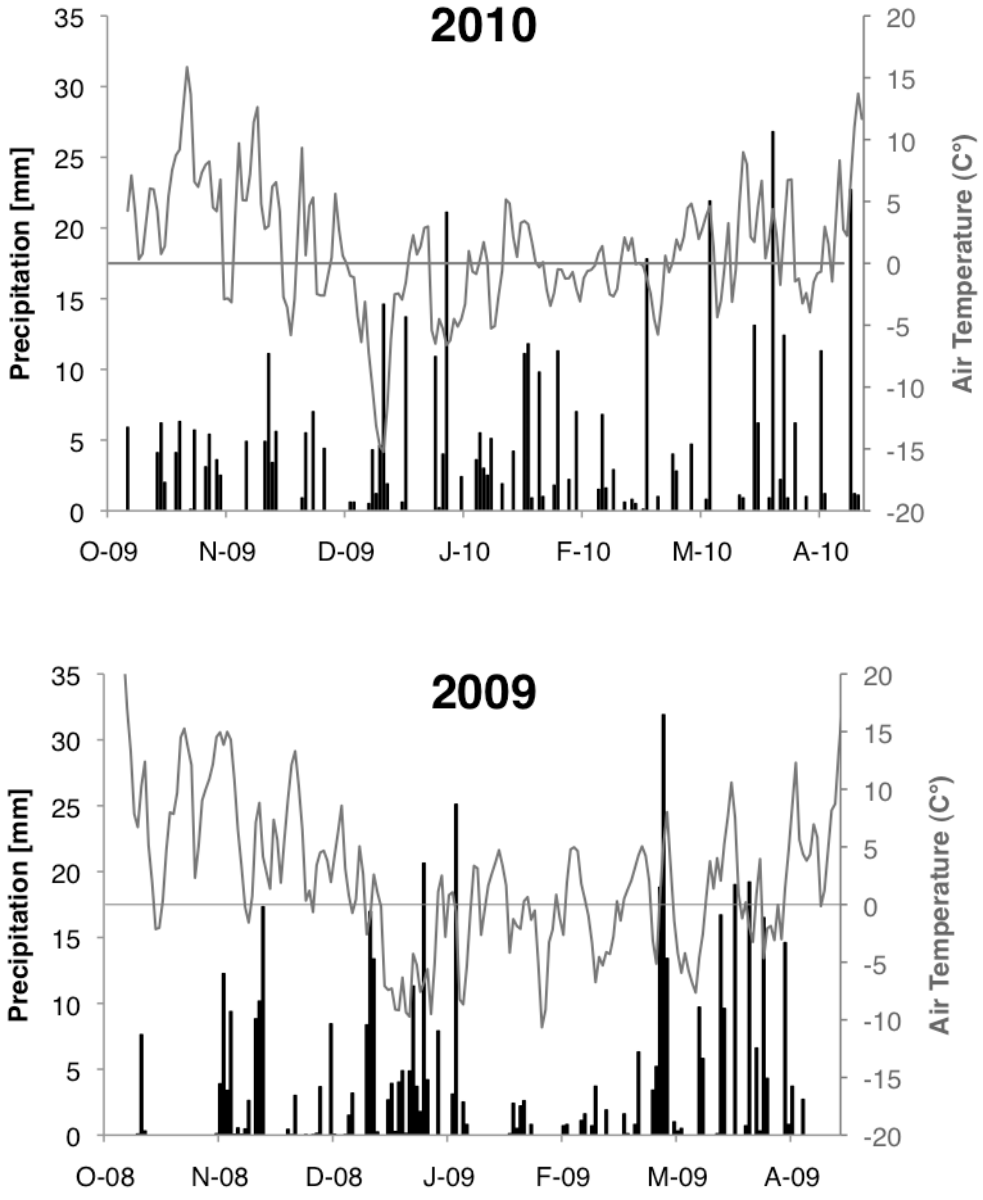


**Figure 1.4** 2010 and 2009 winter months (Oct-April) hyetographs and daily average air temperature from the Treeline weather station. Note the consistant precipitation during 2010, while 2009 experienced dry conditions through late January and much of February, and considerable moisture in early March.

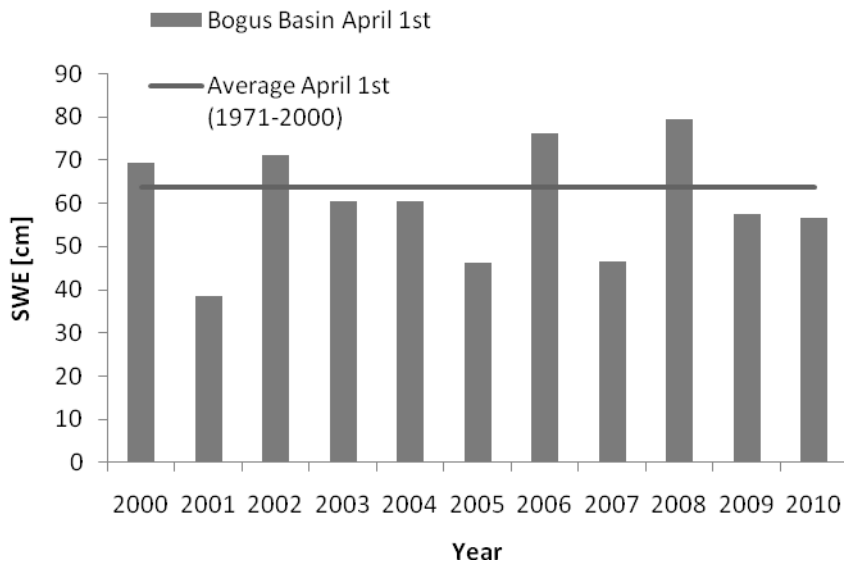


**Figure 1.5** 2000-2010 April 1st SWE measurements and 30 year average from the Bogus Basin Snow Course located at Bogus Basin Ski Resort at 1932 m elevation. (NRCS – Snow Survey)

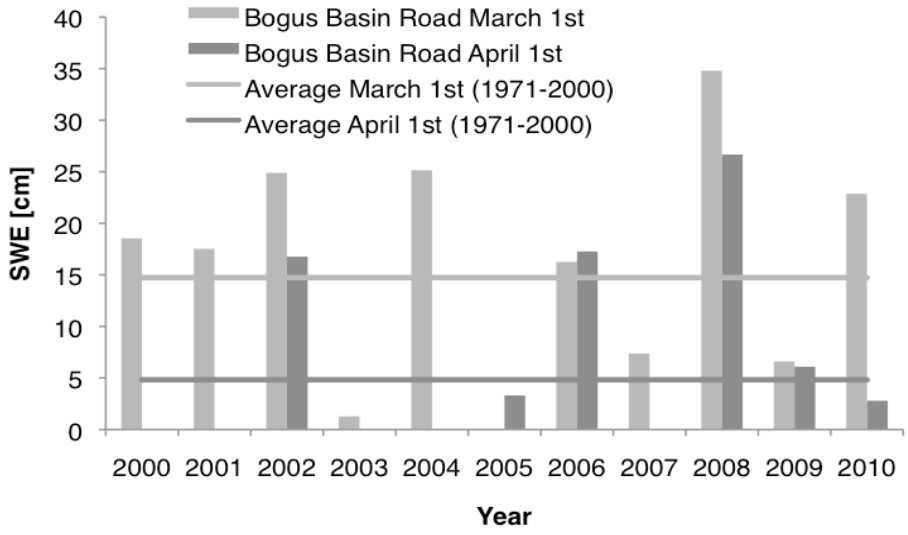


**Figure 1.6** 2000-2010 March 1st SWE measurements and 30 year average from the Bogus Basin Road Snow Course located near Treeline site on Bogus Basin Road at 1630 m elevation. (NRCS – Snow Survey)

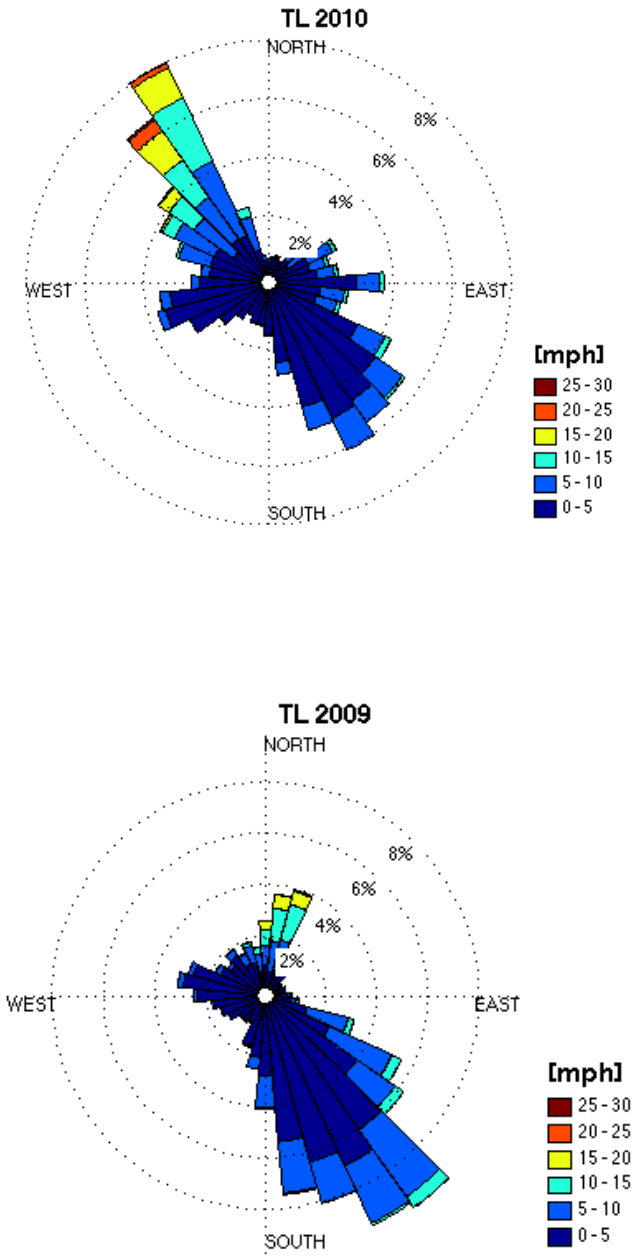


**Figure 1.7** Wind speed and direction roses for October-May at the Treeline site during 2009 and 2010.

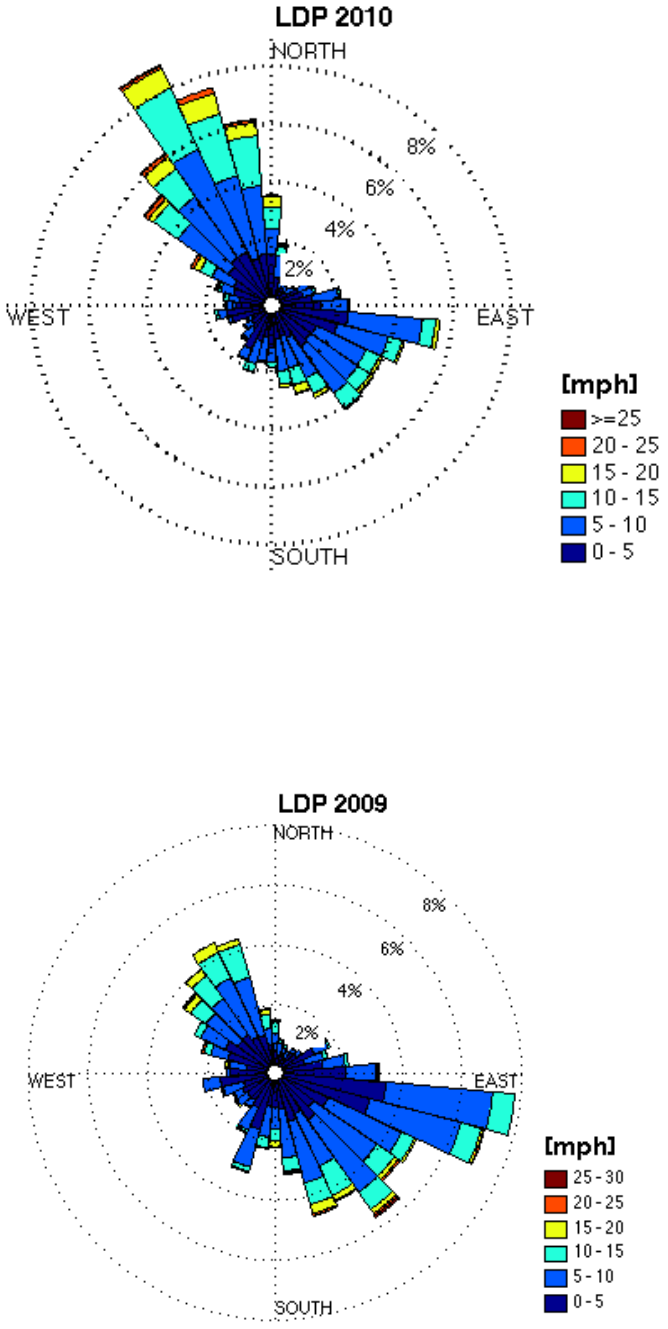


**Figure 1.8** Wind speed and direction roses for October-May at the Lower Deer Point site during 2009 and 2010.

# CHAPTER 2: METHODS

## 2.1 SWE Measurement

The design of this study was approached with the goal of evaluating a distributed model and quantifying the sources of snow spatial variability at three scales. Numerous studies have used snow surveys to estimate water input from melting snow and attempt to quantify spatial variability (Elder *et al*., 1991, 1998; Anderton *et al*., 2004; Jost *et al*., 2007; Motloch and Bales, 2005); however, reporting the variability encountered in the field at assumed maximum accumulation does not necessarily provide information about the causes of variability. To resolve this, surveys in this study were conducted repeatedly at the same locations throughout the snow season with the goal of understanding the processes that cause variability.

Snow water equivalent of a snowpack is calculated as:

$$SWE = h_s\left(\frac{\rho_s}{\rho_w}\right) \qquad (1)$$

where SWE is the snow water equivalent (cm), $h_s$ is the depth of snow (cm), $\rho_s$ is the density of snow (kg/m$^3$), and $\rho_w$ is the density of water (kg/m$^3$). While recent advances in satellite, radar, and radio technology have shown promise for remote measurement of SWE, operational estimates of SWE for water supply forecasting still rely on the methods developed in the early 20$^{th}$ century using aluminum tubes to directly measure snow pack bulk density from snow cores. In this study, snow water equivalent

was measured from snow cores taken with a "Federal" or "Mt. Rose" snow sampler according to the specifications designed by the NRCS and described in Gray and Male (1981). The federal sampler consists of incremented hollow aluminum tubes that screw together and calibrated scale. Measurements are made by vertically inserting the tube into the snowpack until the ground is encountered, extracting the tube and snow core, removing any soil or debris from the bottom, and weighing the tube and snow core. The weight of the empty tube is subtracted from the weight of the tube and the snow core to obtain the water content. Snowpack bulk density can then be calculated by dividing SWE by snow depth. Bulk density is of interest because it can be used to estimate SWE from separate snow depth measurements in what is known as "double sampling" (Berezovskaya and Kane, 2007). SWE measurements made with a federal sampler are representative of the entire snowpack and thus represent a mean SWE for the entire pack.

It is well known that layering within the snowpack from individual snowfall events leads to significant vertical variability in snow density within the pack. Many snow studies have used smaller sample size density measurements along a snow pit wall to discriminate layering within the snowpack and obtain more accurate snow density information. Because this study is not concerned with layering within the snowpack and because this approach is much more time consuming, it is assumed that mean SWE and density are sufficiently accurate. The accuracy of the federal sampler has been debated in the literature. Tests conducted by Work *et al.* (1965) and Goodison (1978) indicate that SWE from federal samplers may be biased over a range from -0.3% to 12%. This overestimate has been attributed to the cutter teeth on the bottom of the tube forcing more snow into the tube. The treatment of this bias in previous studies has been varied.

Molotch and Bales (2005) multiplied all federal sampler measurements by 0.9 based on the results of this test work, while Anderton *et al.* (2002) and Jost *et al.* (2007) make no mention of corrections for error associated with the federal sampler. Work *et al.* (1965) did point out that percentage errors are typically larger for shallow snowpacks than for deeper snowpacks. Due to the complications of sampling shallow snow (<30 cm), a smaller purpose built SWE sampler was often used in shallow conditions for this study. This sampler is a 12-inch long 3-inch diameter plastic tube with a small, calibrated scale, obtained from the Snowmetrics company.

Snow depth was measured using an incremented probe vertically inserted into the snowpack and spatially located using a global positioning system (GPS) unit. During the 2010 snow season, an automatic snow depth and GPS recording device called the Magnaprobe (Patent number 5864059) was used for transect scale snow depth measurements. The Magnaprobe uses a magnetic position sensor attached to a 12-inch diameter plastic basket that slides along a steel rod. The operator vertically inserts the rod into the snowpack until the ground is encountered and with the push of a button, records the height of the basket (i.e., the depth of snow = total length of rod-distance from top of rod to basket) along with GPS location (1-2 meter accuracy) in a backpack data logger. The use of this instrument allowed for orders of magnitude more snow depth measurements than is possible for one person using an incremented probe, handheld GPS, and notebook. The Magnaprobe was developed by Mathew Sturm and Joel Holmgren for sampling arctic snowpacks and typically consists of a 1-meter sampling rod. In this study, for the first time a custom made longer Magnaprobe was used, which had a maximum total depth of 1.65 meters. Although slightly more awkward, it provided depth

measurements that covered nearly all conditions encountered and is therefore the recommended method for snow depth measurements in this semi-arid environment. Snow depth measurements, like SWE measurements, are subject to inaccuracies as well. When probing to the bottom of the snow pack the observer must determine where the snow-soil or snow vegetation interface lies without visual confirmation. Berezovskaya and Kane (2007) in the Alaska tundra showed that overestimation of snow depth may be common due to the inability of observers to distinguish low-density vegetation at the bottom of the snowpack. Other factors influencing the accuracy of snow depth measurements include the presence of ice layers in the snowpack and larger vegetation interactions with the snow depth probe. Under estimation of snow depth is possible when ice layers or larger woody vegetation is encountered with the probing device. Error or uncertainty may also be introduced by deviations from completely vertical insertion of the snow depth and SWE instruments. Every attempt was made to sample snow vertically, however, it is likely that some sampling error occurred.

The approach to determine the spatial locations of samples taken in the field differed for each scale of survey. For the transect scale, the Magnaprobe was used to record GPS location with each measurement, while for the pixel and watershed-scale surveys, survey locations were selected prior to arrival in the field and navigated to with a handheld GPS. The end-points of transects measured in the watershed-scale survey were recorded, and each measurement was inferred by assuming a straight line and even sample spacing along the transect. It should be noted that some inaccuracy in the spatial locations of sample points exists from both the Magnaprobe and the use of handheld GPS units. Some deviation from the pre-selected sample locations likely occurred when

navigating to points in the field using hand-held GPS units due to instrument accuracy. Likewise, the Magnaprobe GPS unit may have been subject to inaccuracy when recording spatial locations in the field due to the availability of satellites and forest cover interference.

## 2.2 SWE Estimation

Several studies investigating SWE spatial variability have shown that snow depth tends to be more variable than snow density (Dickinson and Whiteley, 1972; Stepphun, 1976). This is because snow density varies over a much smaller relative range than snow depth in most conditions. On a given day during mid-winter or spring, mean snowpack density values encountered in the field will fall within a relatively narrow range, typically 250-550 kg/m$^3$. Snow depth, however, shows a much larger range, which relates to the complex processes of accumulation, redistribution, and ablation, as well as small terrain and surface features and can range from 0 to more than 1 meter in distances of less than 100 meters. Sturm *et al*. (2010) proposed using calendar date and climate class to predict mean SWE from snow depth based on the assumption that snow depth is more variable than snow density. Spatial variations in density are, however, much less understood than spatial variations in depth due to the much more time consuming nature of density measurements. Often, snow surveys have several orders of magnitude more depth measurements than density measurements, and density measurements from less than 10 locations is very common.

In this study, SWE spatial variability is quantified using both snow depth and snow density measurements. Due to the aforementioned time consuming nature of snow density compared to snow depth, orders of magnitude more measurements of snow depth were made than that of snow density. Snow depth measurements are also faster and easier to make. Snow depth measurements made with the Magnaprobe take approximately 3-5 seconds (10-20 seconds manually) while snow density measurements

take 5-10 minutes each. Therefore, much of the analysis in this study relies heavily on snow depth measurements. It is assumed that several snow density measurements during each survey could be used to obtain a representative mean snow density for the determination of SWE from snow depth measurements.

It is well known that SWE spatial variability occurs at a range of scales. While large scale modeling approaches, such as the SNODAS product, attempt to provide information about mean SWE at the 1 $km^2$ scale, many studies have shown that micro-scale variability (on the order of 10-100 m) is significant and important to accurately quantify for accurately modeling mean SWE for hydrological applications (Anderton *et al*., 2002; Trujillo *et al*., 2007). To adequately document and quantify this spatial variability, snow surveys were conducted at three different scales across DCEW.

## 2.3 Description of Sampling Strategy

Spatial variability of snow occurs at a variety of scales. In this study, I attempt to quantify snow spatial variability at three scales: the 1 meter spaced transect scale, the 1km$^2$ pixel scale, and the small watershed (27 km$^2$) scale.

### 2.3.1 Transect Scale

To capture the transect scale, one meter spaced sampling was conducted regularly along transects at three different elevations gaining access by skis or snowshoes. The layout of these transects were determined by the topography and characteristics of the three sites. Samples were collected by traversing transect lines and probing to the base of the snowpack with the Magnaprobe with 1 meter spacing along the transect.

The Treeline site consisted of a linear transect 300 meters long traversing the middle of the Treeline basin and adjacent hillslopes. This design was employed to capture the aspect and slope influence of the opposing hillslopes (Figure 2.1). Surveys were conducted bi-monthly during 2010. Treeline was also monitored using time-lapse photography. A waterproof handheld digital camera (Pentax Optio WS 80) was mounted in a bird-house on the Treeline unshielded precipitation gage facing north. The camera was set using interval shoot mode to take one photograph every hour. Batteries and data storage were maintained by visits to the site every ten days throughout the snow season. A video of these images can be viewed at http://www.youtube.com/watch?v=etrRjmzr5UY.

The Lower Deer Point site consisted of two 300 meters transects aligned with the cardinal directions (Figure 2.2). This design attempts to capture a range of forest canopy and vegetation influences found in the vicinity of the weather station. The west end of the transects are located on a ridge top clearing, while the center and east end of the site include areas of 80% canopy cover and thick vegetation. Surveys were conducted bi-monthly during 2010.

The Upper Dry Creek site is located at the highest elevation in DCEW (approx. 2100 m). This sampling design for this site consisted of three linear transects along elevation contours (Figure 2.3). This design was selected as the safest and most efficient method to obtain a large amount of samples and characterize the highest elevation and presumably the greatest and most persistent SWE in the basin. This survey was conducted 5 times during 2010.

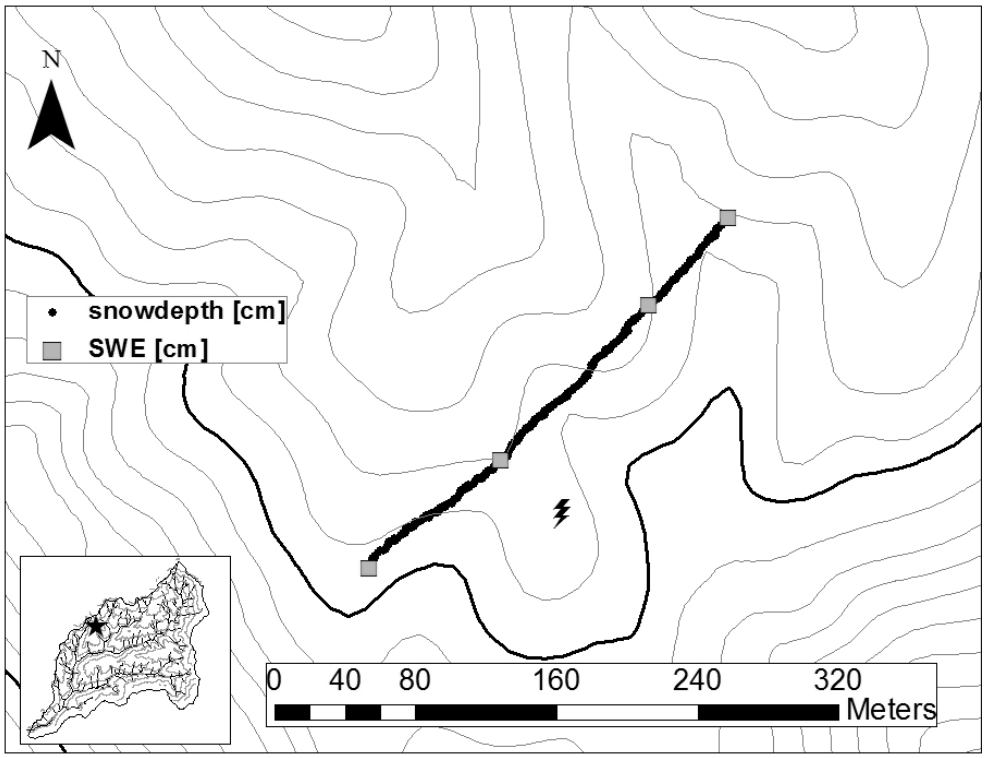


**Figure 2.1** Treeline Site 1 meter spaced snow survey transects.

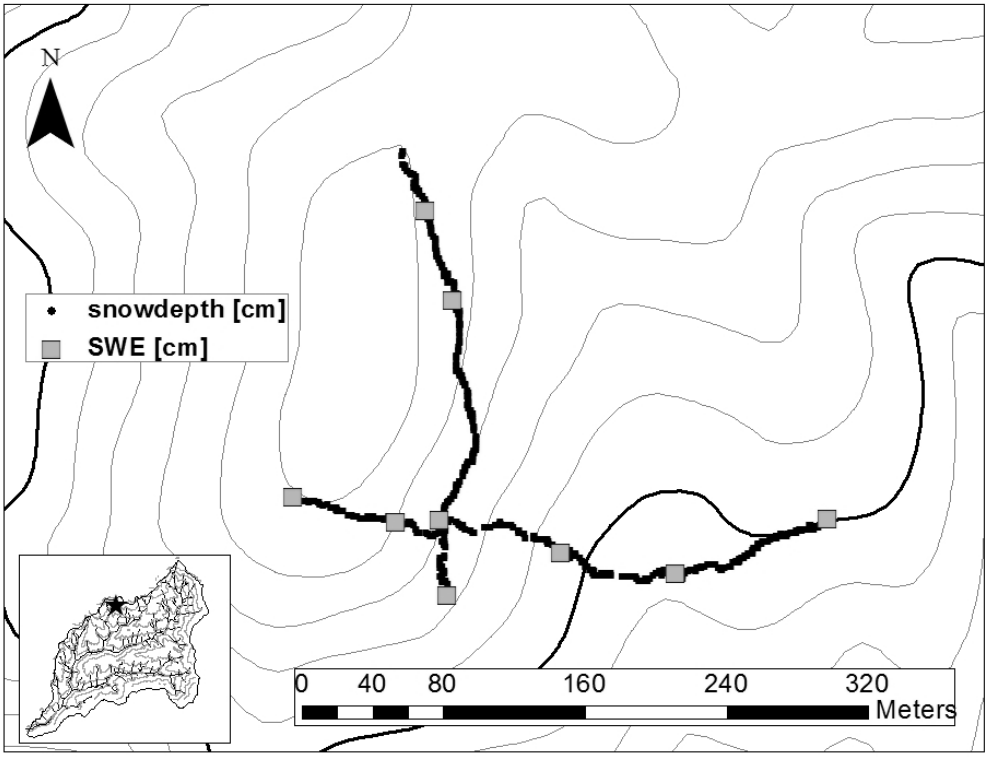


**Figure 2.2** Lower Deer Point Site 1 meter spaced snow survey transects.

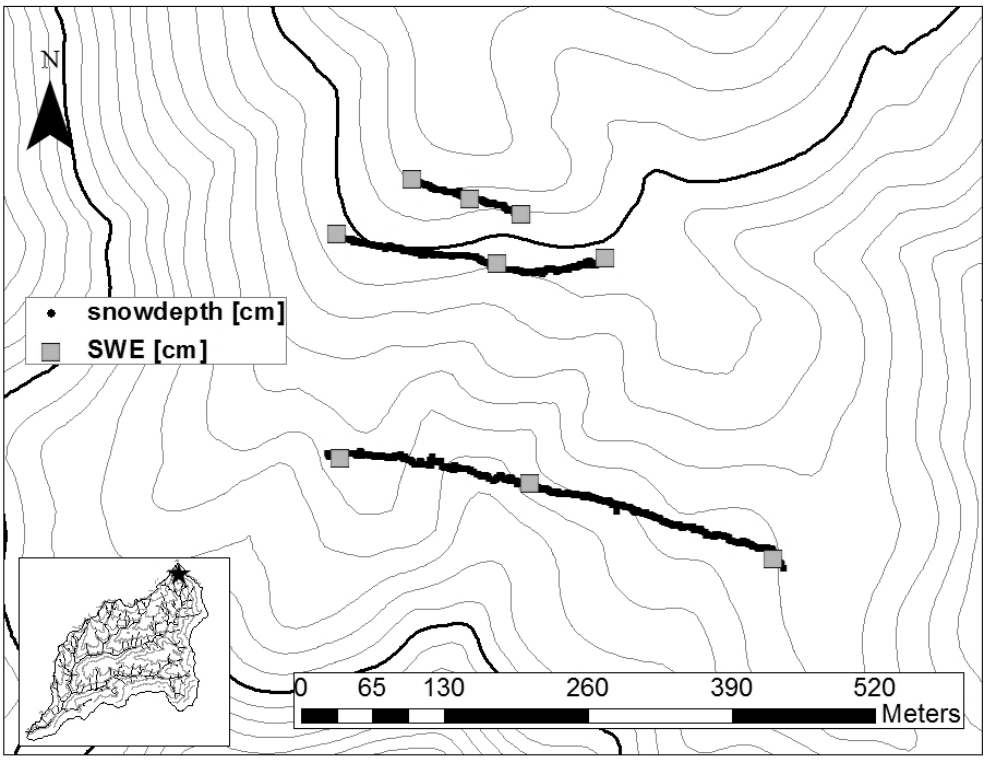


**Figure 2.3** Upper Dry Creek Site 1 meter spaced snow survey transects.

2.3.2 SNODAS Pixel Scale (1 $km^2$)

A gridded 1 km x 1 km survey was aligned with a SNODAS modeling pixel and conducted near the Lower Deer Point site. The 1 $km^2$ pixel covered an array of vegetation types and densities, a variety of slope angles, nearly all aspects, and an approximately 200 meter elevation gradient. The northern portions of the pixel are higher in elevation and more north facing, while the southern portions of the pixel are lower in elevation and more south facing.

The considerations for this survey were that: 1. it was possible to complete with a 6-person field crew in 1 day, 2. it adequately covered the 1 $km^2$ area, and 3. it was suitable for geostatistical analysis with variograms. The 1 $km^2$ survey consisted of 6 east-west 1000 meter transects, separated by 170 meters each. The initial survey in

January consisted of only one measurement every 20 meters along each transect and 1 SWE measurement at the ends and mid-point of the transects. To better accommodate analysis and obtain more samples, the strategy was altered for the remaining three surveys. Along each transect, 5 depth measurements in a cross pattern were made every 20 meters instead of just one, and a north-south portion was also surveyed in between transects. This resulted in a snake-like pattern shown in Figure 2.4. This design resulted in 1750 depth measurements and 18 SWE measurements spaced over the entire $1km^2$. This survey was conducted 4 times throughout the 2010 winter.

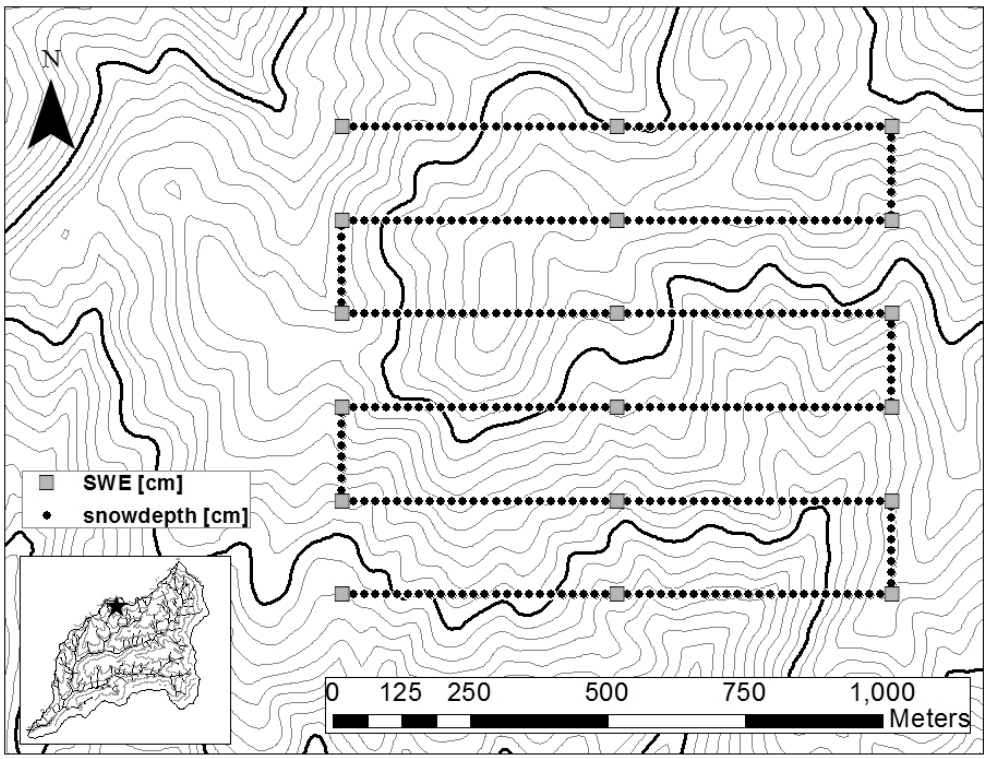


**Figure 2.4** Lower Deer Point 1 km2 scale snow survey transects.

2.3.3 Small Watershed (27 $km^2$) Scale

Watershed scale snow surveys were conducted in mid-March 2009 and 2010 at multiple locations, many of which are too remote to routinely access for regular sampling (Figure 2.5). For this approach, 35 different 50 meter long transects were selected using a DEM. SWE samples were collected at three locations along the transect (endpoints and middle) and snow depth samples were taken every 2 meters. The transect locations and orientations were designed to capture an array of elevations and aspects across the northern portion of the Dry Creek basin with the goal of capturing the range of SWE values present at assumed maximum accumulation.

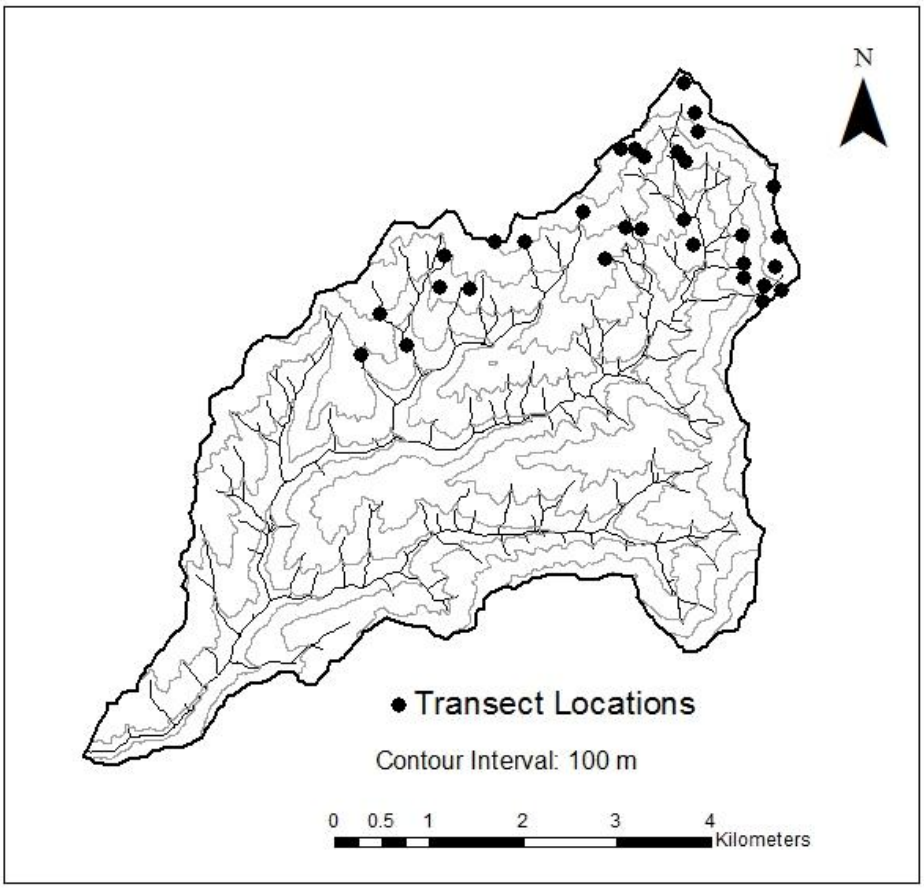


**Figure 2.5** Watershed scale snow survey transects locations.

## 2.4 Influencing Variables

Several topographic and vegetation influencing variables considered to be important controlling factors for the spatial distribution of snow were obtained and evaluated for the presence of correlations with snow depth. Topographic indices were mainly derived from a LiDAR derived digital elevation model (DEM) with a pixel resolution of 1 $m^2$ that was acquired specifically for DCEW. Because this LiDAR DEM did not cover some areas where snow surveys were conducted (northwest portions of the 1 $km^2$ pixel survey fell outside the boundaries of DCEW and were not available in this DEM), a 10 $m^2$ resolution DEM from the USGS National Elevation Dataset was also employed to derive indices.

### 2.4.1 Elevation

Elevation is an important control on snow spatial distribution. Precipitation and temperature are controlled by elevation (Figures 1.2 and 1.3) and SWE is directly influenced by elevation gradients within the basin. Elevation values for each snow depth survey location were derived directly from the DEM.

### 2.4.2 Aspect

Aspect is the compass direction that a hillslope faces. Aspect can influence SWE during both accumulation and ablation. Wind can preferentially deposit more snow on a leeward aspect and scour snow from a windward aspect. Aspect also influences snowmelt by affecting solar radiation inputs. In the Northern Hemisphere, south-facing aspects receive more solar radiation than north-facing aspects due to the position of the sun. Aspect was extracted using ARC GIS Spatial Analyst Extension, Aspect calculation tool.

Aspect values were transformed using the cosine function to correspond with north and south. For example, Cosine 180=-1, and Cosine 360=1.

2.4.3 Slope

Slope is the steepness or elevational gradient of a hillslope. Slope influences snowmelt by affecting solar radiation inputs. Steeper slopes result in more direct incidence angles for direct beam solar radiation. Slope also influences redistribution of snow via avalanches; however, avalanches are not widespread in DCEW. Minor sloughing and wet slides do occur near the Upper Dry Creek site, but the influence of this on SWE distribution is considered minimal. Slope was extracted using ARC GIS Spatial Analyst.

2.4.4 Northness

Northness is an index intended to capture the influence solar radiation by combining slope and aspect. It has been employed by several other studies concerning snow spatial distribution (Molotch and Bales 2005, Veatch *et al*., 2009). Northness is a single parameter that relates to the relative amount of incident solar radiation on a sloped surface. Northness is calculated as: cos(aspect)sin(slope) in radians. Northness ranges from -0.5 to 0.5 where steeper more south-facing slopes are closer to -0.5 and flatter north-facing slopes are closer to 0.5.

2.4.5 Vegetation

Vegetation interacts with a snowpack by becoming partially or fully buried under the snow. In this study, the investigation of the effects of vegetation on SWE is limited to the influence of forest canopies and their role in the interception of snowfall and solar radiation through the canopy. Forest canopy density influences both accumulation, via

canopy interception, and melt via affecting the snow energy balance. Forest canopy density values were obtained from the National Land Cover Dataset (NLCD) (USGS, 2007). NLCD is 30 $m^2$ resolution and derived from Landsat data. Forest canopy density data are primarily used to explore snow-canopy relationships at the Lower Deer Point transect and 1 $km^2$ scale site but are also used in the Upper Dry Creek and basin wide data analysis as well. Because the NLCD is projected on a 30 $m^2$ grid, some values are underrepresented in transect scale comparisons.

### 2.4.6 Wind Exposure

Wind effects snow distribution by preferentially depositing snow in areas sheltered from wind and scouring areas exposed to wind. A directional wind exposure index was calculated from a digital elevation model based on the approach of Lapen and Martz (1993), and Anderton *et al*. (2004). The exposure index was calculated using ARC GIS Spatial Analyst, Neighborhood toolset. The Focal Statistics tool was used to calculate average elevation of a 35-meter radius wedge shaped region in a NW azimuth (270-360˚, the dominant wind direction during 2010) from the cell of interest. The Focal Statistics field was then subtracted from the elevation field to calculate the wind exposure index. The result is a raster dataset that is negative for areas sheltered by upwind topography and positive for areas exposed to wind. Several different azimuth values based on dominant wind direction were used, as well as an average of all azimuths. It was found that 35-meter radius and a NW azimuth provided the highest correlation values for snowdepth.

# CHAPTER 3: ANALYSIS

## 3.1 Variogram Analysis

### 3.1.1 Experimental Variogram

The occurrence of snow on the landscape is the result of numerous physical processes interacting simultaneously. Some of these interactions occur in chaotic, non-linear fashion as though the variation on snow distribution across the landscape may be random. In reality, this distribution is the result of multiple interactions between phases of accumulation, redistribution, and ablation; however, if we treat snow distribution at a given scale as a random process, geostatistics offers a useful approach to quantitatively describe the length scale at which variability occurs and may provide the ability to make predictions and estimates of uncertainty of values at locations that have not been sampled. The semivariogram is often used for this purpose and can be calculated as:

$$\gamma(h) = \left( \frac{1}{2N(h)} \right) \cdot \sum_{i=1}^{N-h} (z_i - z_{i+h})^2 \qquad (2)$$

where $\gamma(h)$ is the semivariance at lag distance h, N is the number of pairs of points at a given lag spacing, and z is snow depth (cm) (Webster and Oliver, 2001). The experimental variogram provides information about the variance of sample data from a population in relation to the separation distance of observations. To understand the

characteristics of the population, the experimental variogram is then used to fit the modeled variogram, which can be used to predict values at unmeasured locations using kriging.

### 3.1.2 Characteristics of the Variogram

The variogram can provide information about the spatial organization of the dataset and there are several characteristics of interest that are used to describe this organization shown in an example in Figure 3.1. The *sill* is the upper bound of the variance, which is the *a priori* variance of the process. If the sill is reached at a finite lag distance, the variogram has a *range,* also known as the *correlation range.* The range is the distance at which autocorrelation becomes zero and indicates the limit of spatial dependence of the process being investigated. The *nugget* is the characteristic of a variogram where as lag distance approaches zero the variance approaches some positive value indicated by the presence of a y-intercept. Nugget variance is an indicator of sampling error or variation that occurs at lengths shorter than the sampling distance.

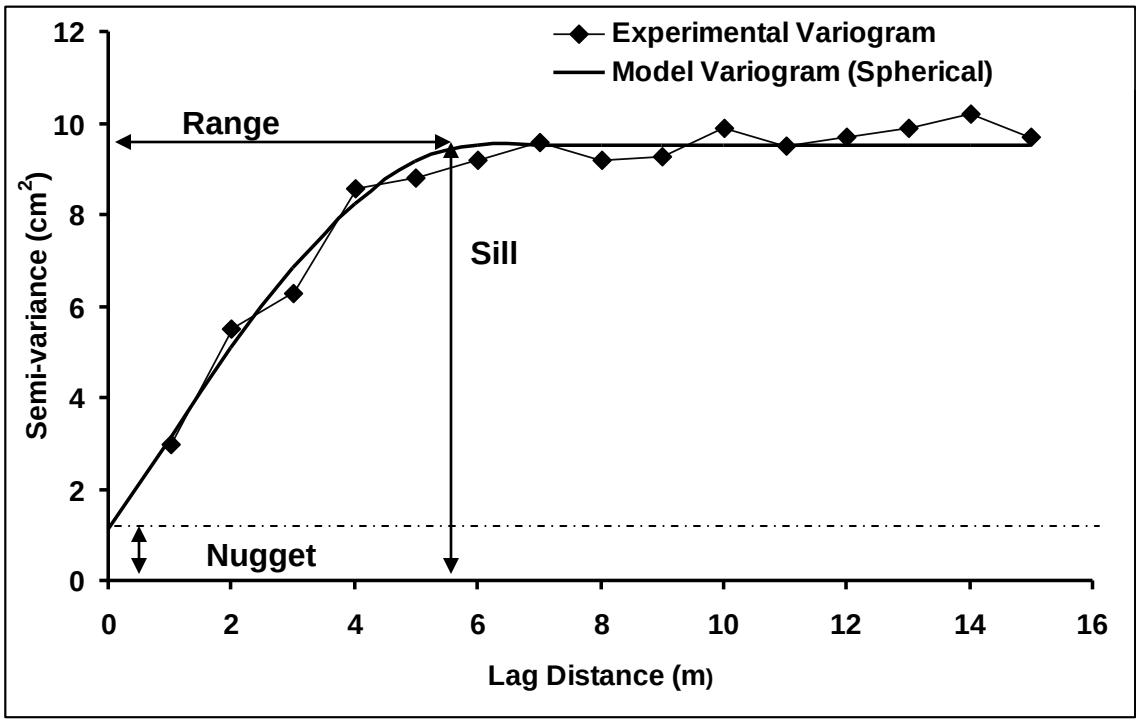


**Figure 3.1** Example variogram showing characteristics of the variogram and example model

3.1.3 Variogram Models

Several mathematical functions have been used to model the variogram. Typical functions used to model the variogram include the bounded linear, exponential, and spherical.

The bounded linear model is the simplest variogram function and consists of two straight lines, one diagonal line extending from the origin or nugget and one horizontal line that exists when only when there is a range and sill at a defined lag. The bounded linear model is written as:

$$\gamma(h) = \begin{cases} c\left(\frac{h}{a}\right) & \text{for } h \le a, \\ c & \text{for } h > a, \end{cases} \qquad (3)$$

where $c$ is the sill variance and $a$ is the range.

The spherical variogram model uses the equation for the volume of a sphere to calculate the portions of the variogram at lags less than the range. The spherical model is written as:

$$\gamma(h) = \begin{cases} c\left\{\frac{3h}{2a} + \frac{1}{2}\left(\frac{h}{a}\right)^3\right\} & \text{for } h \le a, \\ c & \text{for } h > a, \end{cases} \qquad (4)$$

The exponential model asymptotically approaches the sill and the range is a distance at which equals 95% of the sill variance. The exponential model is written as:

$$\gamma(h) = c\left\{1 - \exp\left(-\frac{h}{r}\right)\right\}, \qquad (5)$$

where r is a distance parameter that defines the spatial extent of the model.

All three models were computed for each variogram dataset; however the spherical models showed the best fit to the experimental data, and thus the following results only show the spherical models.

### 3.1.4 Variogram Model Parameter Uncertainty

Estimates of uncertainty in the variogram were computed using a bootstrap monte-carlo procedure coded in MATLAB. The same number of observations as the original dataset was extracted from the original dataset with replacement using a random number generator and the variogram and spherical model were recalculated and fit. This process was repeated 50 times for each dataset and the resulting parameters were evaluated at the 95% and 5% quantiles. The 90% confidence interval of the parameters indicates how stable the resulting parameter estimates are.

## 3.2 SNODAS Model Evaluation

The SNODAS modeling framework provides daily estimates of SWE for the Continental United States with 1 $km^2$ resolution. SNODAS is a physically based energy balance snow accumulation and melt model, coupled with a data ingestion/quality control/downscaling routine and data assimilation routine. The snow model is the main component of the system and is forced with downscaled data from the RUC2 numerical weather prediction model. The model uses a mathematical approach of Jordan (1991) to solve the snow energy balance described in detail below. The downscaled forcing data includes temperature, wind, relative humidity, pressure, and precipitation. The model is updated with an array of satellite and ground-based observations of SWE (including SNOTEL sites) and snow covered area with an assimilation routine, which uses 'nudging' or simple Newtonian relaxation procedure to steer the model toward more accurate predictions. The nudging procedure involves differencing estimated and observed value fields to create nudging fields. The model is re-run and nudged with updated nudging fields (Barrett, 2003).

The NOHRSC website includes an interactive mapping feature that provides model estimates and observational data from weather stations throughout the country. The Lower Weather, Treeline, Lower Deer Point, and Bogus Basin SNOTEL weather stations are available via this interface and observed versus modeled values for temperature, relative humidity, and wind speed can be compared.

3.2.1 Snow Surface Energy Balance

SNODAS simulates the physics of snow accumulation and ablation using the snow surface energy balance equation. Snowmelt can be modeled as the sum of energy fluxes into and out of the snowpack which can be written as:

$$\Delta Q = (S\downarrow - S\uparrow) + (L\downarrow - L\uparrow) + Hs + Hl + Hp + G \qquad (6)$$

where ΔQ is the change in snowpack internal energy, S is shortwave radiation, L is longwave radiation, Hs is sensible heat, Hl is latent heat, Hp is heat from precipitation, and G is ground heat flux. All terms have units of [E $L^{-2}$ $T^{-1}$]. Because these fluxes are not measured at every grid cell within the model, they are parameterized using the approach of SNTHERM.89 (Jordan, 1991) and forced using downscaled forcing data from RUC2 (Barrett, 2003) and potentially other numerical weather predictions models.

### 3.3 Potential Irradiance Theory

In complex terrain, differential ablation often occurs as the result of differential solar radiation inputs. Potential incoming solar radiation is calculated based on the theory put forth by Lee (1963), and Frank and Lee (1966). Potential irradiation theory allows for estimates of incoming solar radiation based on latitude and time of year. Following the approach of DeWalle and Rango (2008), Instantaneous potential solar radiation, $I_S$, and can be calculated from:

$$I_S = (I_0 / e^2)\cos Z \qquad (7)$$

where $I_0$ is the solar constant, e is the radius vector, and Z is the zenith angle. Zenith angle can be computed from the equation:

$$\cos Z = (\sin\theta \sin\delta + \cos\theta \cos\delta \cos\omega t) \qquad (8)$$

where θ is the latitude, δ is the solar declination, and ωt is the hour angle. The hour angle is the product of the Earth's angular velocity (typically 15º/hr) and the time, *t* before or after solar noon.

These estimates can be modified for sloping terrain with the addition of slope and aspect values and by finding an "equivalent horizontal surface" that would receive radiation at the same angel as the slope. Irradiation of an equivalent horizontal surface, $I'_S$, can be calculated as:

$$I'_s = (I_0 / e^2)\cos Z' = (I_0 / e^2)[\sin\theta' \sin\delta + \cos\theta' \cos\delta \cos\omega t'] \qquad (9)$$

where Z' is the angle between the solar beam and a line perpendicular to the slope, θ', is the latitude of the equivalent horizontal surface, which is calculated as:

$$\theta' = \arcsin[\sin k_S \cos(h)\cos\theta + \cos k_S \sin\theta] \qquad (10)$$

where $k_s$ is the slope inclination angle, h is the slope azimuth (degrees clockwise from north), ωt' is the hour angle of the equivalent horizontal surface, which is calculated as:

$$\omega t' = \omega t + a \qquad (11)$$

where a is the difference in longitude between equivalent horizontal surface and slope, and is calculated as:

$$a = \arctan[(\sin(h)\sin k_S)/(\cos k_S \cos\theta - \cos(h)\sin k_S \sin\theta)] \qquad (12)$$

The total daily potential solar irradiation can then be computed by integrating the equation from sunrise to sunset. These computations were made for a 171m x 156 m grid cell encompassing the Treeline site. The slope and aspect values for the computations were derived in ARC map from a 1 meter resolution LiDAR DEM of the watershed. Total accumulated potential solar irradiation was computed at hourly intervals for a ten day increment over 1 meter grid cells within the study site

# CHAPTER 4: RESULTS

## 4.1 SNODAS Model Evaluation

SNODAS was evaluated against observed SWE data at each scale of measurement using data obtained from NOHRSC (2010). Due to the effort required, 1 $km^2$ scale measurements were only made at the Lower Deer Point Site. It is possible that the comparisons of transect scale measurements with SNODAS do not agree because of differing spatial extent. Transect scale comparisons are made acknowledging that observations are limited to smaller regions within a pixel. SNODAS consistently underpredicted SWE at Treeline Site (Figure 4.1) and Lower Deer Point Site (Figure 4.2, 4.3), while it overpredicted late season SWE at the Upper Dry Creek Site (Figure 4.4). Model performance was poorest at the Lower Deer Point site and best at the Upper Dry Creek Site (Table 4.1, 4.2). The 1 $km^2$ scale surveys at Lower Deer Point agreed with the transect scale underprediction of SWE, though greater variability was encountered at the larger scale. Basin wide surveys from both 2009 and 2010 (Figure 4.5) indicated an underprediction of SWE by SNODAS during both years; however, SNODAS did well at capturing the dominant source of variability at the basin scale: the trend of increasing SWE with elevation (Figure 4.6, 4.7).

SNODAS predictions for Treeline underpredicted SWE by between 2-9 cm. SNODAS completely melted all snow from the pixel two times prior to observed total ablation out in late March. SNODAS snow depth values were underpredicted for all sampling events except one sampling event during February (Figure 4.8). Modeled snow

density values diverged from measured snow density during the second sampling event as the model completely melted out the pixel (Figure 4.9). Treeline exhibited patchy snow by mid-February and complete melt out by late March; however, several late season storms produced intermittent snow at this site well into April.

SNODAS predictions for Lower Deer Point included both the transect scale sampling campaign and the 1km$^2$ pixel scale sampling campaign. Both data sets indicated an underprediction of SWE by SNODAS of between 5-25 cm. The 1 km$^2$ data indicate a consistent underprediction of snow depth and a gradually increasing underprediction of snow density throughout the season (Figures 4.10, 4.11). The transect scale data also indicate a consistent underprediction in snow depth and a gradual divergence in snow density throughout the season (Figures 4.12, 4.13). The 1 km$^2$ pixel scale sampling campaign was designed to capture the scale of the model grid cell and determine the true mean SWE for the pixel. It was found that measurements of the transect scale mean SWE and the pixel scale mean SWE were similar during the first two sampling events; however, the pixel scale mean SWE was roughly 10 cm lower than the transect scale mean SWE during the final two sampling events. Snowmelt at the lower elevation and south-facing portions of the 1 km$^2$ pixel during March and April were responsible for this difference.

Upper Dry Creek SNODAS predictions differed from the other sites in that SNODAS SWE was relatively close to observed SWE except during the final sampling event when SNODAS overpredicted SWE by approximately 14 cm. SNODAS modeled snow depth was consistently overpredicted as compared to field measurements, while modeled snow density was consistently underpredicted by the model (Figure 4.14, 4.15).

This resulted in relatively accurate SWE values except during the final sampling event when the model accurately captured snow density and snow depth was still overpredicted, causing an overall overprediction in SWE.

SNODAS snow density values for all study sites were unrealistically low when compared to measured snow density. Measured snow density values were relatively consistent across elevation gradients and increased linearly with time of year. As the season progressed, the snowpack settled and compacted at all study sites. Snow density increased from roughly 200 kg/m$^3$ to 400 kg/m$^3$ by the end of the season. This increase in snow density with time is represented by the model at Lower Deer Point and Upper Dry Creek, but snow density values are consistently lower than measured values. The model significantly underpredicts snow density at the Treeline site and complete melt out of the pixel causes snow density values to unrealistically decrease throughout the season.

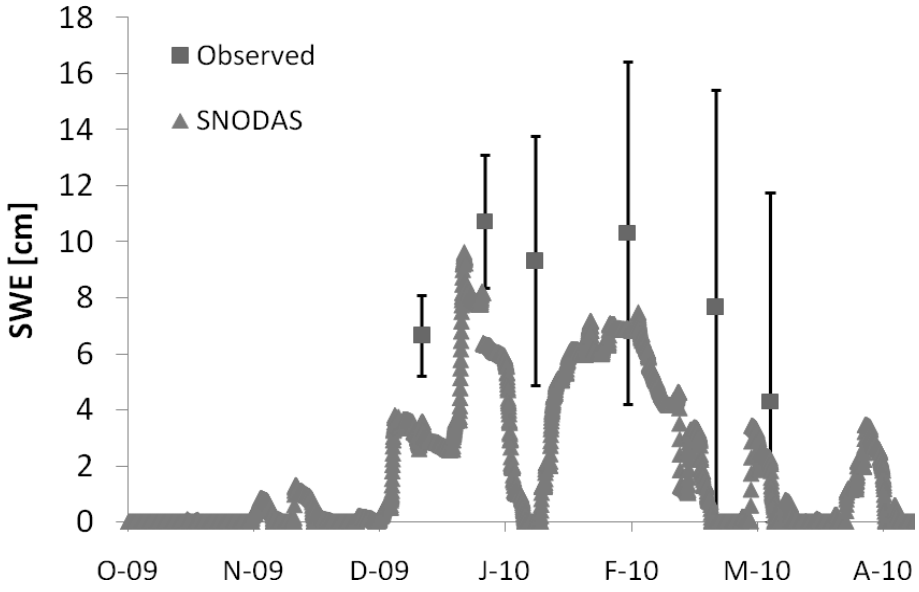


**Figure 4.1** Snow survey results and SNODAS model predictions for Treeline site.

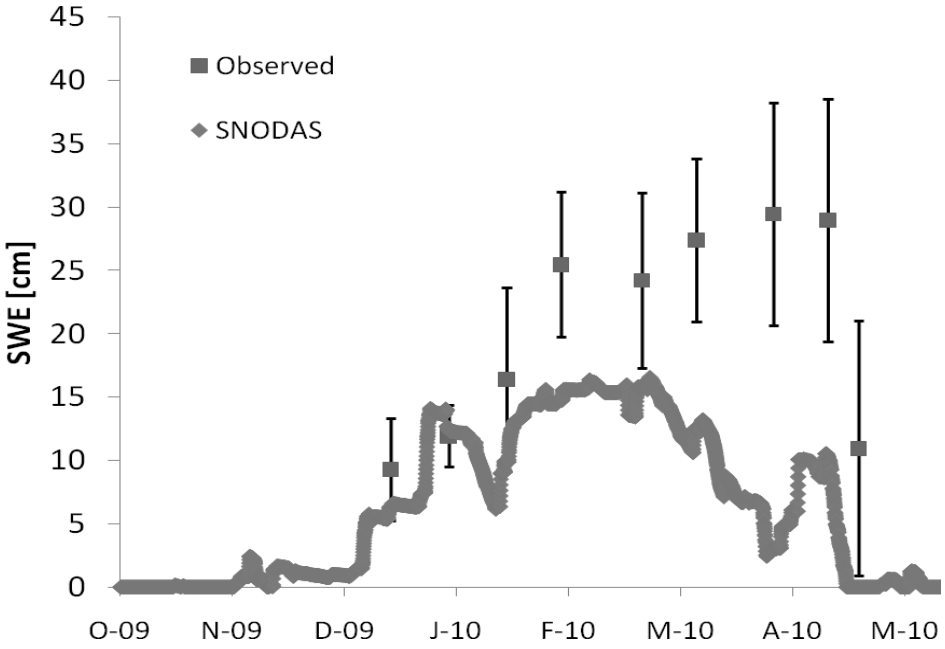


**Figure 4.2** Snow survey results and SNODAS model predictions for Lower Deer Point site.

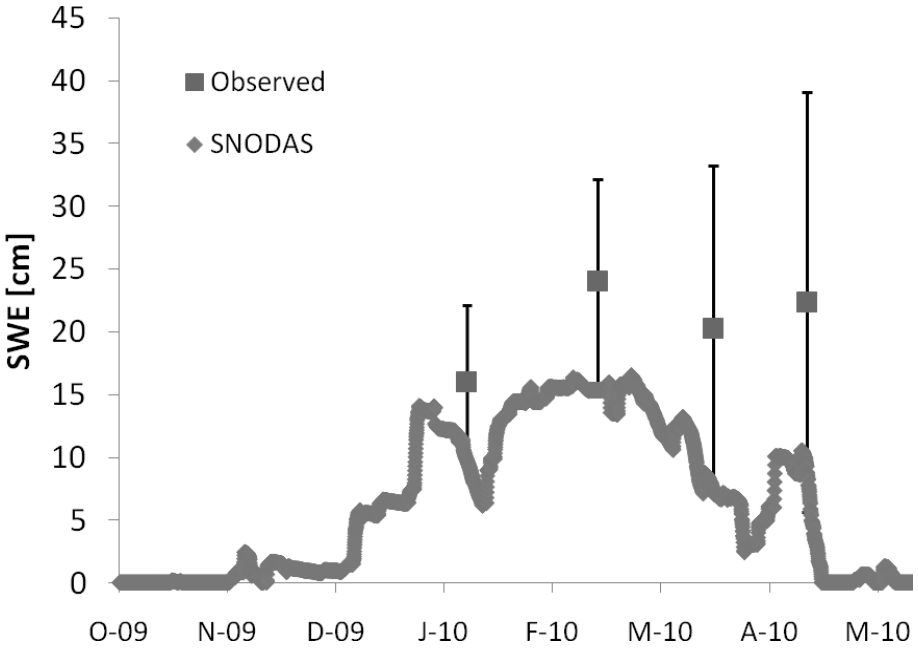


**Figure 4.3** Snow survey results and SNODAS model predictions for the Lower Deer Point 1km$^2$ SNODAS pixel scale survey.

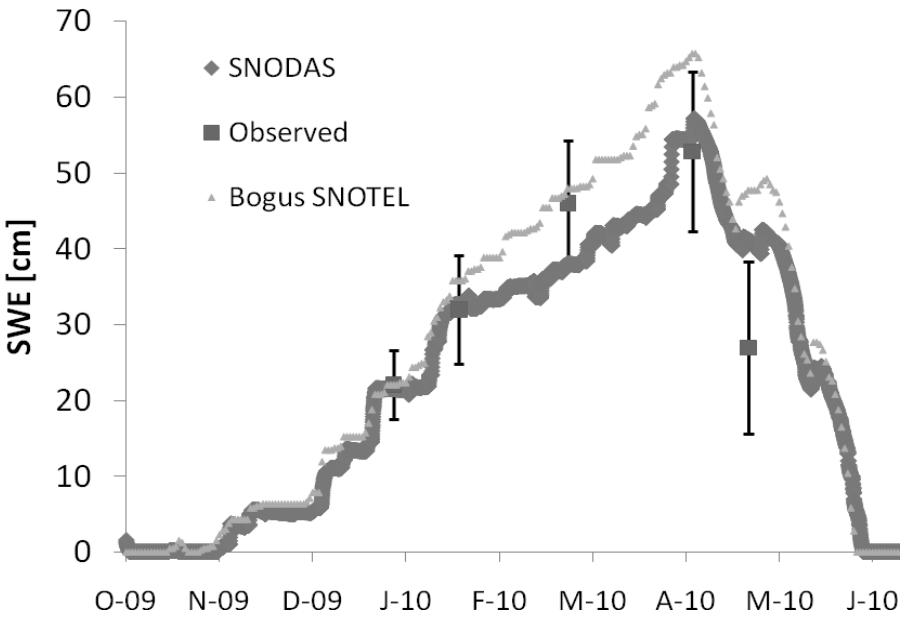


**Figure 4.4** Snow survey results and SNODAS model predictions for Upper Dry Creek site. Also shown is the nearby Bogus Basin SNOTEL snow pillow values that are routinely assimilated into the model.

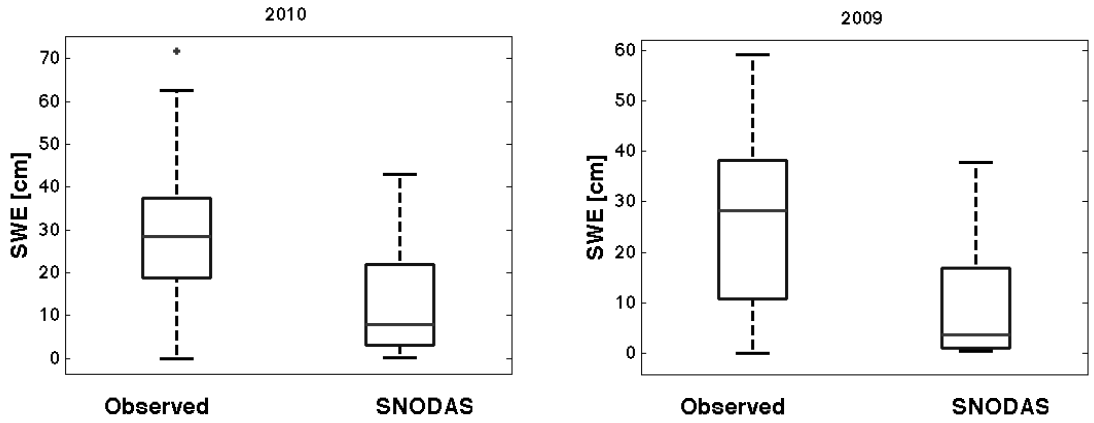


**Figure 4.5** Snow survey results and SNODAS model predictions for basin wide surveys conducted during 2009 and 2010.

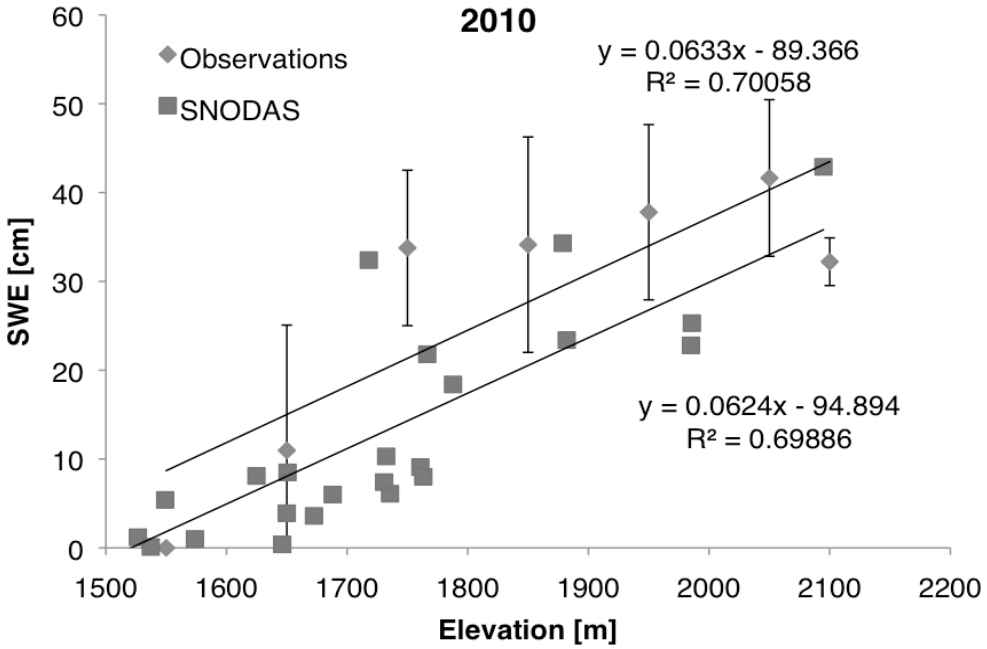


**Figure 4.6** March 21, 2010 Basin-wide snow survey results and SNODAS model predictions for all model pixels covering DCEW. Observations are averaged over 100 meter elevation bins. Error bars are one standard deviation.

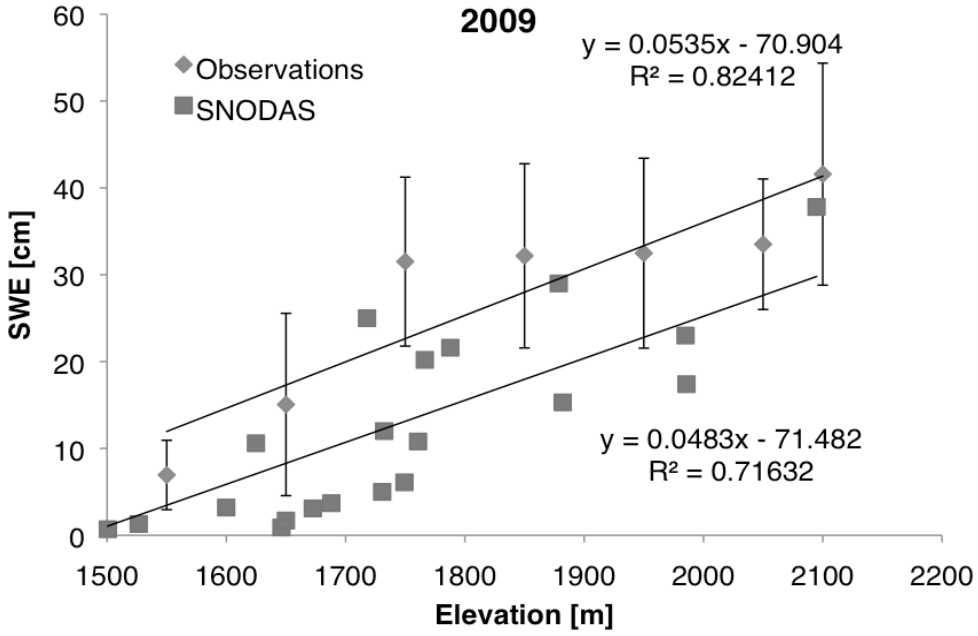


**Figure 4.7** March 16-18, 2009 Basin-wide snow survey results and SNODAS model predictions for all model pixels covering DCEW. Observations are averaged over 100 meter elevation bins. Error bars are one standard deviation.

**Table 4.1** 1 $km^2$ pixel scale modeled and observed snow properties

| Date | SNODAS SWE [cm] | SNODAS Depth [cm] | SNODAS Density [kg/m3] | Avg Measured SWE [cm] | Avg Measured Depth [cm] | Avg Measured Density [kg/m3] |
|---|---|---|---|---|---|---|
| 1/15/10 | 9.4 | 34.05 | 276 | 15.68 | 56 | 286 |
| 2/19/10 | 15.39 | 55.73 | 276.1 | 24 | 78 | 308 |
| 3/22/10 | 7.04 | 25.17 | 279.8 | 19.95 | 57 | 356 |
| 4/16/10 | 7.7 | 24.33 | 316.6 | 22.39 | 53 | 422 |

**Table 4.2** Transect scale modeled and observed snow properties.

| Date/ Location | SNODAS SWE [cm] | SNODAS Depth [cm] | SNODAS Density [$kg/m^3$] | Avg Measured SWE [cm] | Avg Measured Depth [cm] | Avg Measured Density [$kg/m^3$] |
|---|---|---|---|---|---|---|
| Treeline | | | | | | |
| 12/23/09 | 3.04 | 15.02 | 202.3 | 6.7 | 31 | 213 |
| 1/7/10 | 6.31 | 22.07 | 286 | 10.8 | 39 | 276 |
| 1/19/10 | 0.23 | 1.45 | 159.8 | 9.3 | 29 | 322 |
| 2/10/10 | 6.87 | 31.98 | 214.7 | 10.3 | 32 | 318 |
| 3/3/10 | 0.0 | 0.0 | 0.0 | 7.7 | 21 | 363 |
| 3/16/10 | 0.92 | 3.41 | 269.1 | 4.3 | 11 | 385 |
| Lower Deer Point | | | | | | |
| 12/23/09 | 6.62 | 30.79 | 215.1 | 9.3 | 50 | 185 |
| 1/7/10 | 12.32 | 49.27 | 250.1 | 11.9 | 56 | 211 |
| 1/22/10 | 10.07 | 44.43 | 226.6 | 19.8 | 66 | 301 |
| 2/5/10 | 15.11 | 69.64 | 217 | 25.4 | 85 | 298 |
| 2/26/10 | 15.85 | 69.24 | 228.9 | 26.1 | 90 | 289 |
| 3/12/10 | 12.42 | 44.96 | 276.3 | 27.4 | 78 | 352 |
| 4/1/10 | 3.03 | 11.26 | 268.6 | 29.4 | 81 | 364 |
| 4/15/10 | 9.98 | 33.19 | 300.7 | 29.0 | 72 | 400 |
| 4/23/10 | 0.0 | 0.0 | 0.0 | 11.0 | 26 | 419 |

**Table 4.2 Continued** Transect scale modeled and observed snow properties.

Upper Dry Creek

| Date/ Location | SNODAS SWE [cm] | SNODAS Depth [cm] | SNODAS Density [kg/m$^3$] | Avg Measured SWE [cm] | Avg Measured Depth [cm] | Avg Measured Density [kg/m$^3$] |
|---|---|---|---|---|---|---|
| 1/8/10 | 21.51 | 91.67 | 234.6 | 22.1 | 80 | 275 |
| 1/29/10 | 32.61 | 126.21 | 258.4 | 32.0 | 106 | 302 |
| 3/5/10 | 38 | 125.91 | 301.8 | 46.0 | 120 | 384 |
| 4/14/10 | 57.16 | 166.67 | 343 | 52.8 | 130 | 405 |
| 5/2/10 | 41.09 | 117.1 | 350.9 | 27.0 | 75 | 358 |

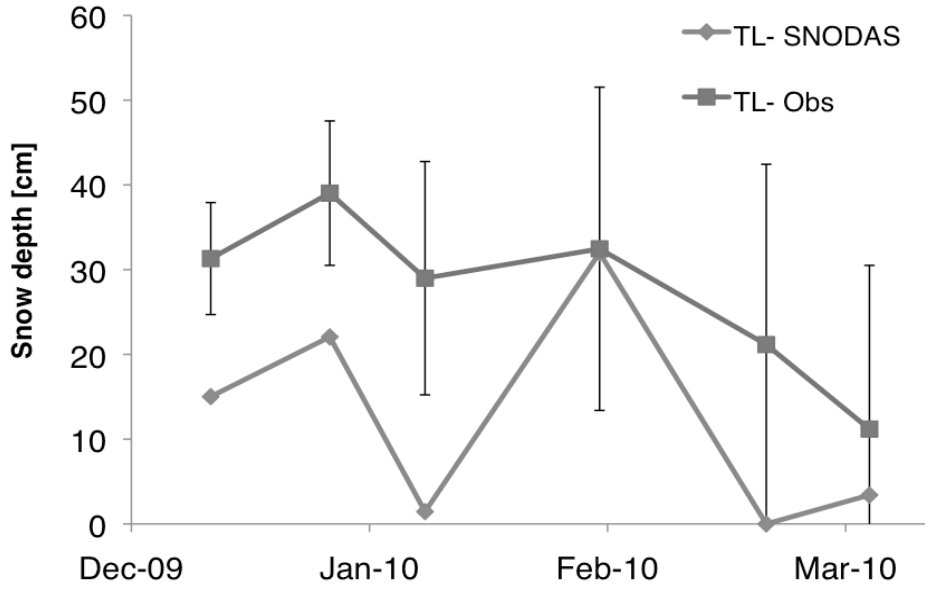


**Figure 4.8** Treeline transect scale observed and SNODAS modeled snow depth.

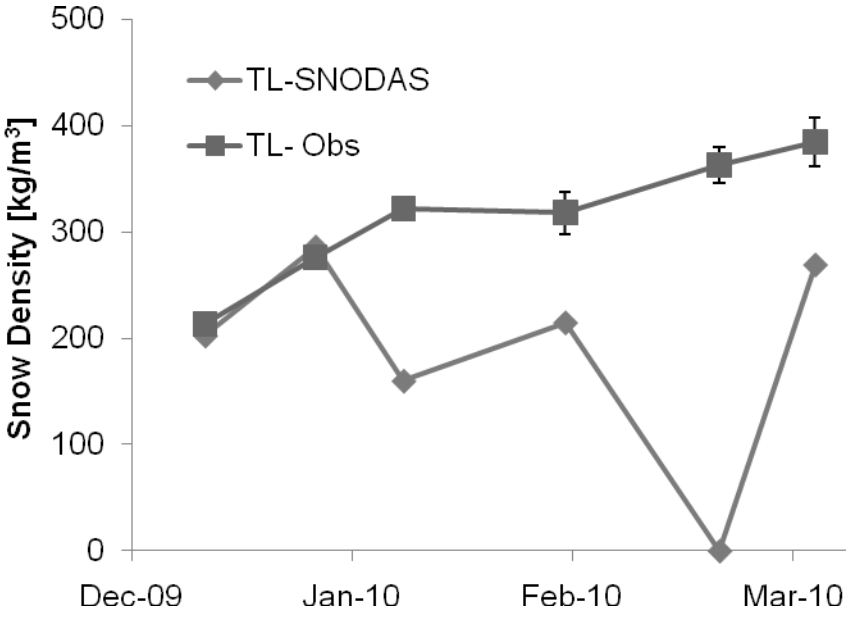


**Figure 4.9** Treeline transect scale observed and SNODAS modeled snow density.

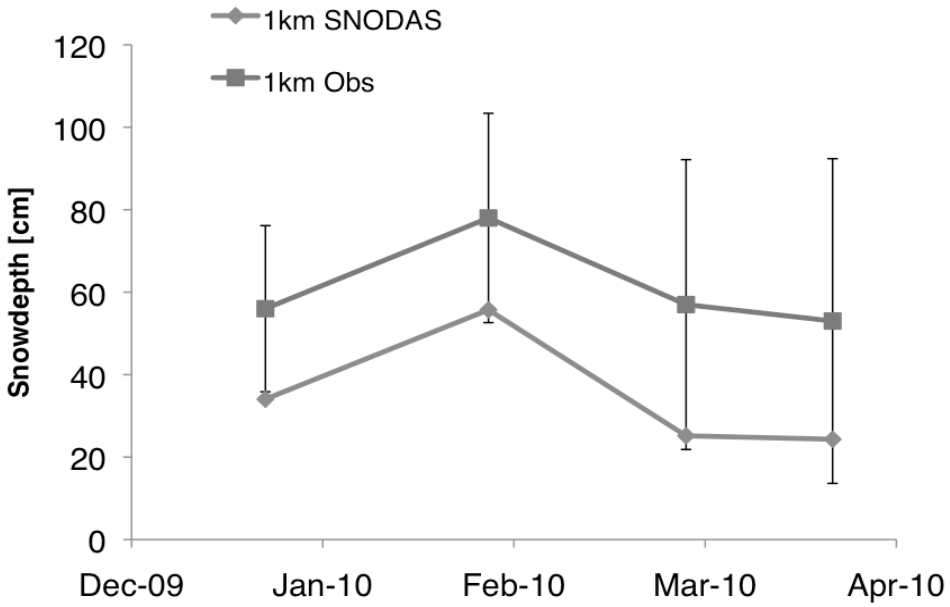


**Figure 4.10** 1 $km^2$ pixel scale observed and SNODAS modeled snow depth.

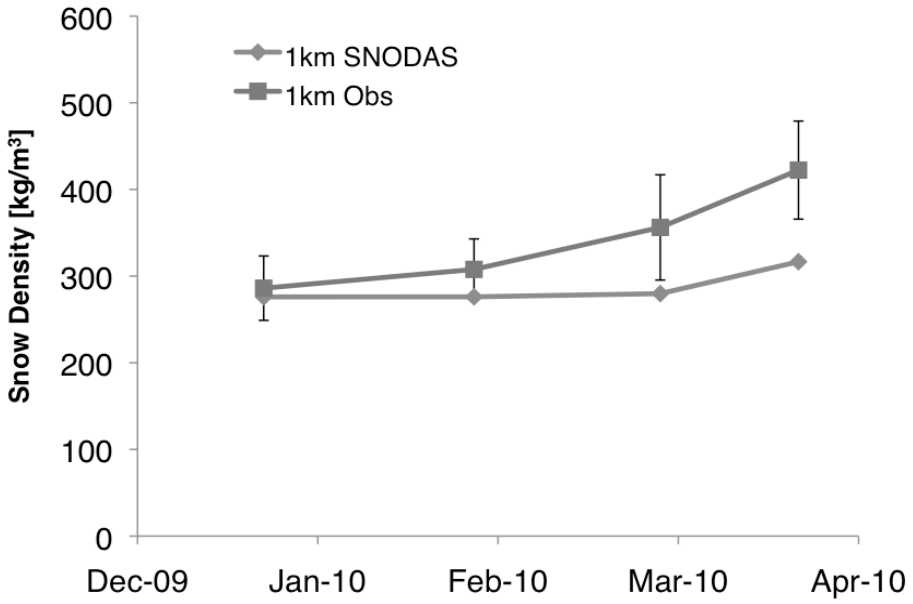


**Figure 4.11** Lower Deer Point1 km$^2$ pixel scale observed and SNODAS modeled snow density.

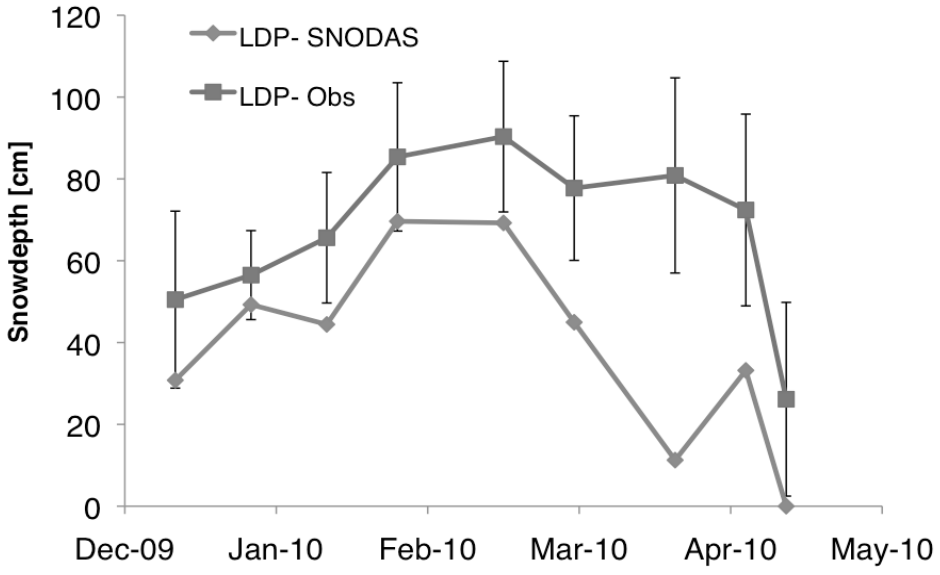


**Figure 4.12** Lower Deer Point tranect scale observed and SNODAS modeled snowdepth.

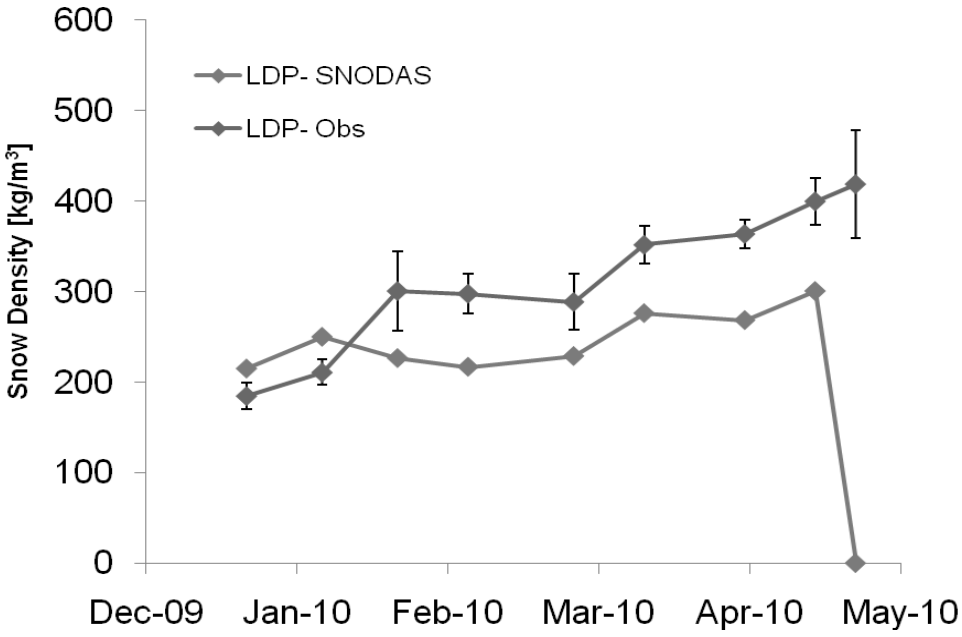


**Figure 4.13** Lower Deer Point transect scale observed and modeled snow density.

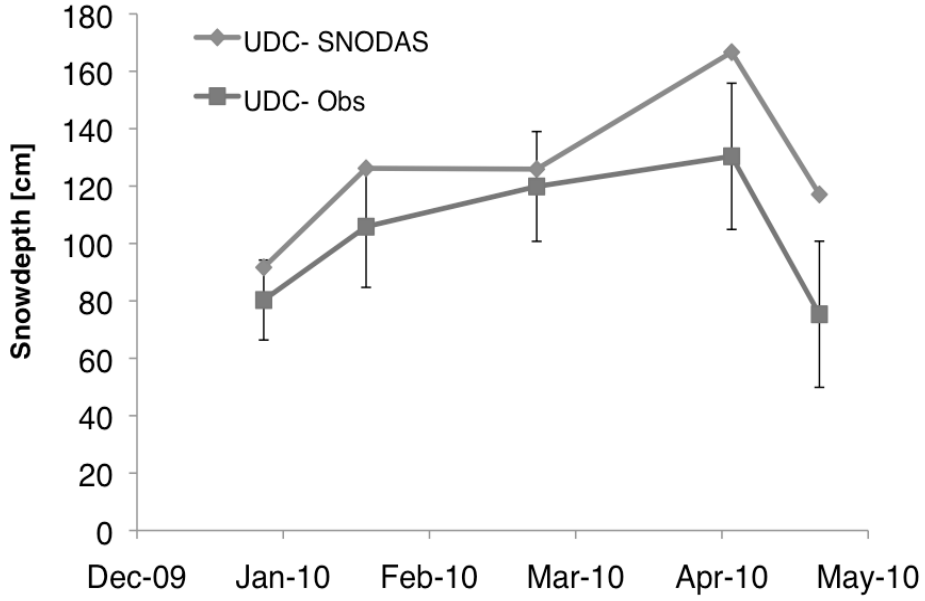


**Figure 4.14** Upper Dry Creek transect scale observed and SNODAS modeled snowdepth.

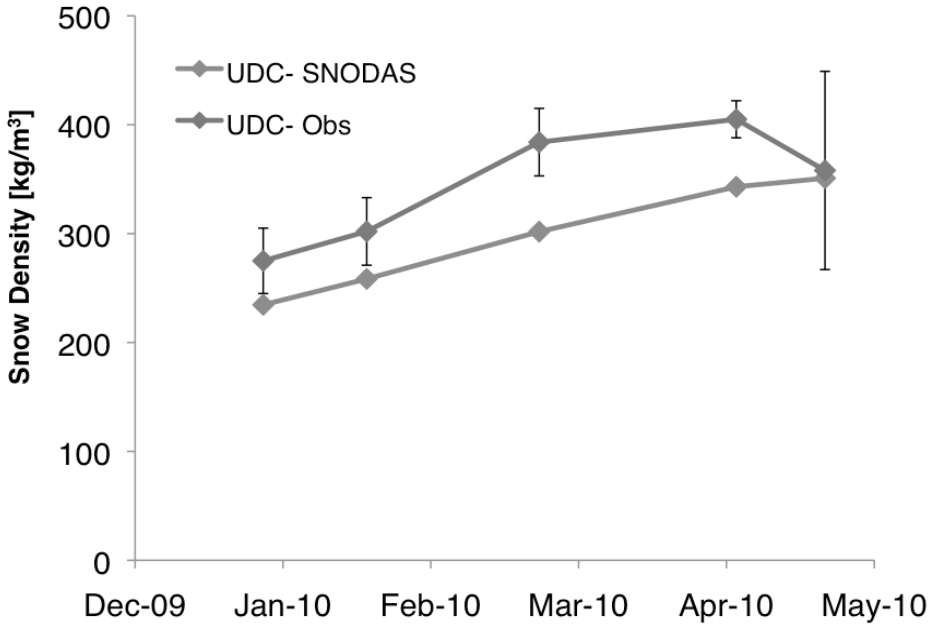


**Figure 4.15** Upper Dry Creek transect scale observed and SNODAS modeled snow density.

### 4.2 Transect Scale Snow Survey Data

Snow depth and snow density data from transects measured at Treeline, Lower Deer Point, and Upper Dry Creek during 2010 are shown in Figures 4.16-4.17. Table 4.3 and 4.4 summarize the snow depth and snow density statistics of each sampling event. Comparison of the three sampling sites indicate that elevation is the strongest control on snow depth at the watershed scale with roughly one meter more snow depth at Upper Dry Creek than Treeline during mid-March. Snow density, however, trends similarly for each site and is relatively consistent across elevation gradients.

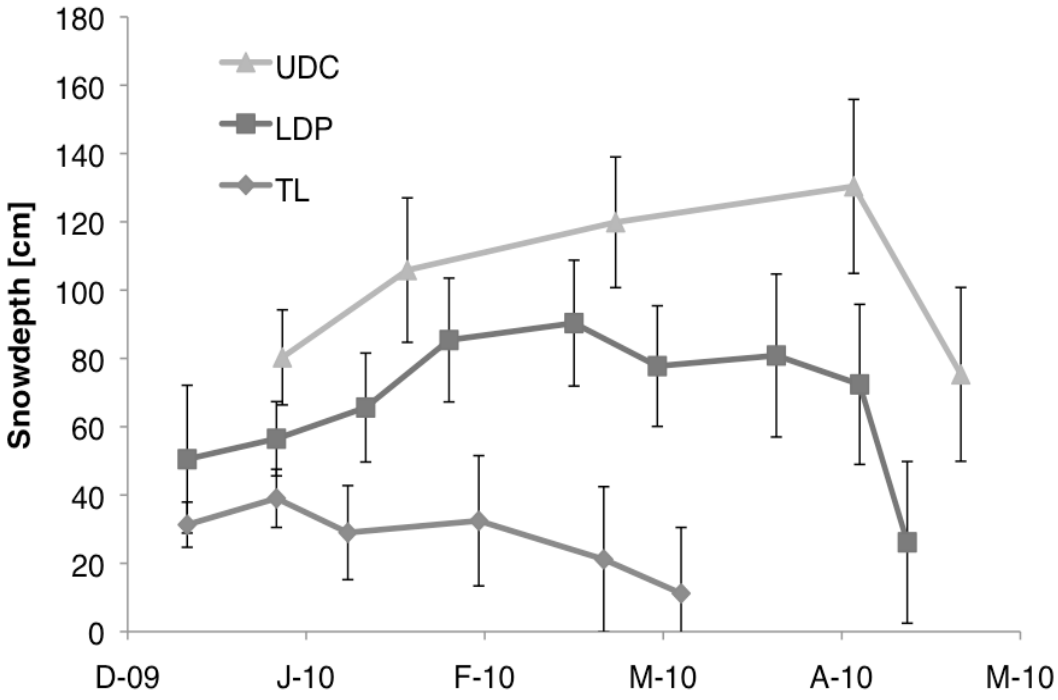


**Figure 4.16** Transect scale measured mean snow depth (symbols) and standard deviation (error bars).

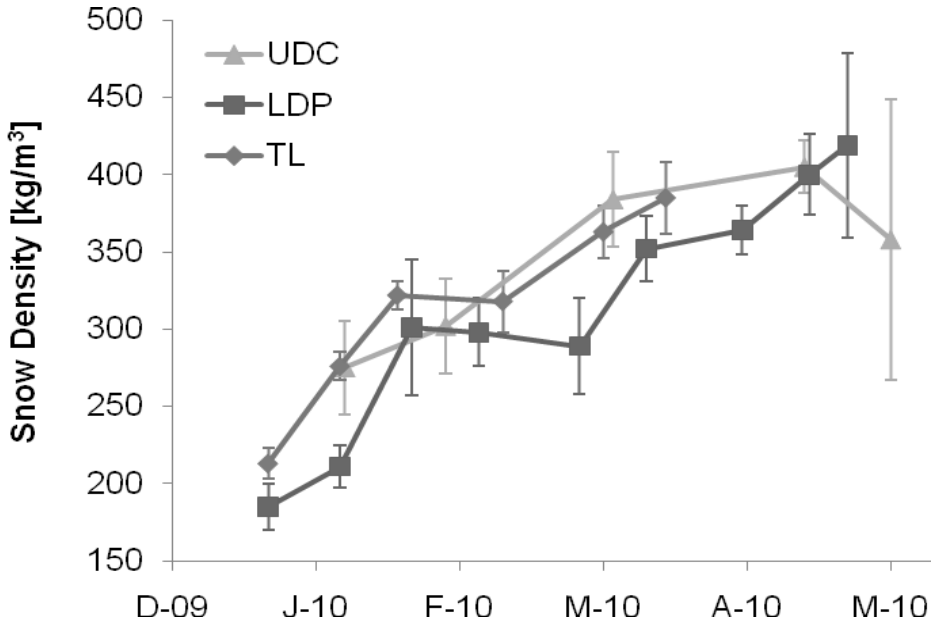


**Figure 4.17** Transect scale measured mean snow density (symbols) and standard deviation (error bars).

**Table 4.3** Transect snow depth statistics

| Date | *n* | mean [cm] | st dev [cm] | cv |
|---|---|---|---|---|
| Treeline Site | | | | |
| 12/23/09 | 299 | 31 | 7 | 0.21 |
| 1/7/10 | 728 | 39 | 9 | 0.22 |
| 1/19/10 | 302 | 29 | 14 | 0.47 |
| 2/10/10 | 704 | 32 | 19 | 0.59 |
| 3/3/10 | 687 | 21 | 21 | 1.01 |
| 3/16/10 | 703 | 11 | 19 | 1.73 |
| Lower Deer Point Site | | | | |
| 12/23/10 | 202 | 50 | 22 | 0.43 |
| 1/7/10 | 451 | 56 | 11 | 0.19 |
| 1/22/10 | 600 | 66 | 16 | 0.24 |
| 2/5/10 | 621 | 85 | 18 | 0.21 |
| 2/26/10 | 632 | 90 | 18 | 0.20 |
| 3/12/10 | 676 | 78 | 18 | 0.23 |
| 4/1/10 | 618 | 81 | 24 | 0.30 |
| 4/15/10 | 618 | 72 | 23 | 0.32 |
| 4/23/10 | 390 | 26 | 24 | 0.94 |

**Table 4.3 Continued** Transect snow depth statistics

| Upper Dry Creek Site | | | | |
|---|---|---|---|---|
| Date | *n* | mean [cm] | st dev [cm] | cv |
| 1/8/10 | 687 | 80 | 14 | 0.17 |
| 1/29/10 | 847 | 106 | 21 | 0.20 |
| 3/5/10 | 818 | 120 | 19 | 0.16 |
| 4/14/10 | 672 | 130 | 25 | 0.20 |
| 5/2/10 | 649 | 75 | 25 | 0.34 |
| avg | 595.2 | 64 | 18 | 0.42 |
| total | 11904 | -- | -- | -- |

**Table 4.4** Transect scale snow density statistics

| Date | *n* | mean [kg/m$^3$] | st dev [kg/m$^3$] | cv |
|---|---|---|---|---|
| Treeline Site | | | | |
| 12/23/09 | 3 | 213 | 10 | 0.05 |
| 1/7/10 | 3 | 276 | 9 | 0.03 |
| 1/19/10 | 3 | 322 | 9 | 0.03 |
| 2/10/10 | 6 | 318 | 20 | 0.06 |
| 3/3/10 | 6 | 363 | 17 | 0.05 |
| 3/16/10 | 5 | 385 | 23 | 0.06 |
| Lower Deer Point Site | | | | |
| 12/23/09 | 2 | 185 | 15 | 0.08 |
| 1/7/10 | 2 | 211 | 14 | 0.07 |
| 1/22/10 | 2 | 301 | 44 | 0.15 |
| 2/5/10 | 8 | 298 | 22 | 0.07 |
| 2/26/10 | 4 | 289 | 31 | 0.11 |
| 3/12/10 | 9 | 352 | 21 | 0.06 |
| 4/1/10 | 4 | 364 | 16 | 0.04 |
| 4/15/10 | 8 | 400 | 26 | 0.07 |
| 4/23/10 | 5 | 419 | 60 | 0.14 |
| Upper Dry Creek Site | | | | |
| 1/8/10 | 12 | 275 | 30 | 0.11 |
| 1/29/10 | 16 | 302 | 31 | 0.10 |
| 3/5/10 | 10 | 384 | 31 | 0.16 |
| 4/14/10 | 8 | 405 | 17 | 0.04 |
| 5/2/10 | 9 | 358 | 91 | 0.25 |
| Total | 125 | | | |
| average | 6.25 | 321 | 26.85 | 0.087 |

4.2.1 Treeline

The Treeline site was measured 6 times during the 2010 winter, starting on December 23, 2009 and ending on March 16, 2010 (Figure 4.18). Maximum accumulation occurred in January and complete ablation occurred in late March. Several storms deposited snow at Treeline during late April and were followed by rapid ablation. Snow density values showed nearly linear increases throughout the season as the snowpack melted and settled. An aspect break of 100˚ was selected to show differences in snow depth on northeast and southwest facing hillslopes throughout the winter (Figure 4.19). Snowdepth values on December 23 and January 7 show a relatively uniform snow distribution across the 300-meter transect. By January 19, aspect differences began to dominate snow distribution due to differential ablation. Time-lapse images of the site illustrate the aspect-induced differences in snow distribution (Figure 4.20). Accumulated potential incoming solar radiation amounts calculated from a DEM using the approach described by DeWalle and Rango (2008) for a ten day period during the spring melt correspond well with snow ablation patterns at Treeline (Figure 4.21). Areas receiving considerably more solar radiation due to slope and aspect become snow free earlier than those receiving less solar radiation. The distribution of aspects and slopes in the SNODAS pixel were similar to those sampled, while SNODAS captures a broader range of elevations (Figure 4.22).

Variograms were fit with the spherical model and uncertainty in the range and sill were evaluated using a bootstrap approach discussed in Chapter 3 (Figure 4.23). The sill variance increased throughout the season, indicating grater variability as the season progressed (Figure 4.24). The range, which indicates the length scale of the process,

increased as the season progressed from 12 meters on January 7 to approximately 50 meters on February 10, where it remained for the final 3 sampling dates (Figure 4.25). The initial sampling event on December 23 produced an unreliable estimate of the range, as noted by the bootstrap approach, while the rest of the sampling dates produced reasonable range parameters. This evolution of the range roughly corresponds with the length of the snow patches that develop on the NE facing hillslopes. A nugget variance was noted in all but the final sampling event, indicating variability at distances less than the sample spacing (Figure 4.26). Variogram parameter values and uncertainties are listed in Table 4.5.

Correlations with influencing variables were explored via scatter plots. It was found that aspect and northness provided the best correlations and showed increasing correlation coefficients throughout the season with a maximum correlation coefficient for aspect of 0.85 and northness of 0.84 on March 16 (Figure 4.27). Forest canopy density was left out of this evaluation due to the lack of significant forest cover at the Treeline site. Correlation coefficients with influencing variables are listed in Table 4.6.

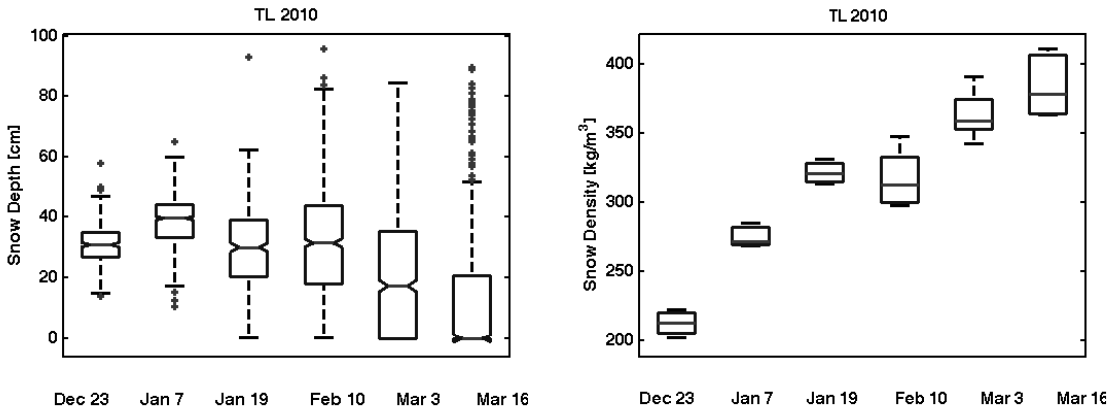


**Figure 4.18** 2010 Treeline snow depth and snow density box plots.

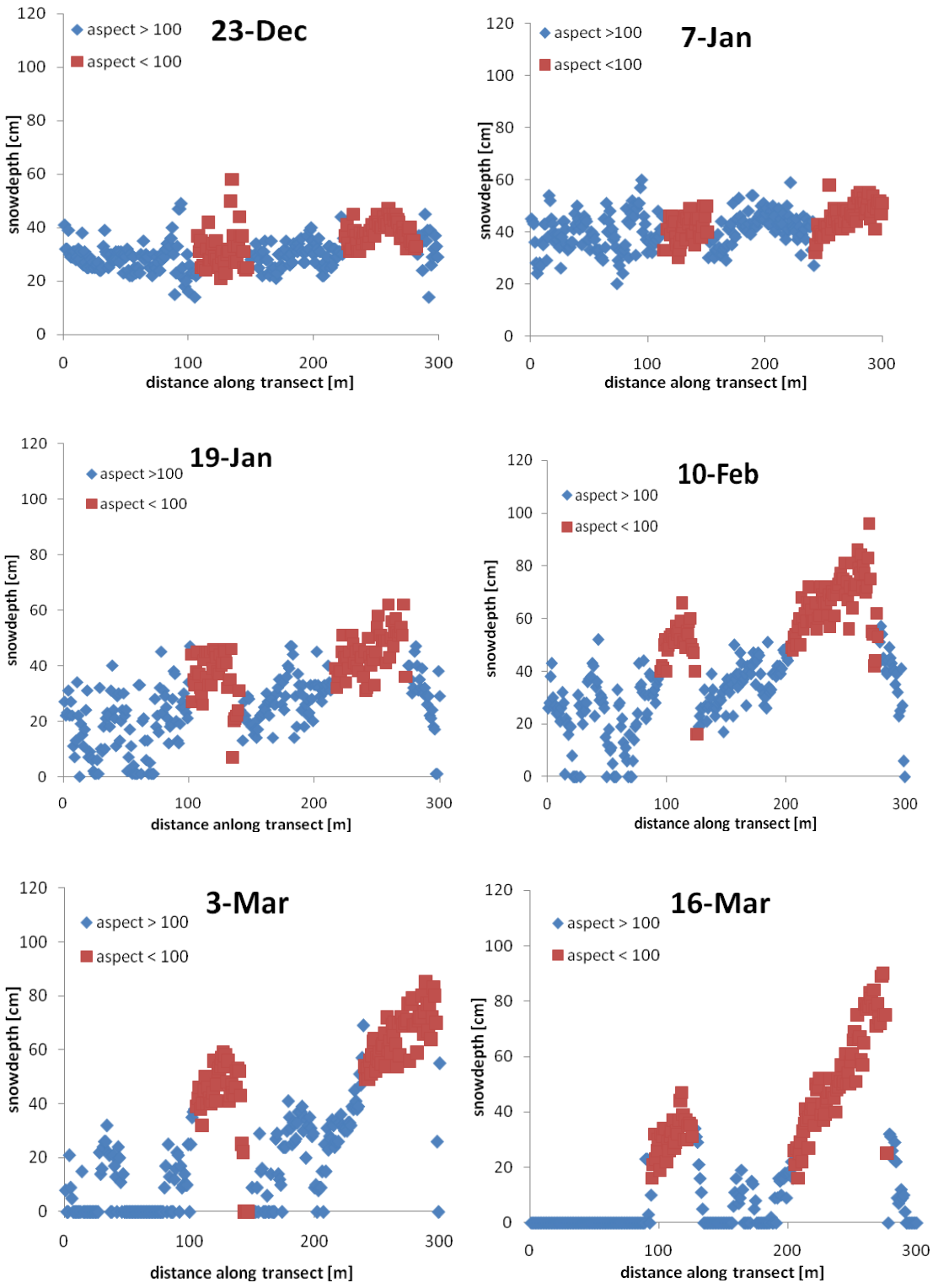


**Figure 4.19** Treeline 300 meter transect showing 100˚ aspect break.

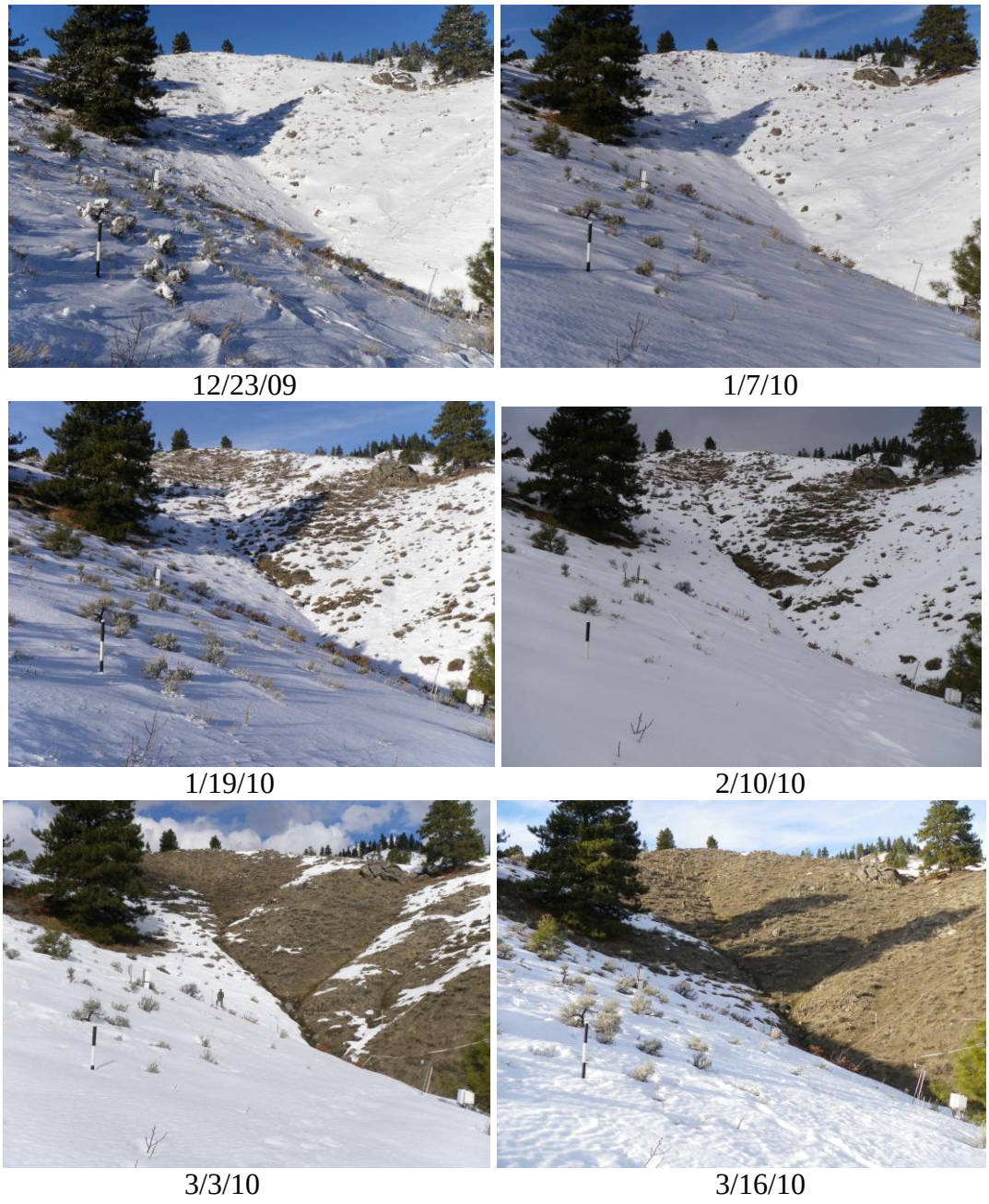


**Figure 4.20** Time-lapse images of the Treeline catchment facing North. Hillslopes on the upper-right side face Southwest, while the lower-left side faces Northeast. A 1 meter marker with 25 cm increments is located in the left foreground. Note: The author sampling with the Magnaprobe in the lower-right image. A video of these images is located at http://www.youtube.com/watch?v=etrRjmzr5UY

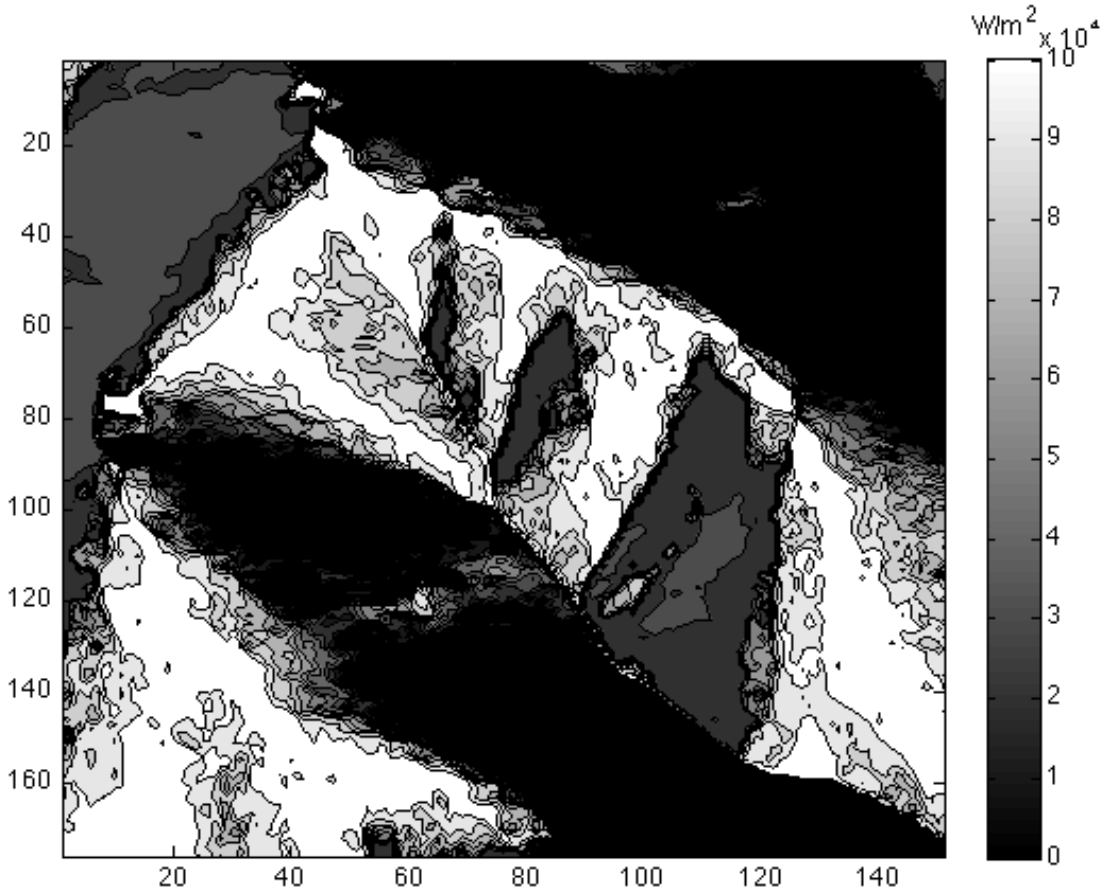


**Figure 4.21** Treeline cathcment modeled accumulated potential solar radiation for March 1 to March 10.

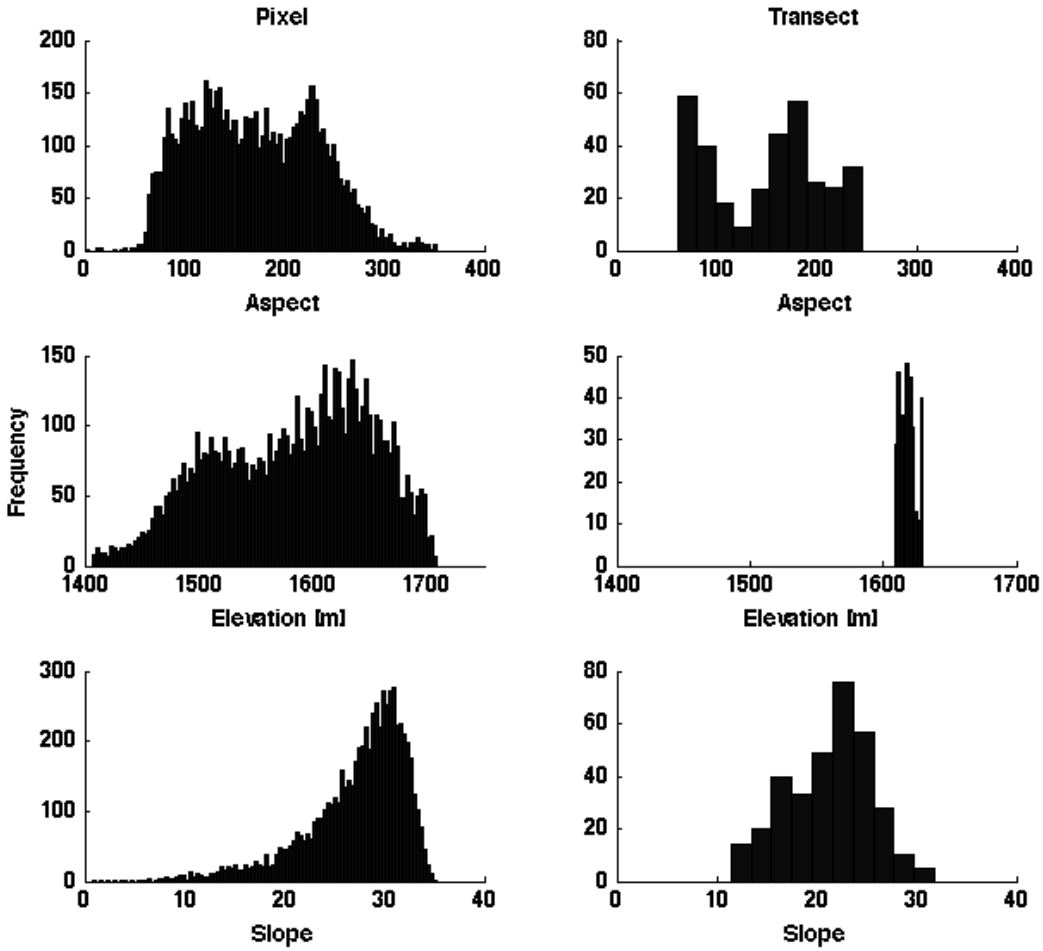


**Figure 4.22** Histogram distribution of landscape characteristics for the measured transect and the Treeline SNODAS pixel.

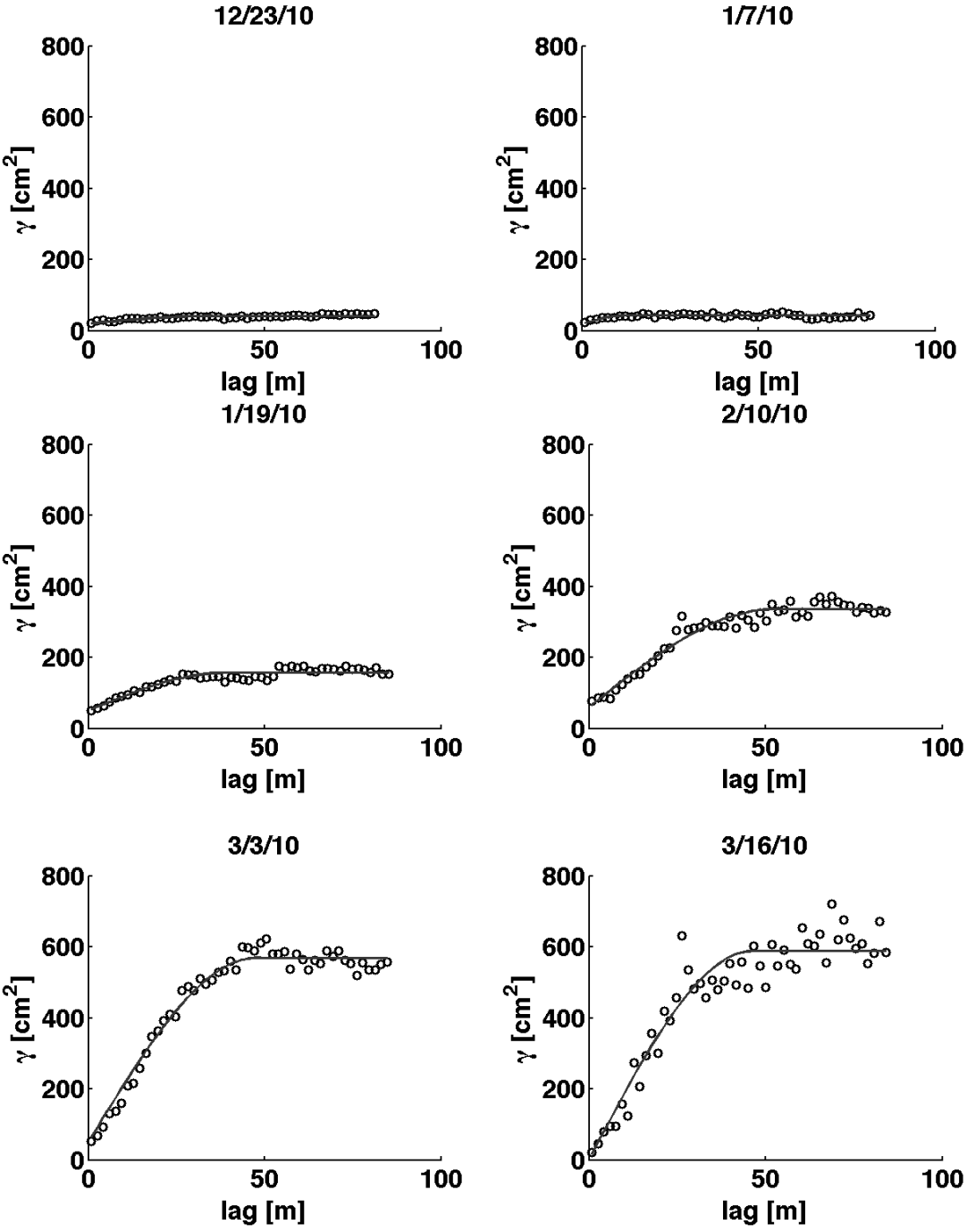


**Figure 4.23** Treeline variograms with spherical models.

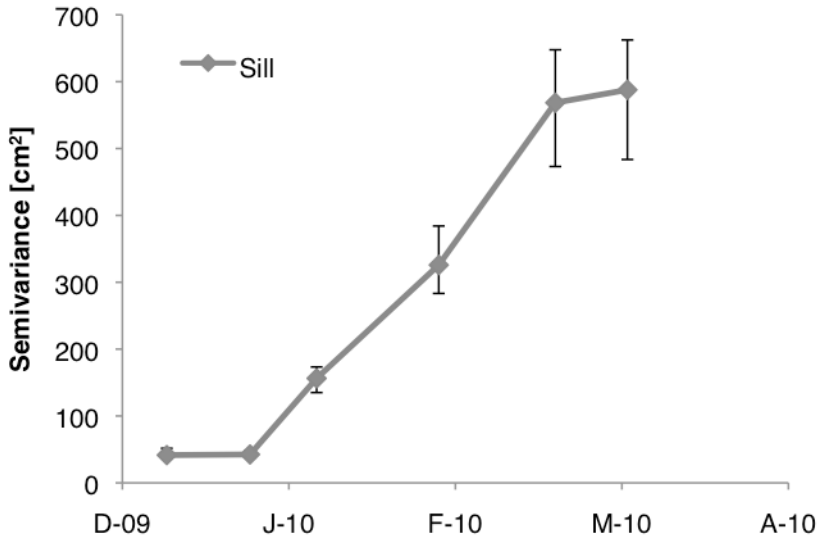


**Figure 4.24** Treeline spherical model variogram sill.

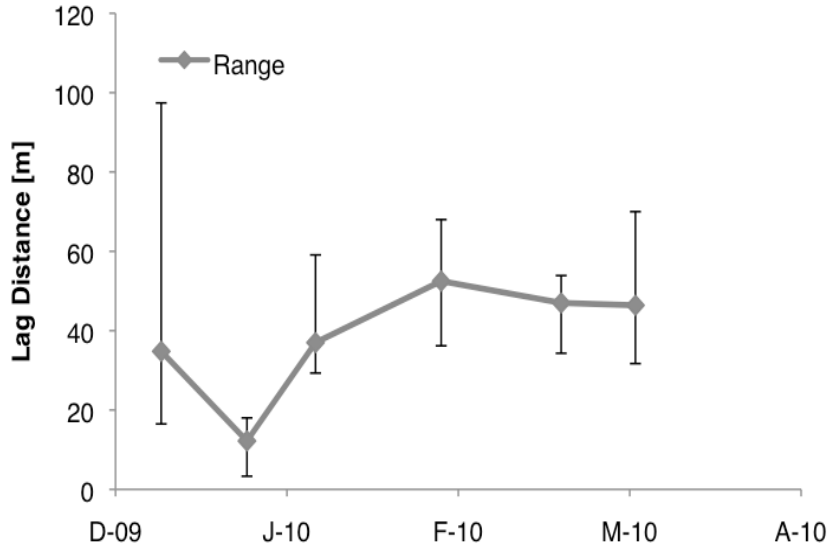


**Figure 4.25** Treeline spherical model variogram range.

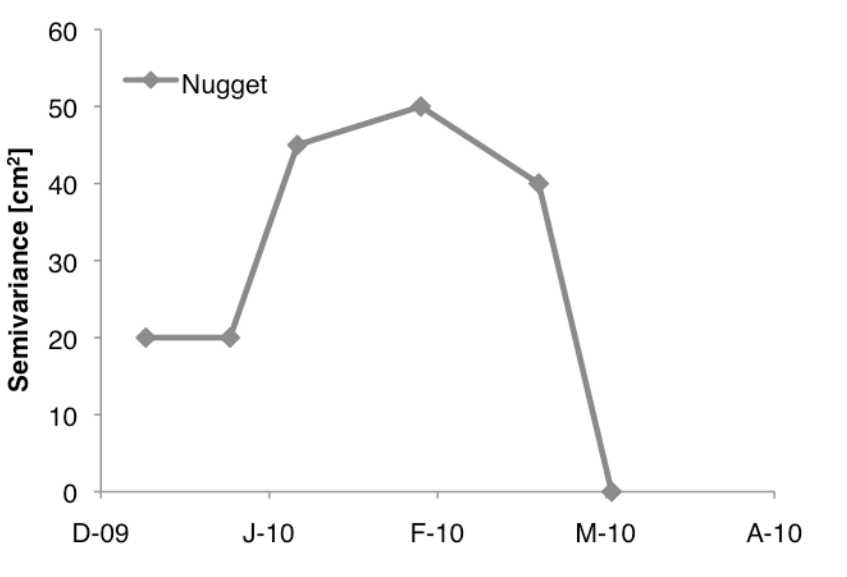


**Figure 4.26** Treeline spherical model variogram nugget.

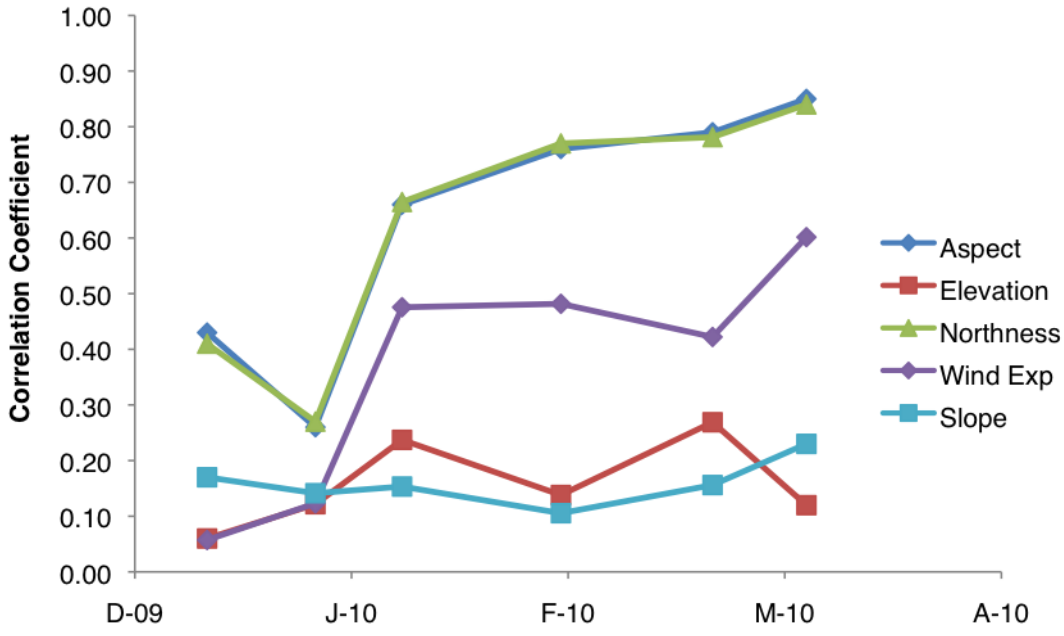


**Figure 4.27** Correlations with influencing variables at the Treeline site.

4.2.2 Lower Deer Point

The Lower Deer Point site was measured 9 times in 2010, starting on December 23 and ending on April 23. Maximum accumulation occurred in late February and melt events began to occur in early March (Figure 4.28). Forest canopy density influenced snow spatial patterns at this site early in the season and NLCD forest canopy density values of greater than or less than 60% were used to illustrate this relationship (Figure 4.29). Snow depth showed moderate correlation (-0.58) with forest canopy density on December 23, as snow settled and melt events occurred this relationship became less strong. Canopy interception reduced snow accumulation on the ground by as much as 58% during the first snowfall event.

Variograms from Lower Deer Point were fit with the spherical model and uncertainty in the range and sill were evaluated using a bootstrap approach discussed in Chapter 3 (Figure 4.30). Variograms calculated from Lower Deer Point show the sill increases as the season progresses (Figure 4.31). It was hypothesized that the range would decrease as the influence of forest canopy became less strong or vice versa. In reality, the December dataset may not have fully captured the forest canopy influence because the range of that process is larger than the greatest lag distance calculated and thus the data are not stationary. The Magnaprobe was not available during the December sampling, thus there are fewer data points (200) from this survey. The early season modeled variograms indicate the presence of a range greater than 100 meters that decreases during the accumulation period; however, the experimental variograms from this time show the possible presence of a smaller range similar to values encountered later in the season if local stationarity is assumed. The range decreases as the season

progresses until the onset of melt during mid-April when the range begins to increase (Figure 4.32). In other words, the length scale of the process in this location decreases throughout the accumulation season and increases during ablation. A nugget variance occurred during all sampling events (Figure 4.33).

Correlations with influencing variables indicated that snow depth was moderately correlated with forest canopy density during the early part of the season (Figure 4.34). This relationship became less strong as the season progressed. It should also be noted that in most cases a 2$^{nd}$ degree polynomial model, in the shape of a parabola, fit the data better and provided greater correlation between snow depth and canopy density. This is in agreement with the findings of Veatch *et al.* (2009), whereby greatest snow depth values were encountered in areas of moderate canopy density. Unfortunately, transect scale snow surveys at the Lower Deer Point site did not cover the entire range of forest canopy density values, leaving a significant gap at the 1-40 % range. Throughout the winter, however, the deepest snow was found in areas with ~40% canopy density. Aspect and wind exposure produced low to moderate correlations with snow depth late in the season.

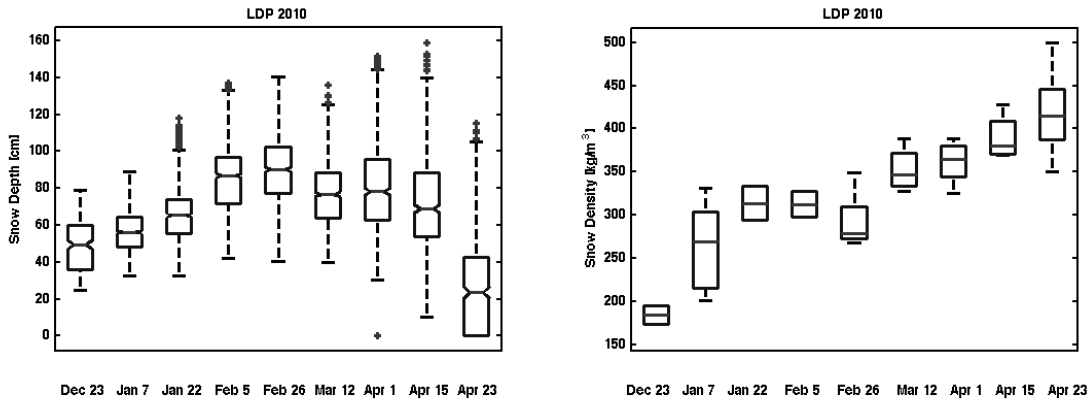


**Figure 4.28** 2010 Lower Deer Point snow depth and snow density box plots.

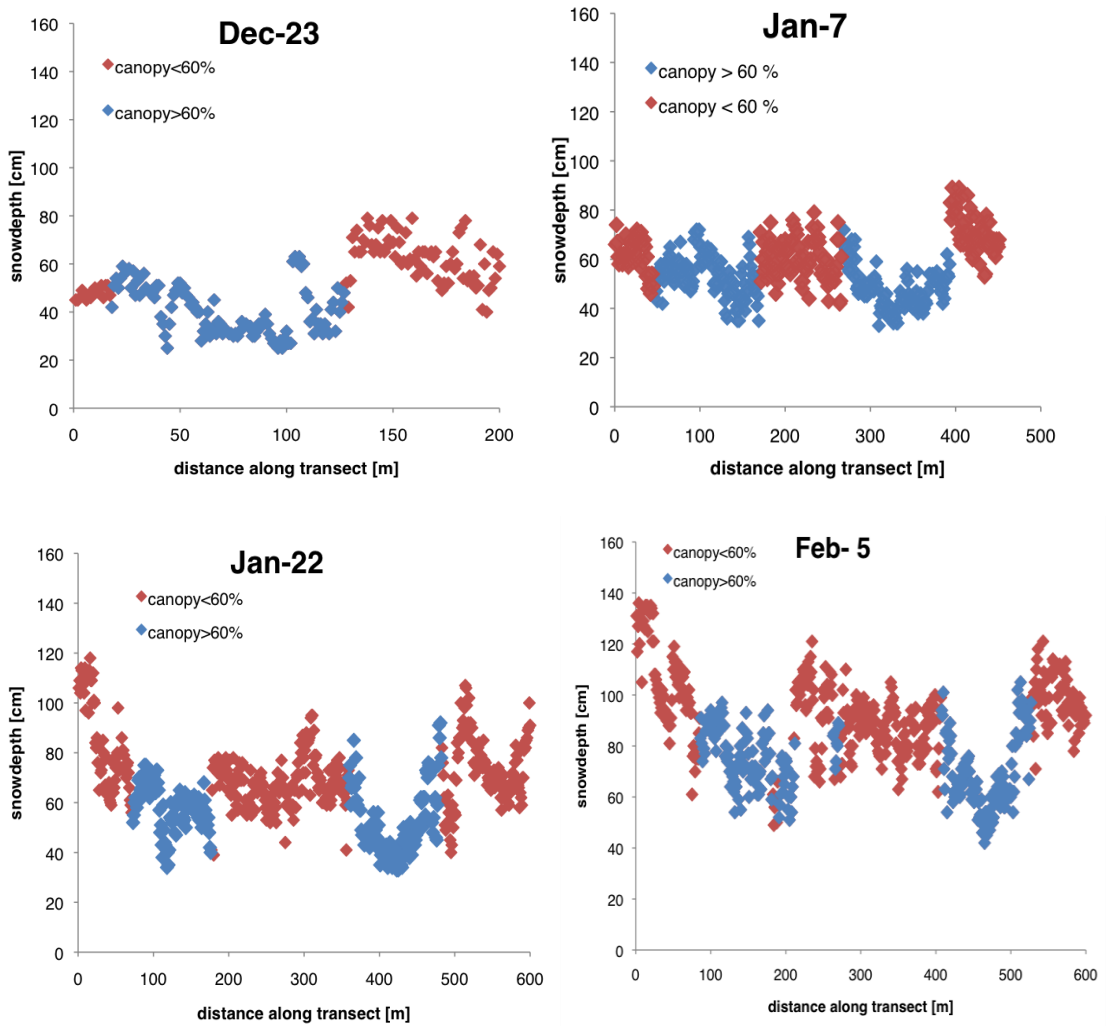


**Figure 4.29** Lower Deer Point snow surveys showing differences snow depth under NLCD forest canopy greater than 60% or less than or equal to 60%.

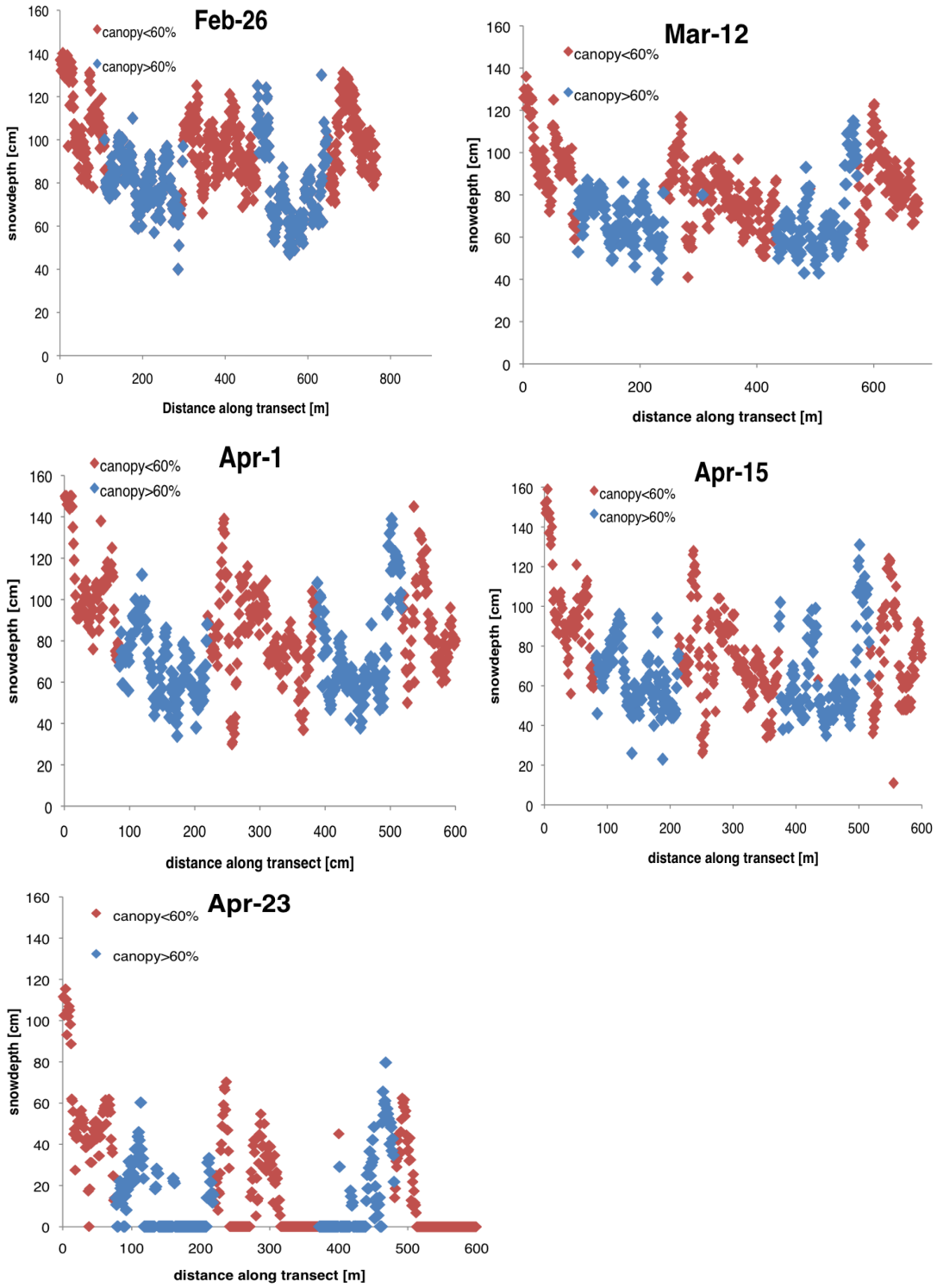


**Figure 4.29 Continued** Lower Deer Point snow surveys showing differences snow depth under NLCD forest canopy greater than 60% or less than or equal to 60%.

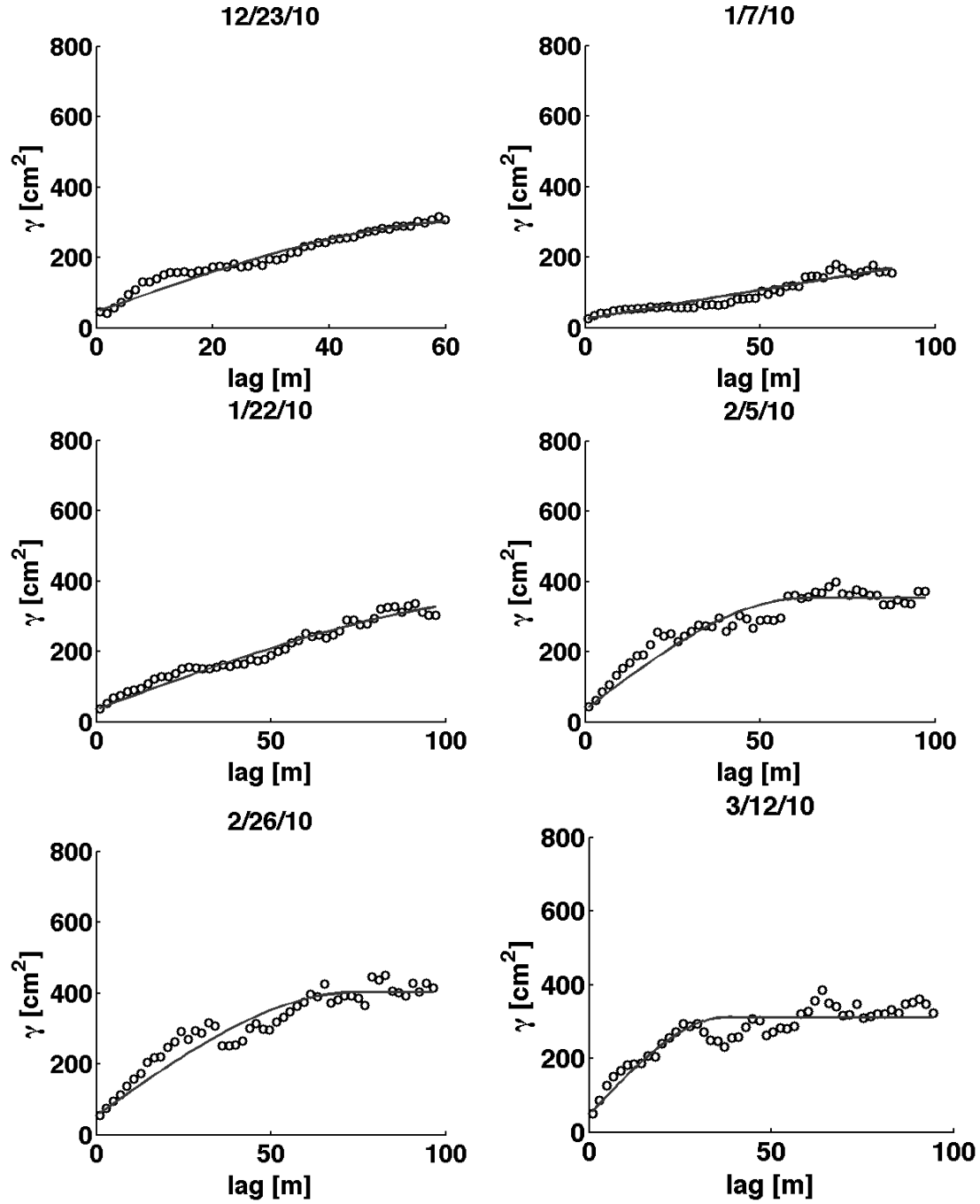


**Figure 4.30** Lower Deer Point variograms with spherical models.

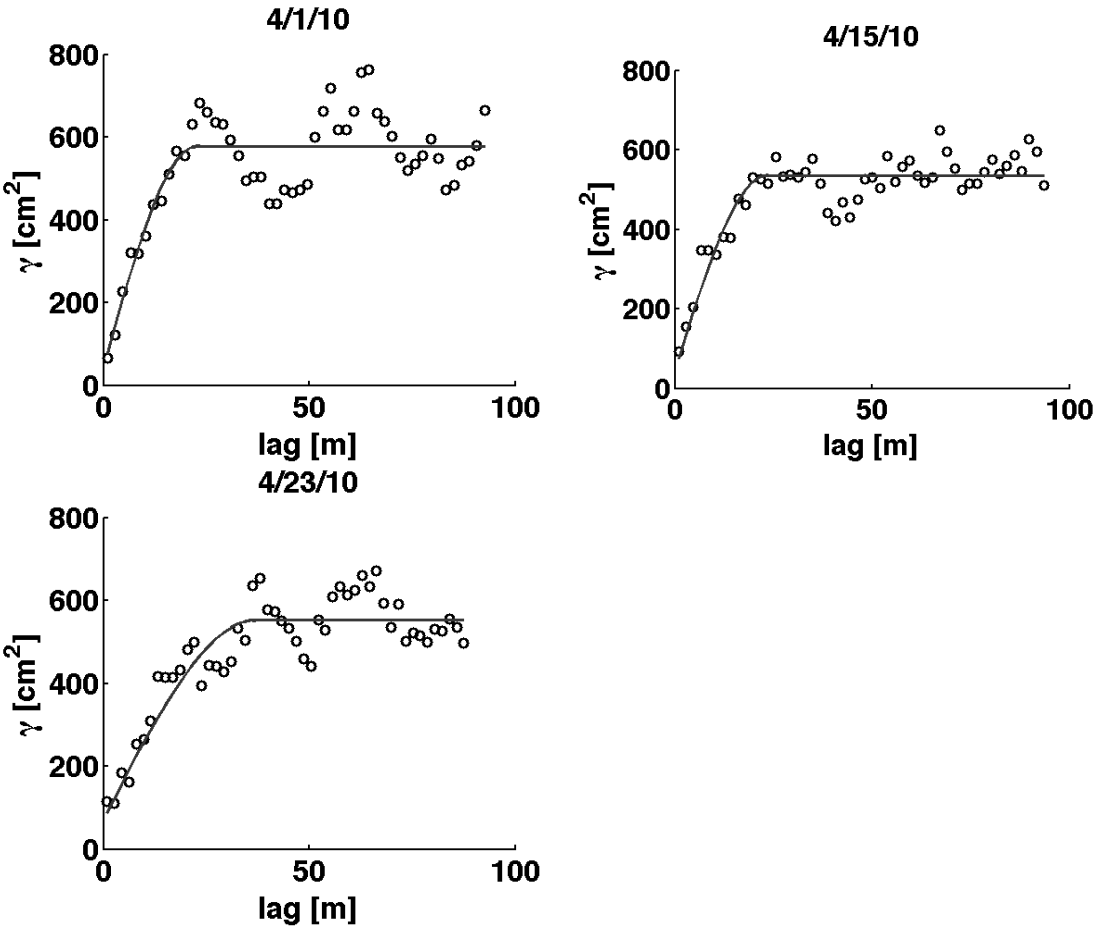


**Figure 4.30 Continued** Lower Deer Point variograms with spherical models.

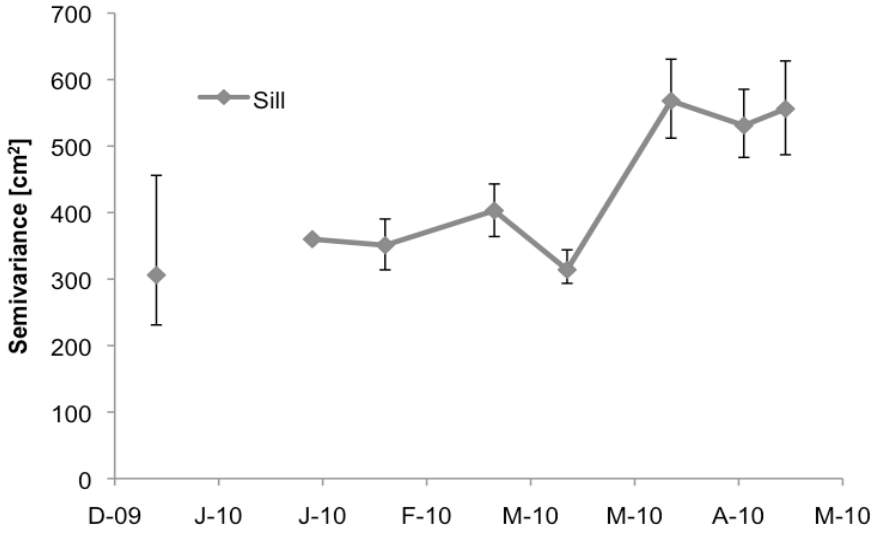


**Figure 4.31** Lower Deer Point sill values.

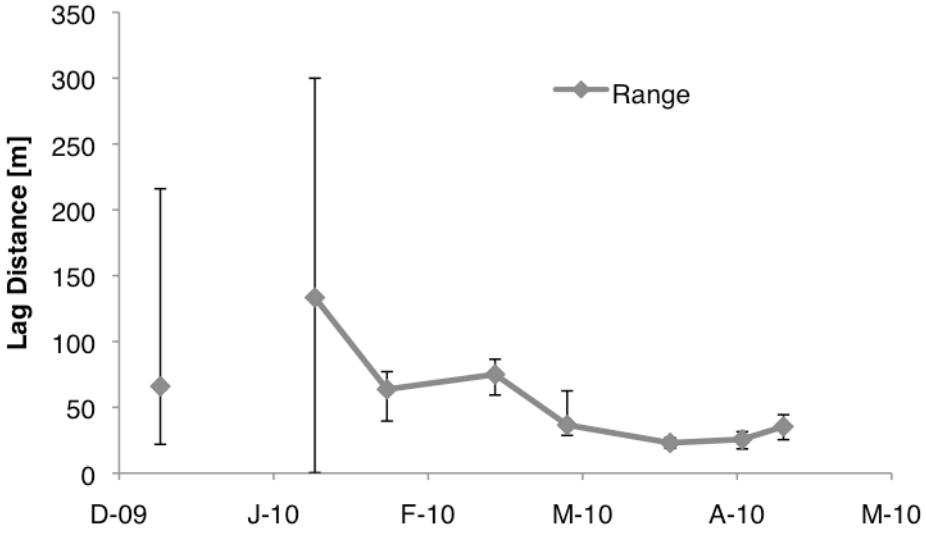


**Figure 4.32** Lower Deer Point range values.

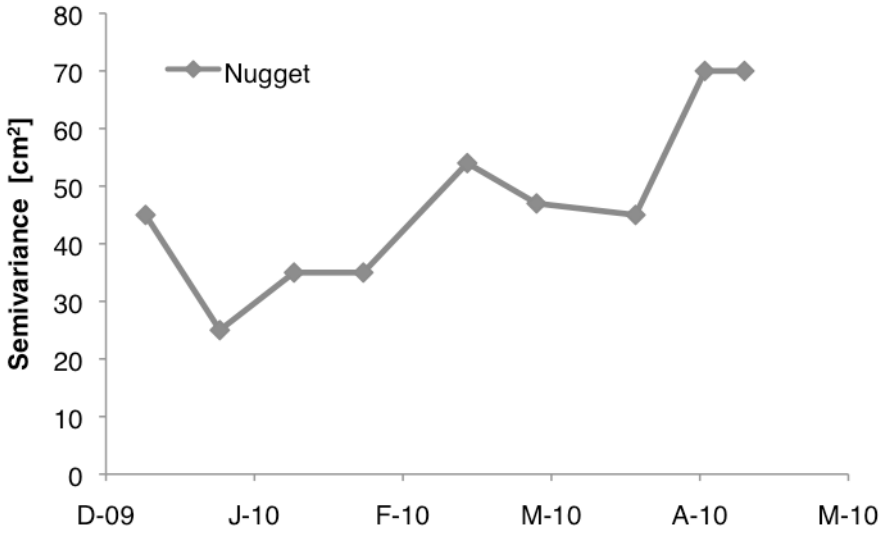


**Figure 4.33** Lower Deer Point nugget values.

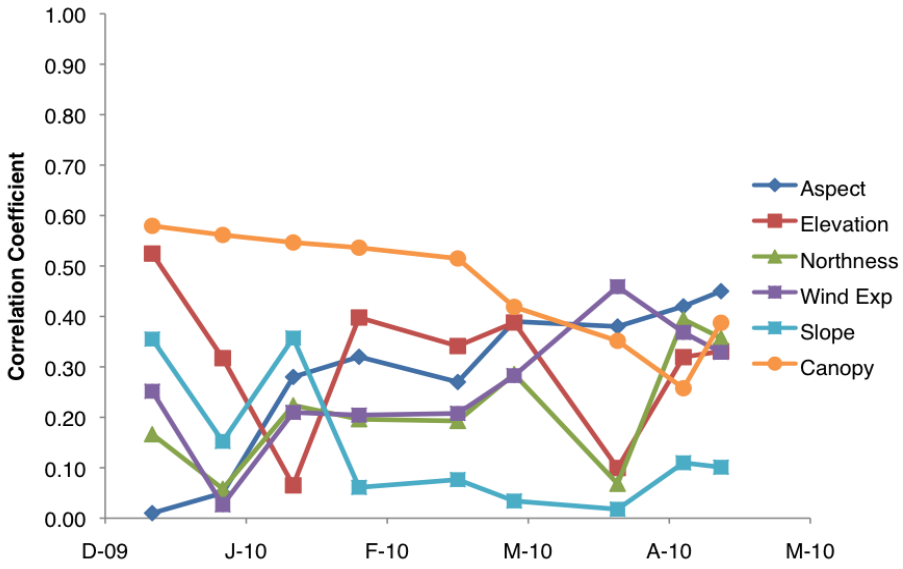


**Figure 4.34** Lower Deer Point correlation coefficients.

4.2.3 Upper Dry Creek

The Upper Dry Creek site was measured 5 times in 2010, starting on January 8 2010 and ending on May 5 2010. Snow density tended to increase linearly with time throughout the season except for the last sampling date where new snow had accumulated in previously bare areas. Maximum accumulation occurred in mid-April (Figure 4.35). Differences in northness were used to illustrate snow depth variability (Figure 4.36). Upper Dry Creek held the deepest snowpack of all sites and not surprisingly showed the greatest range in values at the transect scale. The April 14 sampling date contained snow depth values separated by less than 10 meters that differed by more than 150 cm.

Variograms were fit with the spherical model and uncertainty in the range and sill were evaluated using a bootstrap approach discussed in Chapter 3 (Figure 4.37). The sill increased throughout the season except for a slight decrease from February to March (Figure 4.38). The range indicated large positive uncertainties during the three initial sampling events, which may be the result of non-stationarity in the data. The variograms

from these sampling events appear to increase after reaching the sill. Variograms from this site also showed the greatest "hole effect," whereby the experimental variogram decreases some after reaching the sill and then fluctuates. In previous studies, this periodic behavior in the experimental variogram has been attributed to periodic patterns in the data. Overall, the range appears to decrease throughout the season from about 45 meters to 25 meters (Figure 4.39, Table 4.5). Variograms from Upper Dry Creek exhibited the largest nugget values at the transect scale (Figure 4.40).

Cornices and drifts were observed in the upper portions of the catchment near ridges. Shallower snow was generally found in the upper two transects where slope is greater and the influence of wind is greater leading to negative correlations with slope and elevation. It was hypothesized that the influence of wind would be the greatest at this location due to its higher elevation and exposed topography. The wind exposure index showed moderate correlation with snow depth (-0.57 during the final sampling event (Figure 4.41)); however, it is thought that the influence of wind is not completely captured by this index because snow drifts encountered in the field during the April 14 survey were only 2-3 meters across and thus only consisted of 2-3 snow depth measurements, which appear as outliers in the dataset. Negative correlations between snow depth and elevation and slope are thought to be explained by the influence of wind scouring on the upper two transects at this site. The upper two transects traverse the exposed head wall of the Deer Point summit, while the lower transect traverses a flatter bench below the Boise Ridge road. Greater snow depth was encountered on the lower transect throughout the season, which may be explained by less wind scouring and redistribution.

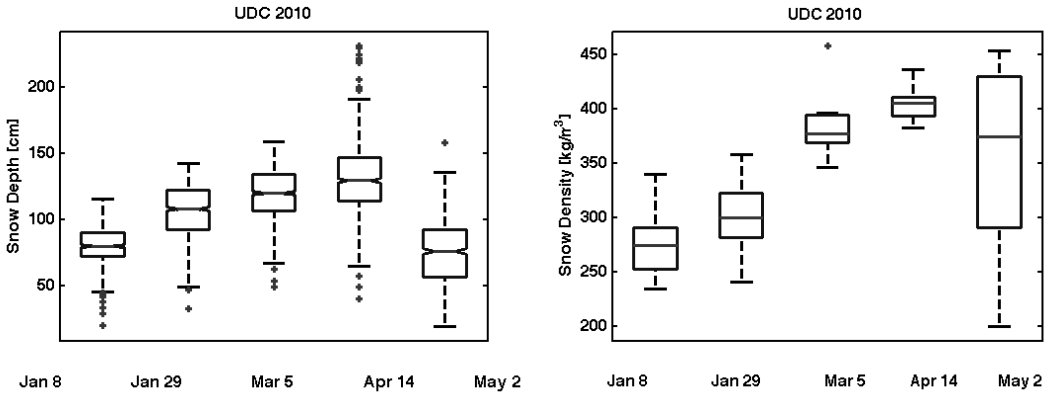


**Figure 4.35** 2010 Upper Dry Creek snow depth and snow density box plots

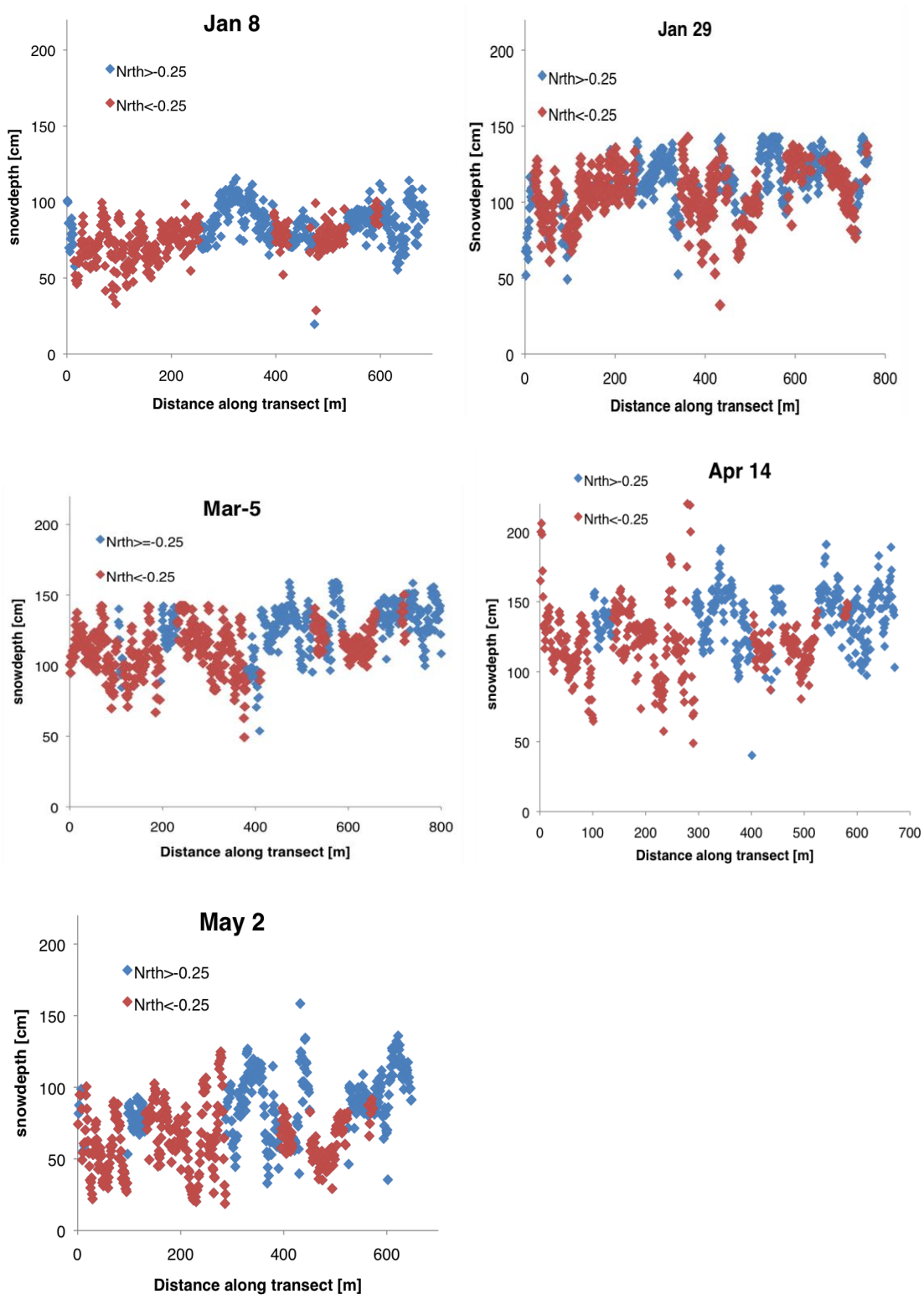


**Figure 4.36** Upper Dry Creek snow survey results showing differences in Northness. Red symbols are less than -0.25 northness or more south facing. Blue symbols are greater than -0.25 northness or less south facing.

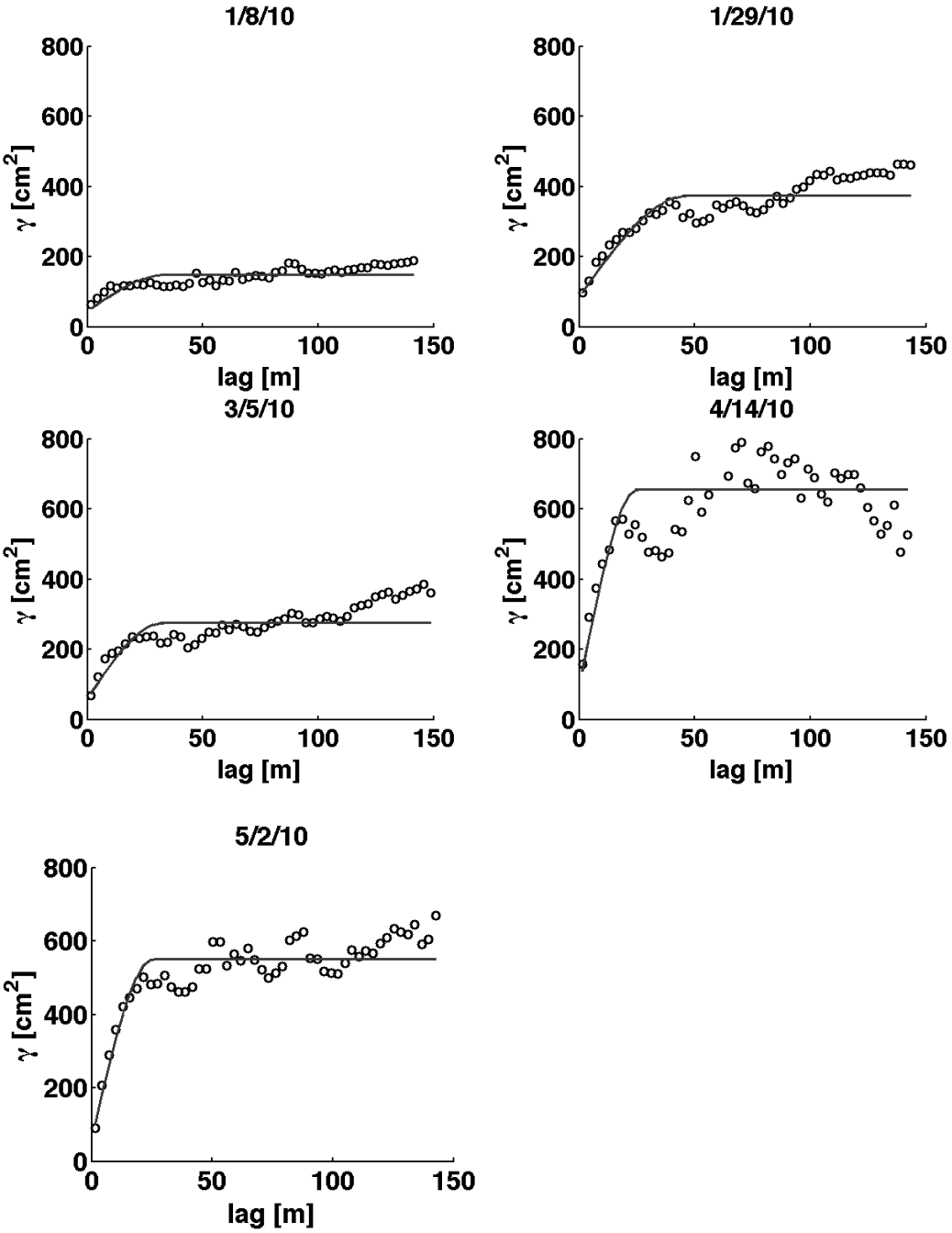


**Figure 4.37** Upper Dry Creek variograms and spherical models.

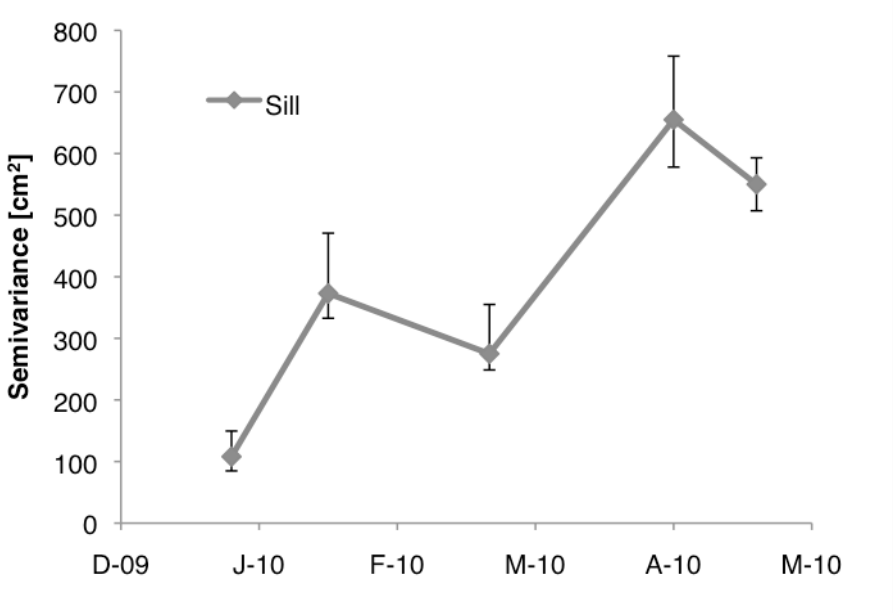


**Figure 4.38** Upper Dry Creek sill values.

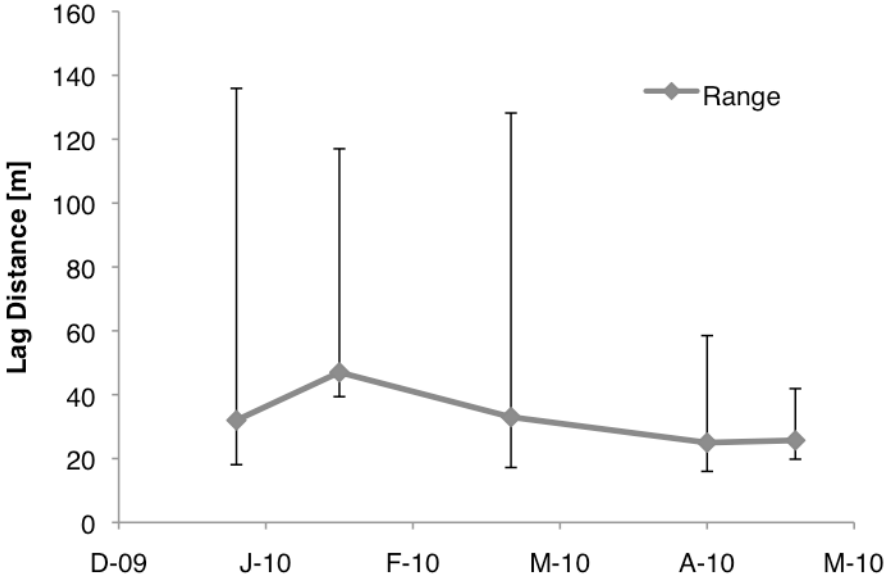


**Figure 4.39** Upper Dry Creek range values.

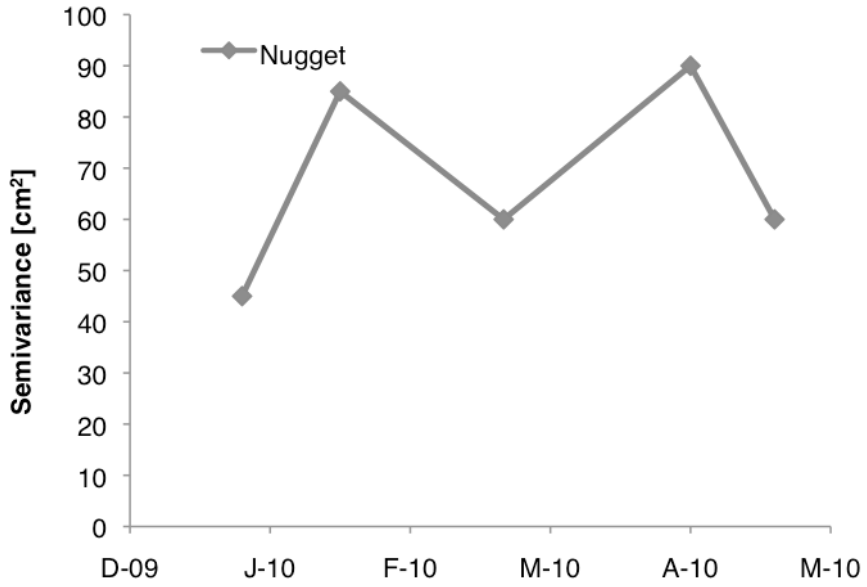


**Figure 4.40** Upper Dry Creek nugget values.

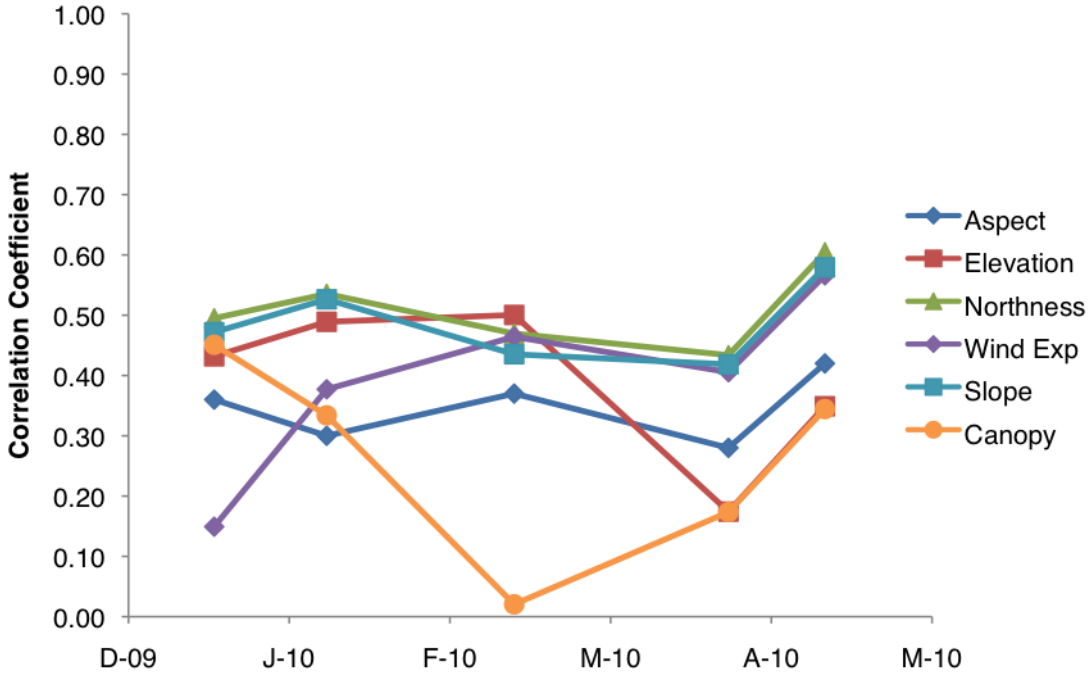


**Figure 4.41** Upper Dry Creek snow depth and influencing variable correlation coefficients.

**Table 4.5** Transect Scale Variogram Model Parameters

| Date/ Location | nugget [$cm^2$] | range [m] | range +error | range -error | sill [$cm^2$] | sill +error | sill -error |
|---|---|---|---|---|---|---|---|
| Treeline | | | | | | | |
| 12/23/09 | 20 | 34.8 | 62.6 | 18.3 | 41.5 | 10.2 | 5.4 |
| 1/7/10 | 20 | 12.2 | 5.8 | 8.9 | 42.48 | 5.7 | 4.7 |
| 1/19/10 | 45 | 37 | 22.1 | 7.7 | 156.3 | 17 | 21.3 |
| 2/10/10 | 50 | 52.5 | 15.5 | 16.3 | 325.8 | 58.3 | 42.5 |
| 3/3/10 | 40 | 47 | 6.9 | 12.7 | 568.5 | 79.2 | 95.4 |
| 3/16/10 | 0 | 46.4 | 23.6 | 14.7 | 587.8 | 74.5 | 104.2 |
| Lower Deer Point | | | | | | | |
| 12/23/09 | 45 | 66 | 150 | 44.1 | 306 | 150 | 75 |
| 1/7/10 | 25 | NA | NA | NA | NA | NA | NA |
| 1/22/10 | 35 | 133.4 | 166.6 | 133 | 360 | NA | NA |
| 2/5/10 | 35 | 63.7 | 13.4 | 24.1 | 350.9 | 39.4 | 37 |
| 2/26/10 | 54 | 75 | 11.5 | 15.7 | 403 | 40 | 39 |
| 3/12/10 | 47 | 36.6 | 25.9 | 7.9 | 314 | 30 | 20.4 |
| 4/1/10 | 45 | 23 | 3.9 | 4.1 | 568 | 62.7 | 56 |
| 4/15/10 | 70 | 25.7 | 5.8 | 7.3 | 531 | 54.4 | 48 |
| 4/23/10 | 70 | 35.4 | 9 | 10 | 556 | 72 | 69 |
| Upper Dry Creek | | | | | | | |
| 1/8/10 | 45 | 32 | 103.9 | 13.9 | 108 | 41.5 | 23.2 |
| 1/29/10 | 85 | 47 | 70 | 7.6 | 373 | 97.8 | 40.3 |
| 3/5/10 | 60 | 33 | 95.2 | 15.8 | 275 | 80 | 26.3 |
| 4/14/10 | 90 | 25 | 33.5 | 9 | 655 | 103.2 | 77 |
| 5/2/10 | 60 | 25.7 | 16.2 | 5.9 | 550.1 | 43 | 43 |

.

**Table 4.6** Transect scale snow depth correlation coefficients

| date | *n* | Elevation [m] | Aspect | Slope | Northness | Wind Exp | Canopy |
|---|---|---|---|---|---|---|---|
| Treeline | | | | | | | |
| 12/23/09 | 299 | NSS | 0.43 | 0.12 | 0.17 | 0.06 | -- |
| 1/7/10 | 332 | 0.12 | 0.26 | 0.14 | 0.27 | -0.12 | -- |
| 1/19/10 | 302 | 0.24 | 0.66 | 0.15 | 0.66 | -0.48 | -- |
| 2/10/10 | 307 | 0.14 | 0.76 | NSS | 0.76 | -0.48 | -- |
| 3/3/10 | 332 | 0.27 | 0.79 | 0.16 | 0.78 | -0.42 | -- |
| 3/16/10 | 308 | -0.12 | 0.85 | -0.75 | 0.83 | -0.60 | -- |
| Lower Deer Point | | | | | | | |
| 12/23/09 | 202 | 0.52 | NSS | 0.36 | -0.17 | 0.25 | -0.58 |
| 1/7/10 | 452 | 0.32 | NSS | 0.15 | NSS | NSS | -0.56 |
| 1/22/10 | 600 | NSS | 0.28 | 0.36 | 0.22 | -0.21 | -0.55 |
| 2/5/10 | 622 | 0.40 | 0.32 | -0.06 | 0.20 | -0.20 | -0.54 |
| 2/26/10 | 632 | 0.34 | 0.27 | -0.08 | 0.19 | -0.21 | -0.51 |
| 3/10/10 | 676 | 0.39 | 0.39 | -0.03 | 0.29 | -0.28 | -0.42 |
| 4/1/10 | 619 | 0.10 | 0.38 | NSS | NSS | 0.25 | -0.35 |
| 4/15/10 | 619 | 0.32 | 0.42 | -0.11 | 0.39 | NSS | -0.26 |
| 4/23/10 | 390 | 0.33 | 0.45 | -0.10 | 0.36 | -0.21 | -0.39 |
| Upper Dry Creek | | | | | | | |
| 1/8/10 | 687 | -0.43 | 0.36 | -0.47 | 0.49 | -0.15 | 0.45 |
| 1/29/10 | 847 | -0.49 | 0.30 | -0.53 | 0.54 | -0.38 | 0.33 |
| 3/5/10 | 818 | -0.50 | 0.37 | -0.44 | 0.47 | -0.46 | NSS |
| 4/14/10 | 672 | -0.17 | 0.28 | -0.42 | 0.43 | -0.41 | 0.17 |
| 5/2/10 | 649 | -0.35 | 0.42 | -0.58 | 0.60 | -0.57 | 0.34 |

## 4.3 1 $km^2$ Pixel Scale Snow Survey Data

1 $km^2$ pixel scale snow surveys were conducted near the Lower Deer Point site four times during 2010 starting January 15 and ending April 16 (Figure 4.42; Tables 4.7 and 4.8). Maps of each survey showing snow depth proportional bubbles illustrate the spatial variability of SWE encountered throughout the season (Figures 4.43-4.46). As described in the methods section, the sampling design was altered after the first survey to better accommodate analysis with variograms and obtain more samples. Mean snow depth was greatest at mid-February (Figure 4.47); however, deepest individual snow values were encountered during the final survey in April. Snow density increased throughout the season (Figure 4.48).

Variograms computed from the experimental data indicate some non-stationarity in the data, as there is not an obvious sill. The data appear to continue to increase in variance with increasing lag distance (Figure 4.49). The models fit to the data indicate an increasing sill throughout the season as variability increases (Figure 4.50). The variogram models show a correlation range that increases from 106 meters in February to 250 meters in April (Figure 4.51). Nugget variances are relatively consistent with the transect scale surveys, with nugget variances of roughly 60-70 $cm^2$ (Figure 4.52). Uncertainty in the sill and range was evaluated using a bootstrap approach, and parameter estimates and uncertainties are listed in Table 4.9. The range exhibited uncertainties of roughly 20-40 meters, except during the final survey, which indicated an uncertainty of 135 meters.

Elevation, northness, and wind exposure show the strongest relationship with snow depth throughout the season (Figure 4.53). Canopy density was hypothesized to play an important role in snow distribution at this scale; however, correlations between

the two were not as strong as elevation, northness, and wind exposure. Fitting 2nd order polynomial models to the canopy versus snow data did increase the correlation coefficient in these data sets as well suggesting that moderate canopy density (~40-60%) accumulates the greatest amount of snow.

Little ablation had occurred during the January and February surveys, while the March and April surveys exhibited significant melt along the low elevation and southern portions of the survey. The two southern most transects show significant snow-free portions by mid-March owing to both lower elevation and south-facing aspects. The more north-facing, higher elevation transects near the northern edge of the study site continued to accumulate snow up to the final survey and the deepest snow of the season was encountered at these locations.

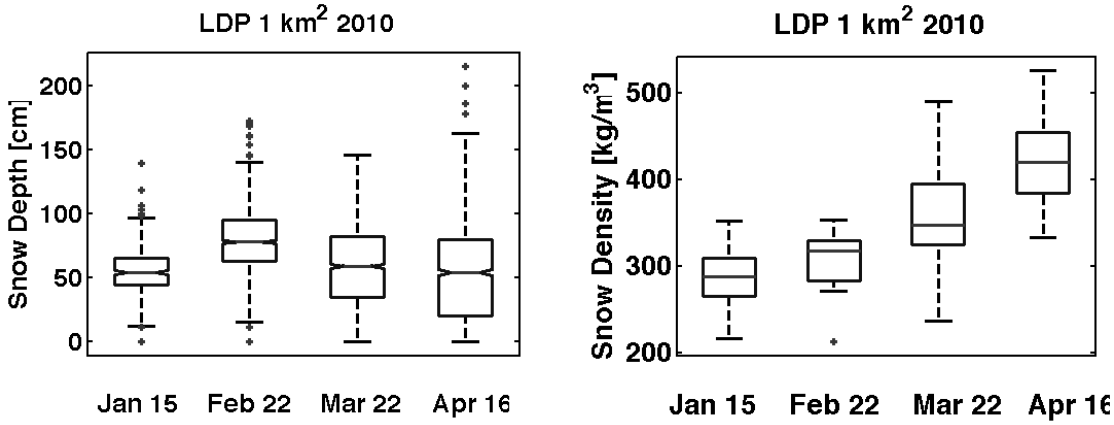


**Figure 4.42** 2010 Lower Deer Point 1 km2 snow depth and snow density box plots.

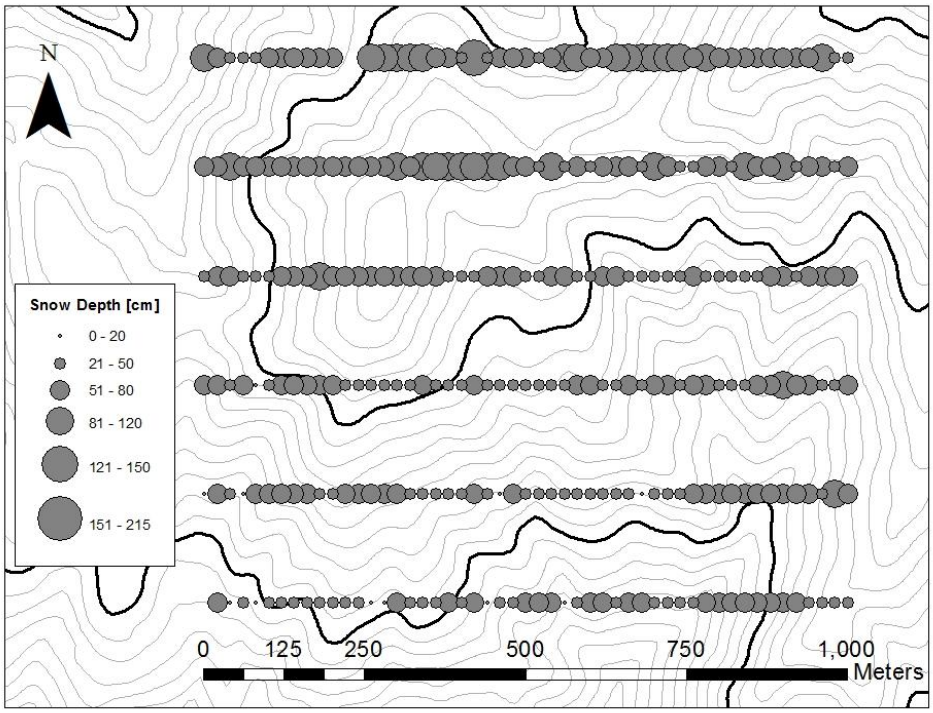


**Figure 4.43** 1 km$^2$ pixel snow depth Jan-15, 2010

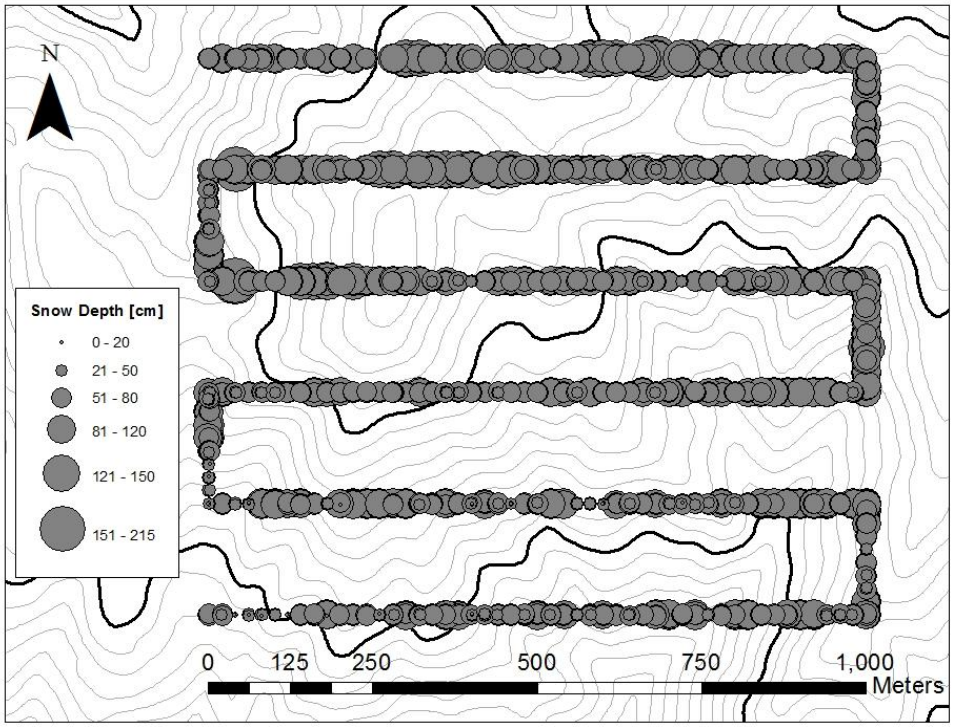


**Figure 4.44** 1 km$^2$ pixel snow depth Feb-19, 2010

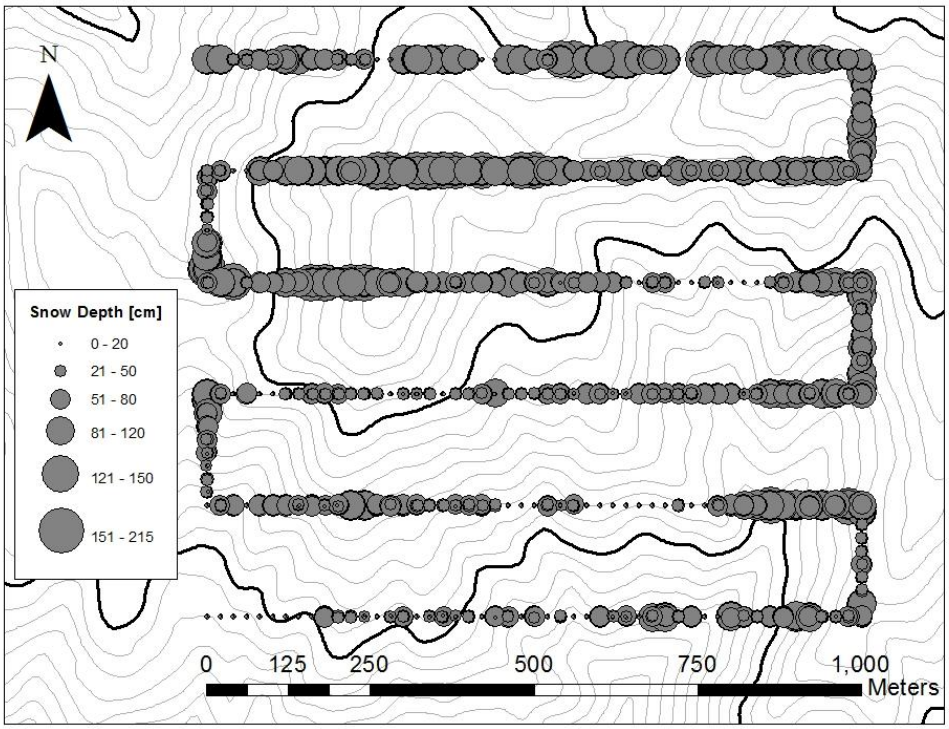


**Figure 4.45** 1 km$^2$ pixel snow depth Mar-22, 2010

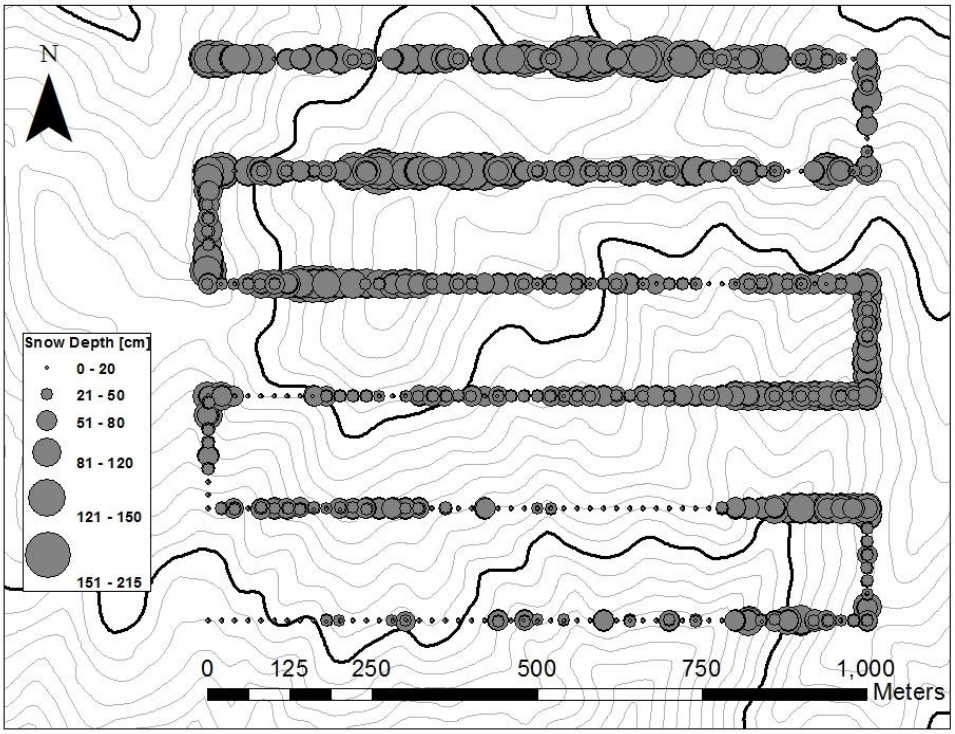


**Figure 4.46** 1 km$^2$ pixel snow depth Apr-16, 2010

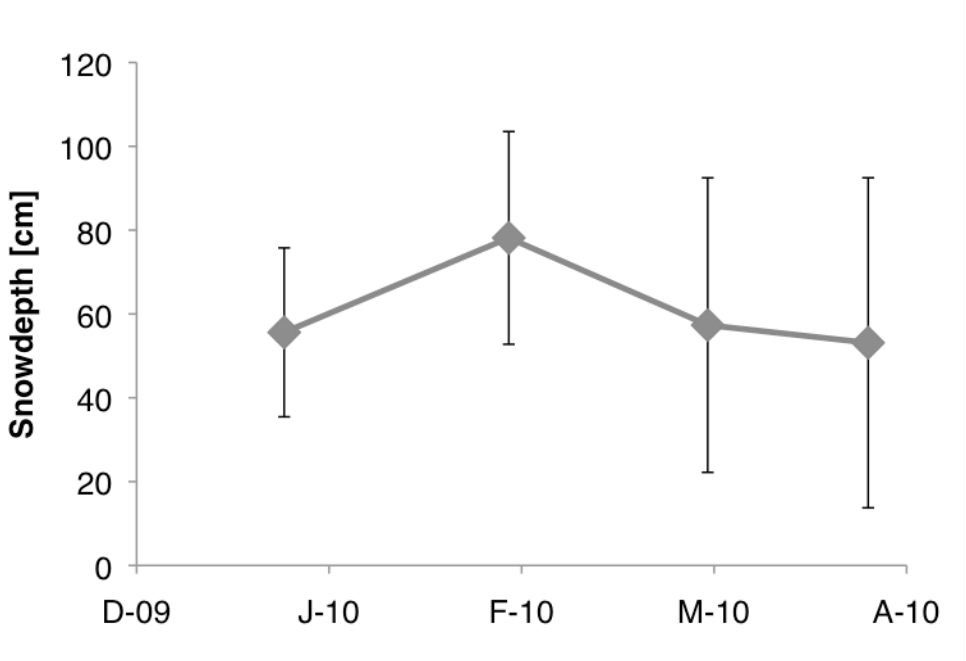


**Figure 4.47** 1 km$^2$ pixel scale mean snow depth and standard deviation (error bars).

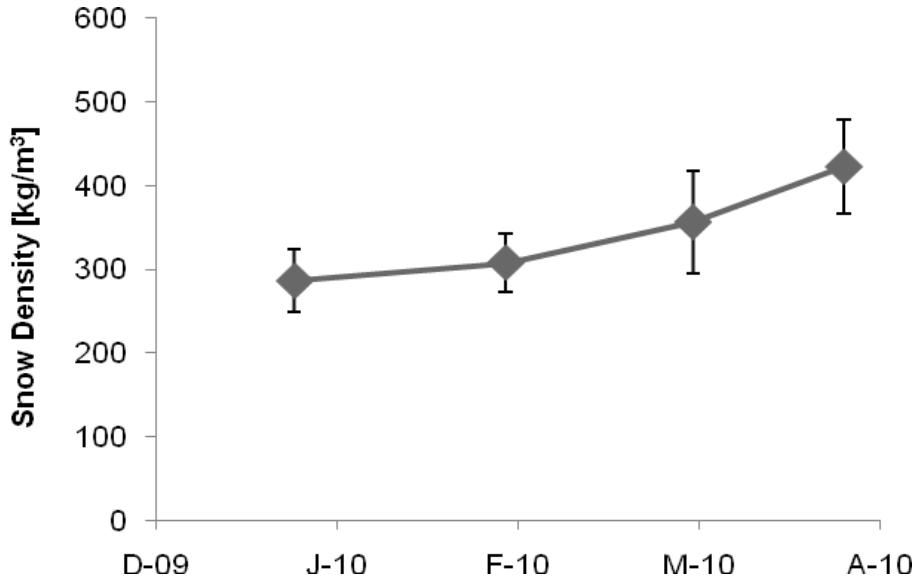


**Figure 4.48** 1km$^2$ pixel scale mean snow density and standard deviation (error bars).

**Table 4.7** 1 km$^2$ pixel snow depth statistics

| Date | *n* | mean [cm] | st dev [cm] | cv |
|---|---|---|---|---|
| 1/15/10 | 303 | 56 | 20 | 0.36 |
| 2/19/10 | 1725 | 78 | 25 | 0.32 |
| 3/22/10 | 1725 | 57 | 35 | 0.61 |
| 4/16/10 | 1725 | 53 | 39 | 0.74 |
| avg | 1369.5 | 61 | 30 | 0.51 |
| total | 5478 | -- | -- | -- |

**Table 4.8** 1 km$^2$ pixel snow density statistics

| Date | *n* | mean [kg/m$^3$] | st dev [kg/m$^3$] | cv |
|---|---|---|---|---|
| 1/15/10 | 18 | 286 | 37 | 0.13 |
| 2/19/10 | 18 | 308 | 35 | 0.11 |
| 3/22/10 | 16 | 356 | 61 | 0.17 |
| 4/16/10 | 18 | 422 | 57 | 0.13 |
| avg | 17.5 | 343 | 47 | 0.14 |
| total | 70 | -- | -- | -- |

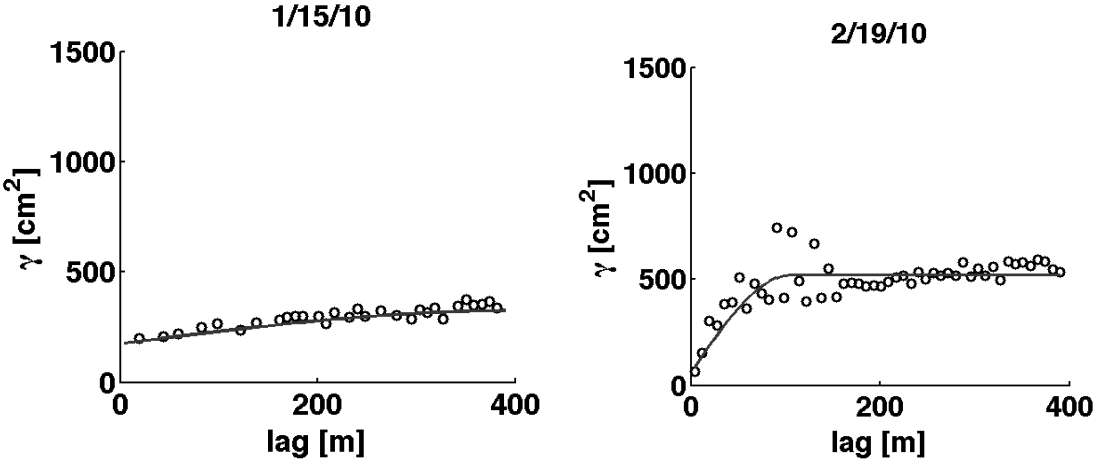

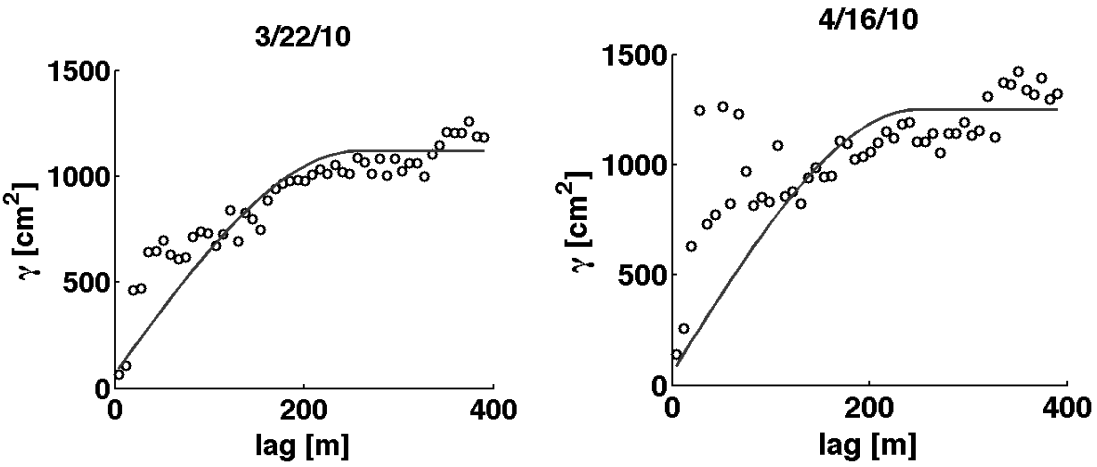


**Figure 4.49** Lower Deer Point 1 km$^2$ variograms.

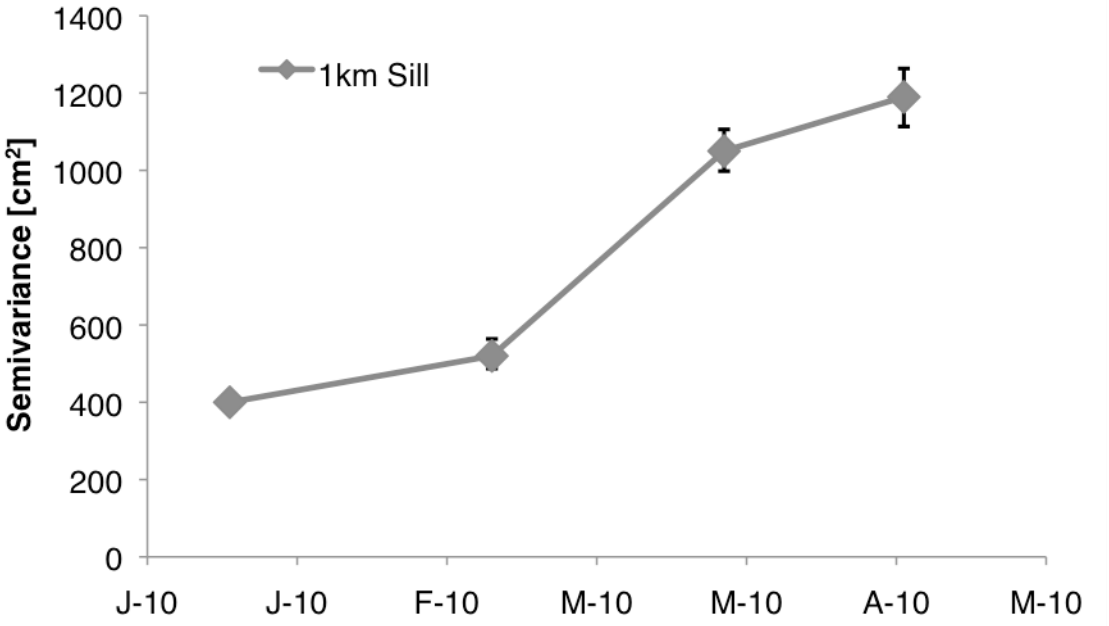


**Figure 4.50** 1 km$^2$ pixel scale variogram sill parameter. Error bars are bootstrap uncertianty 90% confidence interval.

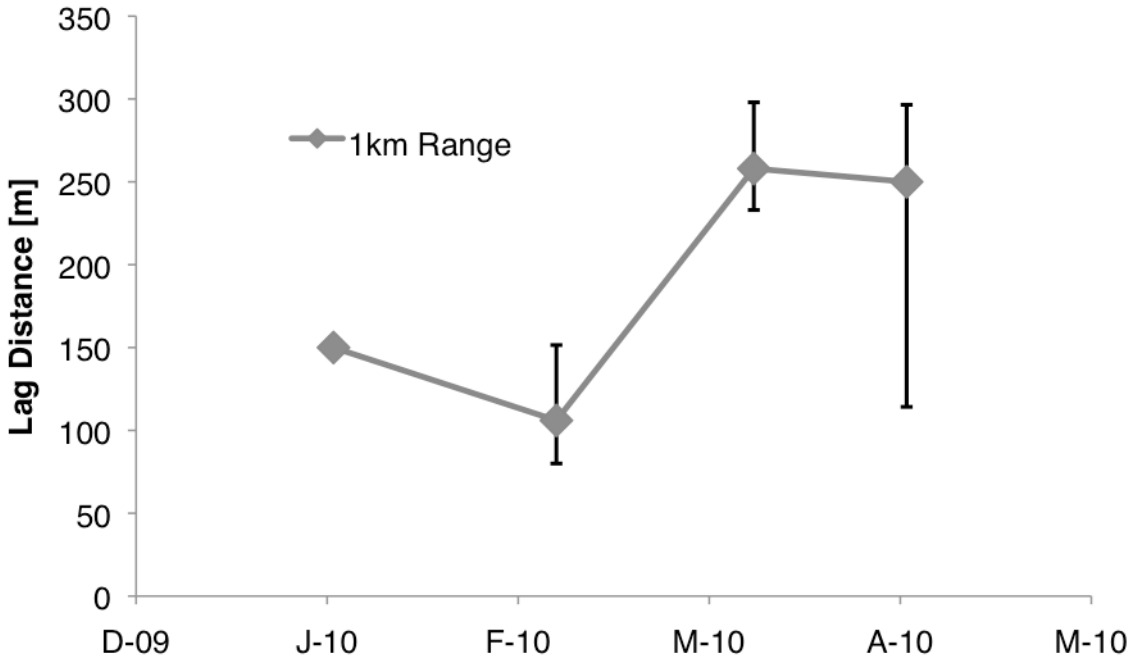


**Figure 4.51** 1 km$^2$ pixel scale variogram range parameter. Error bars are bootstrap uncertianty 90% confidence interval.

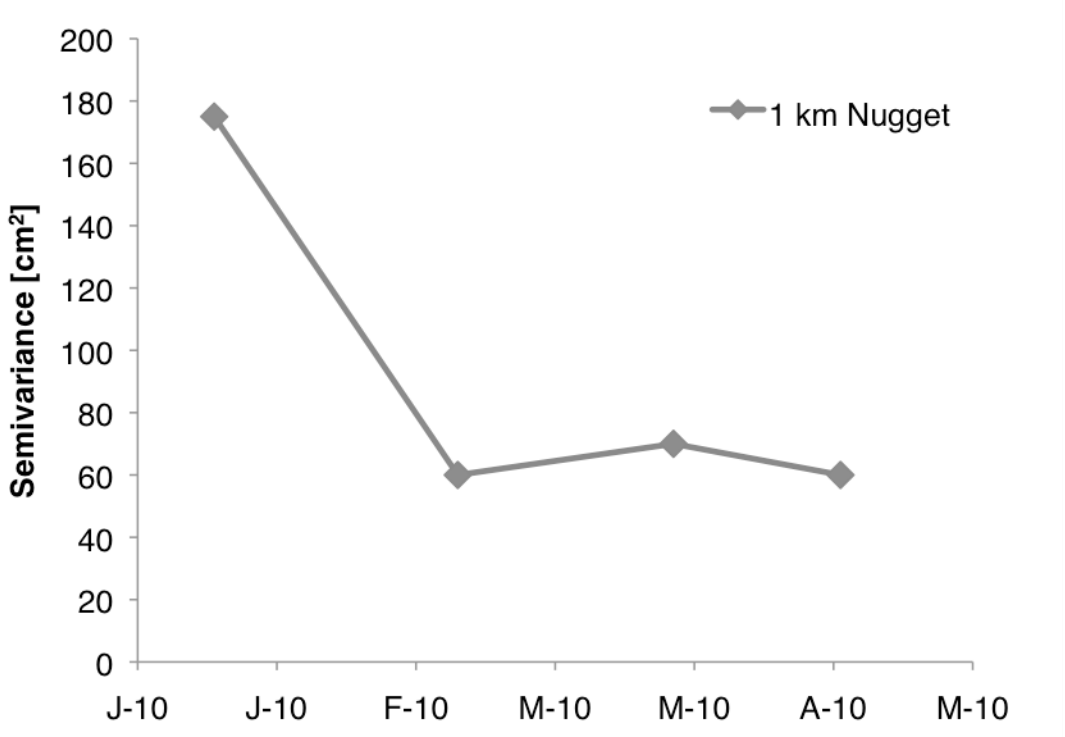

**Figure 4.52** 1 km$^2$ pixel scale variogram nugget parameter.

**Table 4.9** 1 km$^2$ pixel variogram parameter table

| Date | nugget [cm$^2$] | range [m] | range +error | range -error | sill [cm$^2$] | sill +error | sill -error |
|---|---|---|---|---|---|---|---|
| 1/15/10 | 175 | 150 | NA | NA | 400 | NA | NA |
| 2/19/10 | 60 | 106 | 45.5 | 26 | 520 | 43.9 | 32.8 |
| 3/22/10 | 70 | 258 | 40 | 25 | 1050 | 56 | 52 |
| 4/15/10 | 60 | 250 | 46.5 | 135.8 | 1190 | 73.4 | 76.5 |

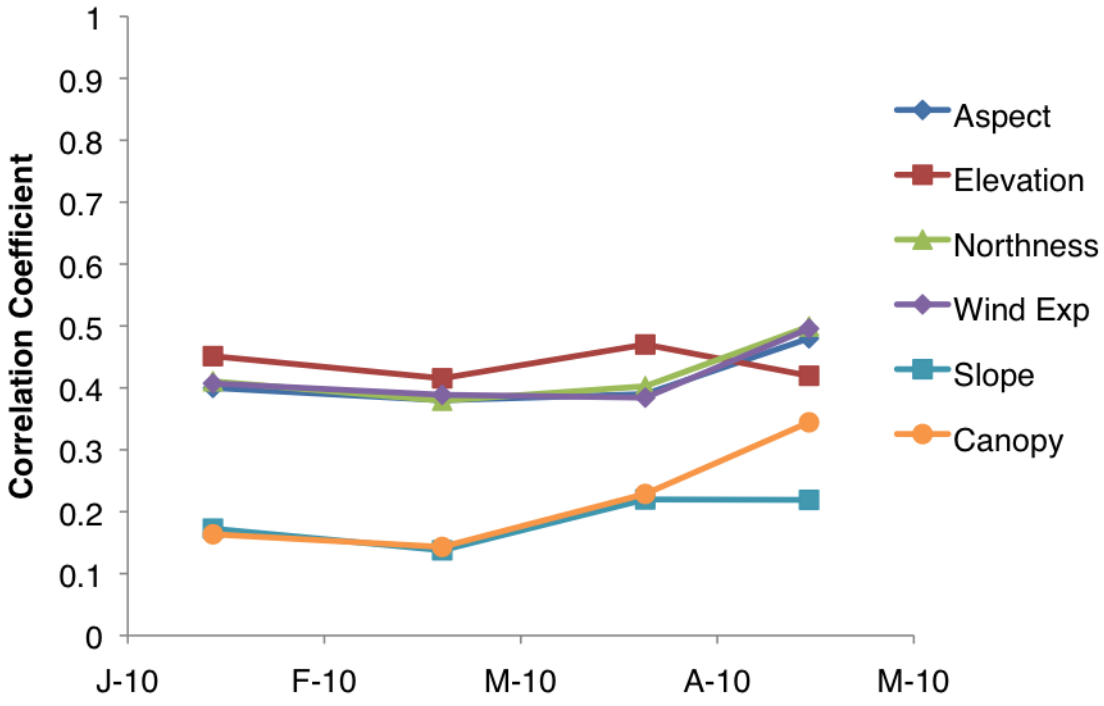


**Figure 4.53** 1 km$^2$ pixel scale influencing variable correlation coefficients.

**Table 4.10** 1 km$^2$ scale correlation coefficients for snow depth and influencing variables

| Date | *n* | Elevation | Aspect | Slope | Northness | Canopy Density | Wind Exposure |
|---|---|---|---|---|---|---|---|
| 1/15/10 | 303 | 0.45 | 0.40 | -0.17 | 0.41 | 0.16 | -0.41 |

| | | | | | | | |
|---|---|---|---|---|---|---|---|
| 2/19/10 | 1725 | 0.42 | 0.38 | -0.14 | 0.38 | 0.14 | -0.39 |
| 3/22/10 | 1725 | 0.47 | 0.39 | -0.22 | 0.40 | 0.23 | -0.38 |
| 4/16/10 | 1725 | 0.42 | 0.48 | -0.22 | 0.50 | 0.34 | -0.50 |

### 4.4 Basin-Wide Snow Survey

Snow depth, snow density, and SWE values from both years are surprisingly similar for both years (Figure 4.54, Table 4.11). Mean SWE values based on both depth and density measurements show only a 1 cm difference between 2009 and 2010; however, histograms from both years show some differences in snowdepth values encountered in the field (Figure 4.55). Measurements were taken along transects at the same locations both years, although with fewer depth samples per transect at some locations in 2010. 2010 data has numerous zeros at lower elevations where snow had melted out. During 2009, a snowstorm occurred during the survey, which resulted in snow coverage even at lower elevations. Overall, the snow/no-snow elevation line was higher in 2010 than 2009, but the 2010 snowpack was deeper at higher elevations.

Correlations with influencing variables showed stronger relationships during the 2010 season with all variables except slope (Figure 4.56, Table 4.12). Elevation showed the strongest correlation during both years (Figure 4.57 and 4.58) followed by aspect in 2010, and canopy density during 2009.

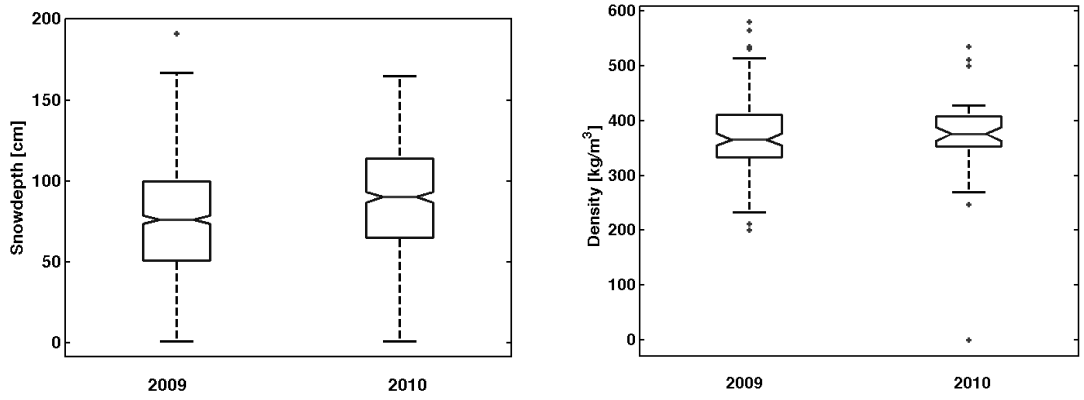


**Figure 4.54** Basin-Wide snow depth and density box plots.

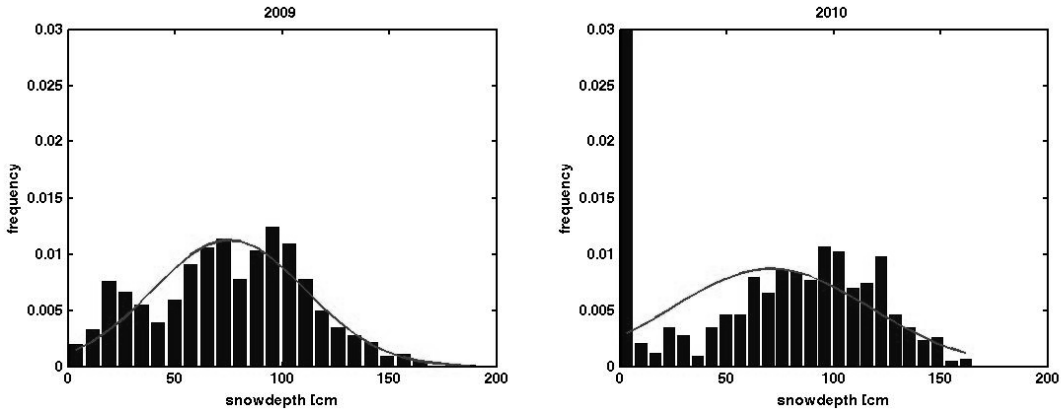


**Figure 4.55** Basin-wide snow survey snow depth histograms (bars) and normal probability density function (line).

**Table 4.11** Basin-Wide Snow Survey Statistics

| Date/parameter | *n* | mean | std dev | *cv* |
|---|---|---|---|---|
| snow depth [cm] | | | | |
| 2009 | 846 | 76 | 35 | 0.46 |
| 2010 | 642 | 71 | 44 | 0.61 |
| snow density [kg/m$^3$] | | | | |
| 2009 | 103 | 375 | 74 | 0.2 |
| 2010 | 44 | 379 | 71 | 0.19 |
| SWE [cm] | | | | |
| 2009 | 846 | 29 | 14 | 0.5 |
| 2010 | 642 | 27 | 18 | 0.64 |

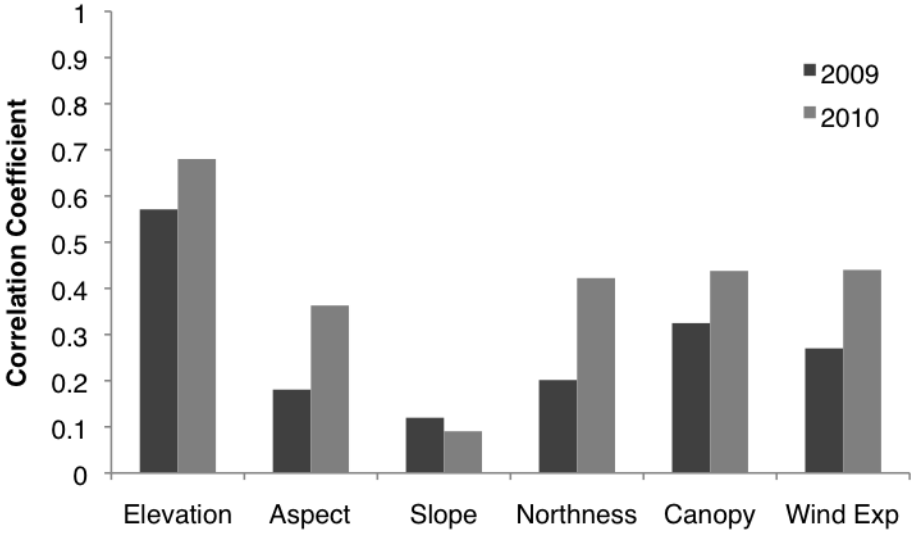


**Figure 4.56** Correlation coefficients for 2009 and 2010 basin-wide surveys.

**Table 4.12** Basin-wide correlation coefficients for snow depth and influencing variables

| Year | *n* | Elevation | Aspect | Slope | Northness | Canopy Density | Wind Exposure |
|---|---|---|---|---|---|---|---|
| 2009 | 846 | 0.57 | 0.18 | -0.12 | 0.20 | 0.32 | -0.27 |
| 2010 | 642 | 0.68 | 0.36 | 0.09 | 0.42 | 0.44 | -0.44 |

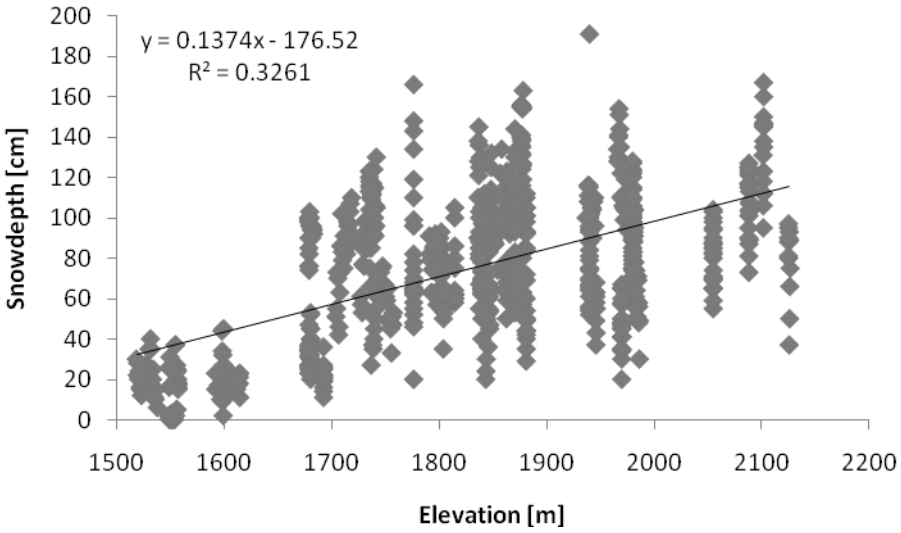


**Figure 4.57** 2009 Basin-wide Elevation trend.

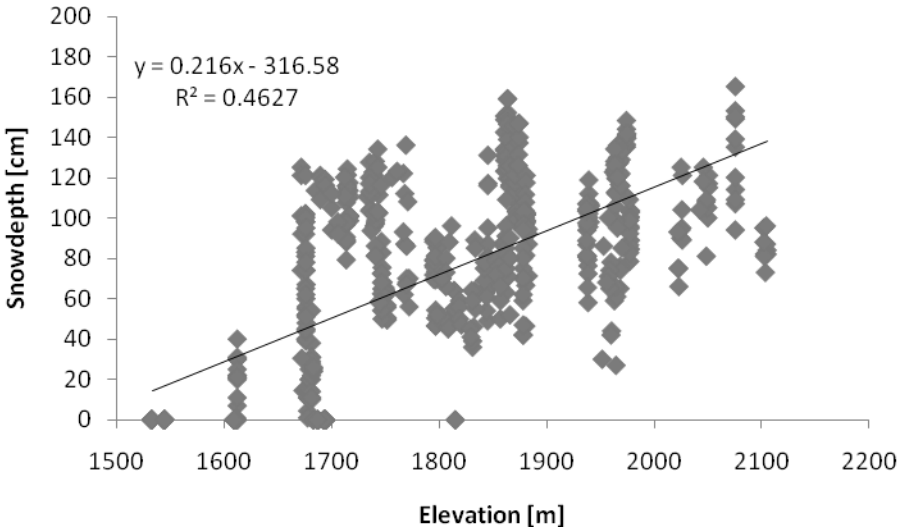


**Figure 4.58** 2010 Basin-wide Elevation trend.

# CHAPTER 5: DISCUSSION

This work investigated the sources and evolution of snow spatial variability and the performance of the SNODAS modeling product. The hypothesis tested is that spatial variability of snow is explained by three interacting processes: 1) differential accumulation, 2) redistribution, and 3) differential ablation. Evidence for each of these processes was encountered during the study. Their influence was determined through analysis of spatial correlations and influencing variables.

Differential accumulation of snow due to elevation is the dominant source of watershed-scale and SNODAS pixel scale (1 $km^2$) spatial variability. Both the watershed-scale and pixel scale surveys show the strongest correlations with elevation, except the final pixel scale survey where aspect and northness shows greater correlation than elevation. Differential accumulation via differences in elevation are evident when the three transect scale survey campaigns are compared (Figure 4.12) and in the precipitation lapse rate (Figure 1.2). By mid-March, over the roughly 550 meter increase in elevation from Treeline to Upper Dry Creek, there is a 1 meter increase in snow depth on average. Differential accumulation is also evident as the result of forest canopy interaction with snowfall at the transect scale at Lower Deer Point. Early season snow distribution at Lower Deer Point showed greater variability and moderate correlation with forest canopy density. Areas under dense forest canopy accumulated less snow than areas in forest openings. This relationship became less strong as the season progressed. It

is likely that variability resulting from the influence of forest canopy density occurs at smaller scales (< 30 $m^2$) than the NLCD Forest Canopy dataset and the influence of canopy shading may have reduced the dependence of snow depth on forest canopy density.

Evidence for redistribution of snow deposited on the ground was not found to be a strong control on snow distribution at any scale in this study. It was assumed that the wind exposure index would provide information about snow redistribution at the transect scale. While the wind exposure index did provide some moderate correlations with snow depth at all scales, it is thought that those correlations are the result of differential ablation due to aspect or solar radiation influence. The wind exposure index was calculated from a DEM using a NW azimuth (270-360˚) that may have captured some preferential deposition due to wind, but also likely captured aspect differences. The only evidence for redistribution encountered during these surveys is the presence of outlier values measured at Upper Dry Creek during the April 14 survey. Snowdrifts were noted in the field and snow depth values of over 200 cm were measured at two locations along the transects. These snowdrifts were only 1-3 meters across so the data provides only 1-3 measurements of each drift, thus correlations of snowdrifts with any controlling variables are absent.

Differential ablation is an important control on spatial variability of snow at all three scales of measurement. The data from the Treeline transect scale surveys illustrate a clear picture of differential ablation across slope and aspect differences due to differential input of solar radiation. Because the Treeline site experienced relatively uniform snow accumulation during the early season, the late season spatial variability can

be completely attributed to the influence of differential ablation. The final transect-scale sampling dates at Lower Deer Point and Upper Dry Creek were made when significant melt was occurring and differential ablation likely influences these data. However, significant spatial variability prior to ablation and lack of significant correlation with any of the influencing variables renders it difficult to attribute this variability to a distinct process or influencing variable.

The relative influence of elevation, aspect, slope, wind, and vegetation is different for the various scales of measurement. Snow depth was found to have moderate to high correlations with elevation at the watershed scale and the pixel scale. Solar radiation parameters (aspect, slope, and northness) and vegetation showed moderate correlations with transect scale snowdepth at Treeline and Lower Deer Point, respectively.

Overall, correlations with a single influencing variable were not significantly strong, except in the case of aspect and northness at the Treeline site (correlation coefficient of 0.85 by the end of the season). Interactions between influencing variables and random variability due to surface roughness and small scale interactions between snow and the landscape make the determination of landscape property influences difficult.

The pixel scale surveys also indicated the influence of differential ablation. Figures 4.38 – 4.41 show the spatial distributions of snow depth over the 1 $km^2$ area during each survey. As snow continued to accumulate at higher elevations and more north-facing areas, portions of the pixel became snow free at lower more south-facing areas. Differential ablation began as early as mid-February in some portions of the

survey, while the deepest snow encountered during the campaign was measured during the final survey in higher elevation areas protected from solar radiation.

The evolution of the variogram range indicated that different scales and landscape environments provide different trends in correlation lengths as the snowpack evolves. At the Treeline site, the range decreased as the season progressed from roughly 10 meters to roughly 50 meters. These distances are approximately similar to the separation distances of sagebrush coppices and hillslope aspect differences, respectively. At the Lower Deer Point site, the range decreased with time from roughly 75 meters to roughly 25 meters as variability increased. These correlation lengths are the result of the influence of forest canopy interception and shading. This indicates that during accumulation, larger distances are subject to reduced snow under forest canopy, while during subsequent ablation variable transmittance of solar radiation through the canopy reduces the length of these correlations. The evolution of the range at Upper Dry Creek decreased from roughly 50 meters to roughly 25 meters. This evolution of the range corresponds approximately with changes in hillslope aspect differences.

SNODAS model predictions were most accurate at the Upper Dry Creek Site and least accurate at the Lower Deer Point site. It was hypothesized that sub-pixel variability would render SNODAS predictions unrepresentative of field conditions. While this was encountered at individual model pixels, it was found that SNODAS captured the elevation trend throughout the basin. Therefore, SNODAS is capable of representing the dominant source of variability at the watershed scale, despite underpredicting the magnitude of SWE. Model underprediction of snow density occurred at all study sites. While snow depth was found to be highly variable throughout the watershed, snow

density values and their trend throughout the season were relatively consistent. Snow density increased linearly with time at all locations. Early season modeled snow density values tended to be closer to measured values, but as the season progressed, modeled snow density did not increase as much as observed snow density. Snow depth was underpredicted by the model in most locations, except for the Upper Dry Creek site. The overprediction of snow depth at Upper Dry Creek balanced the underprediction of snow density, yielding relatively accurate predictions.

The accuracy of SNODAS in complex terrain where significant snow depth variability is present is surprisingly reasonable. Model underprediction of snow depth at two sites and overprediction of snow depth at one site are likely due to the proximity of measurements to the SNOTEL site and lack of assimilated snow information at lower elevations. Inaccuracies in the model forcing data, such as the amount and type of precipitation, likely reduce the model accuracy; however, the influence of assimilated snow cover imagery may also be an important source of error. Barrett (2003) stressed SNODAS' trouble with forested landscapes due to the inability of snow-covered area images to properly capture snow or no-snow under dense forest canopy. Model underprediction of SWE at Lower Deer Point may be related to this issue and future work to improve SNODAS should include modeling snow in forested landscapes.

The evolution of measured snow density in this study is consistent across multiple scales and environments. Snow density of a seasonal snowpack increases linearly with time until complete ablation. SNODAS could also be improved by a more accurate representation of snow density throughout the winter.

SNODAS could also likely be improved by more data assimilation across elevation gradients. SNODAS assimilates SNOTEL data to update the model and move it toward a more accurate prediction of conditions on the ground. SNOTEL sites, however, are not stratified across a wide range of elevations. Most SNOTEL sites are located between 6000-7000 feet elevation. SNOTEL sites are also point measurements that can misrepresent the overall basin scale snow conditions if located in an area that preferentially accumulates snow.

This study found that variability occurs over scales of tens of meters. SNODAS model predictions may be inherently biased due to the model averaging the relevant influencing variables, such as elevation and aspect, over 1 km areas, effectively averaging out the variability and causing underprediction. SNODAS could be improved by better handling of sub-pixel variability.

# CHAPTER 6: CONCLUSIONS

The goal of this study was to evaluate the SNODAS modeling framework and estimate accuracy and sub-pixel variability of model estimates within DCEW. This study also sought to quantify the evolution of SWE spatial variability at three different scales using the variogram and to gain a quantitative understanding of the landscape characteristics and physical processes that influence the spatial distribution of SWE at these scales.

SNODAS model comparison with snow survey field data indicte that SNODAS captures the influence of elevation at the watershed scale while underpredicting the magnitude. SNODAS underpredicted, snow depth, snow density and SWE in both transect and 1 $km^2$ pixel scale surveys at Lower Deer Point and Treeline. SNODAS performed much better in the higher elevation, Upper Dry Creek site with an overprediction of SWE during ablation. It is thought that the close proximity of the Bogus Basin SNOTEL station and its use in the assimilation of ground truth data are responsible for the better performance at Upper Dry Creek. Modeled snow density did not compare well with measured snow density and may explain some the descrepency between modeled and observed SWE. Modeled snow density was unrealistically low for a seasonal snowpack at all study sites.

Results from the transect scale surveys indicate that in non-forested, lower elevation sites (Treeline) solar radiation or northness is the dominant control leading to

differential ablation patterns and a high degree a variability durring ablation. There was little evidence for differential accumulation in this environment beyond the variability associated with interaction with shrubs and small scale surface roughness. The correlation range of the snow-cover process increased throughout the season as differential ablation became more prevalent. In the forested, mid-elevation site (Lower Deer Point) surveys indicate that differential accumulation occurs as a result of forest canopy interception, and that moderate forest canopy denisties (40-60%) tend to accumulate the deepest snow. At the transect scale, the correlation between forest canopy and snowdepth decreased as the season progressed. The correlation range of the snow depth decreased with time until significant ablation began to occur, at which time it began to increase. Results from the Upper Dry Creek Site indicate that small-scale topography influences SWE deposition, resulting in differential accumulation in less wind exposed areas such as areas with lower slope and farther from the ridge line. Differential ablation does occur in these areas as noted by the correlation with northness, but is thought to be not as important as differential accumulation.

The 1 $km^2$ pixel scale surveys indicate that even relatively small elevation gradients (~200m) play a significant role in determining SWE variability. Differential accumulation occurred along elevation gradients and in conjunction with wind exposure indicies, while differential ablation occurred as a result of differential solar radiation inputs and elevational temperature differences.

Basin-wide surveys indicate that elevation, canopy density, and wind exposure indicies are important controls on snow distribution. Two seasons with the same percent of average SWE, based on the Bogus Basin snow course, had significantly different snow

distribution patterns and very different relationships with influencing variables. This work indicates that small scale variaiblity, on the order of 20-60 meters, is important for describing basin-wide SWE, especially in shallow snow where accumulation and ablation occur repeatadly throughout the season. This work also demonstrates that snow density tends to increase linearly with time until ablation regardless of the variabilty in snow depth. This work is representative of snow evolution and SNODAS model performance in mid-elevation semi-arid landscapes with complex terrain.

# REFERENCES


Anderton, S. P., White, S. M. and Alvera, B. (2002), Micro-scale spatial variability and the timing of snow melt runoff in a high mountain catchment. *Journal of Hydrology 268,* 158-176.

Anderton, S.P., S.M. White, B. Alvera. (2004), Evaluation of spatial variability in snow water equivalent for a high mountain catchment. *Hydrological Processes. 18.* 435-453.

Armstrong,R. L. and Brun,E. (2008), *Snow and Climate: Physical Processes, Surface Energy Exchange and Modeling* pp. 1-256. Cambridge University Press.

Bales R.C., Molotch N.P., Painter T.H., Dettinger M.D., Rice R., Dozier J. (2006), Mountain hydrology of the western United States. *Water Resources Research **42:** WO8432,* doi.10.1029/2005WR004387.

Barnett T.P., Adam J.C., Lettemeier D.P. (2005), Potential impacts of a warmer climate on water availability in snow dominated regions. *Nature. 438*:303-309

Barrett, A. *National Operational Hydrologic Remote Sensing Center Snow Data Assimilation System (SNODAS) Products at NSIDC*. NSIDC Special Report 11. 19 pp: National Snow and Ice Data Center. Boulder, CO USA. 2003

Berezovskaya S. and D. Kane. (2007), Measuring snow water equivalent for hydrological applications: Part1, accuracy of observations. *Proceedings of the 16$^{th}$ International Northern Research Basins Symposium and Workshop, Petrozavodsk, Russia*. Pp. 29-37.

Blöschl, G. (1999), Scaling issues in snow hydrology. *Hydrological Processes 13*: 2149-2175

Carrol T., Cline D., Olheiser C., Rost A., Nilsson A., Fall G., Bovitz C., Li L. (2006), NOAA's National Snow Analysis. *Proceedings of the 74th Annual Western Snow Conference, Las Cruces, New Mexico.*

Cayan D.R., Kammerdiener, S.A., Dettinger, M.D., Caprio, J. M., Peterson, D.H. (2000), Changes in the onset of spring in the Western United States. *Bulletin of the American Meteorological Society. 83*:399-415

DeWalle, D. R. and Rango, A. (2008), *Principles of Snow Hydrology*. pp. 22-47 Cambridge University Press

Dickinson, W. T. and H. R. Whiteley, (1972), A sampling scheme for shallow snowpacks. *IASH Bulletin, 17***:** 247-258.

Elder K. J. Dozier, J. Michaelsen. (1991), Snow accumulation and distribution in an alpine watershed. *Water Resources Research. 27*: 1541-1552

Elder K. W. Rosenthal, R. Davis. (1998), Estimating the spatial distribution of snow water equivalent in a montane watershed. *Hydrological Processes. 12*: 1793-1808.

Frank, E. C. and Lee R. 1966. *Potential Solar Beam Irradiation on Slopes: Tables for 30 to 50 Latitude*. Res. Paper RM-18. Rocky Mtn. For. and Range Exp. Sta.:US Department of Agriculture, Forest Service.

Goodison, B.E. (1978), *Accuracy of snow samplers for measureing shallow snowpacks: an update.* Proc 35th Annu. Meet. West. Snow Conf., pp. 44-58

Granger, R.J., J.W. Pomeroy and R.L.H Essery. (2006), Boundary layer growth over snow and soil patches. *Hydrological Processes. 20:* 943-951.

Gray D.M. and Male D.H. (1981), *Handbook of snow: principles processes, management and use.* pp. 567-581. Pergamon Press.

Helms, D. S.E. Phillips, P.F. Reich. (2008), The History of Snow Surveying and Water Supply Forecasting. USDA, NRCS pp. 3-7

Homan, J. W., Luce, C. H., McNamara, J. P. and Glenn, N. F. (2011), Improvement of distributed snowmelt energy balance modeling with MODIS-based NDSI-derived fractional snow-covered area data. *Hydrological Processes*, n/a. doi: 10.1002/hyp.7857

Jordan R.(1991), A one-dimensional temperature model for a snow cover; Technical documentation for SNTHERM.89. CRREL Special Report 91-16, 64p.

Jost G., Weiler M., Gluns D.R., Alila Y.(2007), The influence of forest and topography on snow accumulation and melt at the watershed-scale. *Journal of Hydrology. 347*:101-115.

Kormos, P. (2005), Accounting for time and space variations of [delta]18O in a snowmelt isotopic hydrograph separation in the Boise Front. Master's Thesis, Boise State University, Boise, Idaho, United States.

LaMontagne, A.(2009) Characteriztion and quantification of ground heat flux for shallow snow. Master's Thesis. Boise State University, Boise Idaho, United States.

Lapen, D.R. and L.W. Martz. (1993), The measurement of two simple topographic indicies of wind sheltering-exposure from raster digital elevation models. *Computers and Geosciences. Vol. 19. Issue 6.* pp. 769-779.

Lee, R. (1963), Evaluation of Solar Beam Irradiation as a Climatic Parameter of Mountain Watersheds, Hydrology Paper No. 2, Ft. Collins, CO: Colorado State University

Li, L. and J. Pomeroy. (1997), Estimates of threshold wind speeds for snow transport using meteorological data. *Journal of Applied Meteorology. 36*. 205-213.

Luce C.H., D.G. Tarboton, K.R. Cooley. (1999), Sub-grid parameterization of snow distribution for an energy and mass balance snow cover model. *Hydrological Processes. 13*: 1921-1933.

McNamara, J.P., D. Chandler, M. Seyfried, S. Achet. (2005), Soil moisture states, lateral flow, and streamflow generation in a semi-arid, snowmelt driven catchment. *Hydrological Processes. 19*. 4023-4038.

Molotch N.P. and R.C. Bales. (2005), Scaling snow observations from the point to the grid element: implications for observation network design. *Water Resources Research. 41*: W11412

National Operational Hydrologic Remote Sensing Center (NOHRSC). 2010. *Snow Data Assimilation System (SNODAS) Data Products at NSIDC*. Boulder, Colorado USA: National Snow and Ice Data Center. Digital media.

NRCS – Snow Survey. 2010. Snow course historical data. Digital Media http://www.id.nrcs.usda.gov/snow/data/historic.html.

Rango, A., J. Martinec, A. Chang, J. Foster, and V. van Katwijk. (1989), Average areal water equivalent of snow on a mountain basin using microwave and visible satellite data. In *IEEE Transactions on Geoscience and Remote Sensing 27*:6:740-745.

Rott, H., S. Yueh, D.W. Cline, C. Duguay, R. Essery, C. Haas, F. Heliere, M. Kern, G. Macelloni, E. Malnes, T. Nagler, J. Pulliainen, H. Rebhan, A. Thompson. (2010), *Cold Regions Hydrology High Resolution Observatory for Snow and Cold Land Processes. Proceedings of the IEEE Vol. 89 No. 5.*

Rutter, N., D. Cline, and L. Li, (2008), Evaluation of the NOHRSC Snow Model (NSM) in a One-Dimensional Mode. *J. Hydrometeor. 9,* 695-711.

Schmugge, T.J., W.P Kustas, J.C. Ritchie, T.J. Jackson, A. Rango. (2002), *Remote sensing in hydrology. Advances in Water Resources. 25,* 1367-1385.

Stepphun, H., (1976), Areal water equivalents for prairie snowcovers by centralized sampling. *Proceedings, 44th Annual Western Snow Conference,* 63-68.

Sturm, M., B. Taras, G. E. Liston, C. Derksen, T. Jonas, J. Lea. (2010), Estimating local to global snow water resources using snow depth data and snow climate classes. *Journal of Hydrometeorology. 11,* 1380–1394.

Trujillo, E., J. A. Ramirez, and K. J. Elder. (2007), Topographic, meteorologic, and canopy controls on the scaling characteristics of the spatial distribution of snow depth fields, *Water Resour. Res., 43,* W07409, doi:10.1029/2006WR005317

Webster, R. and Oliver M. (2001), *Geostatistics for Environmental Scientists*. p.47-131. John Wiley and Sons, ISBN 0-471-96553-7

Williams, C.J. (2005), Characterization of the spatial and temporal controls on soil moisture and streamflow generation in a semi-arid headwater catchment. Master of Science Thesis. Boise State University, Boise, Idaho. United States of America.

Williams, C.J., McNamara, J.P., and Chandler, D.G., (2009), Controls on the spatial and temporal variation of soil moisture in a mountainous landscape: the signatures of snow and complex terrain. *Hydrology and Earth System Science, 13:* 1325-1336.

Work, R.A.; H.J. Stockwell, T. G. Freeman, and R.T. Beaumont. (1965), *Accuracy of field snow surveys, western United States, including Alaska.* Tech. Rep. 163, U.S. Army Cold Reg. Res. Eng. Lab., Hanover, N. H.

United States Geological Survey. (2007), *NLCD 2001 Land Cover*. United States Geological Survey: Sioux Falls, SD.

Veatch, W., Brooks, P. D., Gustafson, J. R. and Molotch, N. P. (2009), 'Quantifying the effects of forest canopy cover on net snow accumulation at a continental, mid-latitude site'. *Ecohydrology, 2:*115–128.